UNIVERSITÀ DEGLI STUDI DI PARMA
DIPARTIMENTO DI INGEGNERIA DELL'INFORMAZIONE

Dottorato di Ricerca in Tecnologie dell'Informazione
XXVI Ciclo

Lara González Villanueva

MULTIMODAL BEHAVIOURAL ASSESSMENT IN REHABILITATION

DISSERTAZIONE PRESENTATA PER IL CONSEGUIMENTO
DEL TITOLO DI DOTTORE DI RICERCA

GENNAIO 2014

UNIVERSITÀ DEGLI STUDI DI PARMA

Dottorato di Ricerca in Tecnologie dell'Informazione

XXVI Ciclo

MULTIMODAL BEHAVIOURAL ASSESSMENT IN REHABILITATION

Coordinatore:

Chiar.mo Prof. Marco Locatelli

Tutori:

Chiar.mo Prof. Stefano Cagnoni

Ing. Luca Ascari, PhD

Dottorando: *Lara González Villanueva*

Gennaio 2014

This work has been funded by the European Commission
under the MIBISOC project (Grant Agreement: 238819)
within the action Marie Curie Initial Training Network of the 7FP.

Alla mia metà

Contents

List of Figures

List of Tables

List of Algorithms

List of Acronyms

ACK	Acknowledgement
AI	Artificial Intelligence
CP	Computational Perception
CRC	Cyclic Redundancy Check
CSMA-CA	Carrier Sense Multiple Access – Collision Avoidance
CTP	Computational Theory of Perceptions
DGNG	Double Growing Neural Gas
DIKW	Data-Information-Knowledge-Wisdom
EEG	Electroencephalography
FCS	Frame Check Sequence
FFSM	Fuzzy Finite State Machine
FRBS	Fuzzy Rule-Based System
GLMP	Granular Linguistic Model of a Phenomenon
GNG	Growing Neural Gas
GNG-U	Growing Neural Gas with Utility
GUI	Graphical User Interface
ID	Identifier
IGNG	Incremental Growing Neural Gas
ISR	Interrupt Service Routine

LED	Light-Emitting Diode
LQI	Link Quality Indication
MAC	Media Access Control
MGNG	Merge Growing Neural Gas
MEMS	Micro-Electro-Mechanical Systems
MPF	Memory Prediction Framework
NG	Neural Gas
NL	Natural Language
PAN	Personal Area Network
PDA	Personal Digital Assistant
PDU	Protocol Data Unit
PLL	Phase-Locked Loop
PM	Perception Mapping
RF	Radiofrequency
RSSI	Received Signal Strength Indicator
RS232	Recommended Standard 232
SMO	Sequential Minimal Optimization
SGONG	Self-Growing and Self-Organized Neural Gas
SOM	Self Organizing Map
SVM	Support Vector Machine
TDMA	Time Division Multiple Access
TTL	Transistor–Transistor Logic
WBAN	Wireless Body Area Network
WSN	Wireless Sensor Network

Abstract

After suffering from a serious injury, illness or surgery, the patient usually needs to follow a long and critical physical rehabilitation program to recover the former strength, mobility and fitness. Procedures for monitoring patients' movements are widely used in this context and are mainly aimed at identifying and maximizing life quality and movement potential. Many rehabilitation programs rely on classical treatments based on physiotherapy, which requires trained specialists and their precious experience. However, sometimes, these treatments lack standardized and objective information for properly evaluating patients' performance.

Creating non-invasive systems, using a low-power scheme at low cost, for monitoring the patients' movements and interpreting properly the data acquired in order to provide them with a useful feedback, is one of the current challenges and the main aim of this PhD dissertation. As a contribution to the assessment of rehabilitation exercises, a hardware and software suite is proposed, both for human motion acquisition and tracking and data analysis.

Firstly, to capture human motion, a prototypical wearable sensing system, based on a robust communication scheme and a data alignment algorithm, is developed and tested. It is composed of a number of small modules that embed high-precision accelerometers and wireless communications to transmit the information related to the body motion to a workstation. The system includes a device for video acquisition during the training sessions in order to provide, additionally, visual feedback to the patient.

Afterwards, three different methods are investigated for the analysis of motion data. The first one is based on neural gas networks, which are considered in a implementation of the Memory Prediction Framework theory. The Granular Linguistic Model of a Phenomenon, which is based on the Computational Theory of Perceptions, is used in combination with a Fuzzy Finite State Machine in the second approach to develop a tool that analyses the exercise and provides a linguistic description of it. The last method proposes a hybrid neuro-fuzzy system which merges the two previous schemes in order to join their advantages while compensating their drawbacks.

From the experimental results obtained, it can be concluded that, both from a practical and a theoretical point of view, the proposed suite can introduce improvements in the current state of the art in the field of human motion monitoring for rehabilitation.

Chapter 1

Introduction

Rehabilitation is to be a master word in medicine.

Dr. William Mayo

1.1 Motivation

Human motion monitoring and analysis can be an essential part of a wide spectrum of applications ranging from entertainment and gaming to surveillance and medical diagnosis [1], including physical rehabilitation among other potential areas of interest. The main aim of rehabilitation is to enable patients to regain the highest possible level of motor functions and independence after a stroke or another kind of accident [2]. There is strong evidence that after-stroke patients benefit from exercise programmes in which functional tasks are directly and intensively trained [3]. To achieve this objective, patients' activities need to be monitored and consequently corrected. Classical treatments, as physiotherapy, are mainly based on the experience of the specialists and may lack objective information for a proper evaluation of patients' performances. Applying motion sensors technology to these therapies involves accurate identification [4], tracking and post-processing of movement, which can help to improve the diagnosis and the rehabilitation process [5, 6], as they provide objective and quantitative information which can be added to the expertise of the clinicians [7].

Among several ways available for recording patients' activities, automatic human motion tracking systems are becoming more and more attracting because of their potential, allowing to acquire a huge amount of information regarding the poses or movements of the subjects [8]. However, at the same time, they still have major practical limitations. Motion tracking systems, especially those where human movements can be detected using on-body sensors, often include wires between them and other unwieldy elements that have to be worn, as shown in Figure 1.1 (from [9]).

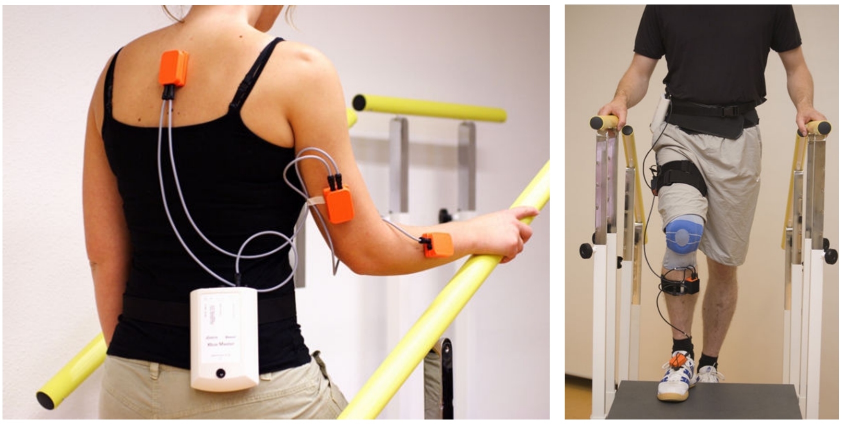

(a) Upper body monitoring. (b) Lower body monitoring.

Figure 1.1: Commercial system for human motion monitoring [9].

This shortcoming makes them unsuitable for certain types of therapies, like sports rehabilitation, as they may limit the patient's movements and negatively influence the measures [10]. Additionally, existing systems are not easily affordable.

Therefore, in the context of an exercise session within a rehabilitation program there are mainly two or three questions to be answered:

1. *How* to effectively monitor the patient's movements?

2. *How* is the patient performing the exercise?

3. *How* to inform and make the patient aware of her/his performance to boost the improvement?

One of the most promising approaches in building wearable health monitoring systems is based on emerging Wireless Body Area Networks (WBANs) [11], consisting of multiple sensor nodes, placed strategically on the human body, each capable of sampling, processing and communicating information related to the patient's movements. On the other hand, to answer the second question it is necessary to perform an accurate analysis on the acquired data, while the answer to the last one is *feedback*.

1.2 Aim of the thesis and research approach

Creating non-invasive systems, using a low-power scheme at low cost, for monitoring the patients' movements and interpreting properly the data acquired in order to provide them with a useful feedback, is one of the current challenges and the main aim of this thesis.

The work described in this dissertation has been funded by the European Commission under the MIBISOC project (Grant Agreement n. 238819), "Medical Imaging using Bio-Inspired and Soft Computing", within the action Marie Curie Initial Training Network of the 7FP, being Henesis S.r.l. [12] the hosting partner. Within the project requirements, it has been focused mainly on two research lines: the use of Wireless Sensor Networks (WSNs) for human motion monitoring and the application of Artificial Intelligence (AI) techniques to data analysis.

In order to answer the questions mentioned previously, the overall aims of this multidisciplinary research are manifold, *i.e.*, to: (i) investigate and conceive an effective and robust multimodal sensing system, (ii) investigate the application of bio-inspired and soft computing techniques to motion data analysis, and (iii) step forward in behavioural assessment for quantitative and qualitative monitoring of a rehabilitation process. The project can be split into three phases:

1. Proposal: investigation of the state of the art, identifying the shortcomings of the current approaches and the requirements to be fulfilled.

2. Technical research: development and implementation of the sensing system,

including data fusion and its validation to determine its feasibility and usefulness for rehabilitation.

3. Applied research: investigation of various techniques for motion data analysis, to be used for behaviour recognition and gesture evaluation.

The work carried out in this thesis has dealt with developing processes at different levels of abstraction, that can be represented as a hierarchy by the DIKW (Data-Information-Knowledge-Wisdom) pyramid in Figure 1.2 (from [13]). At the lowest level there is the data, *i.e.*, the acceleration signals, the direct and objective observations of the phenomena. Over it, there is the information level, which is inferred from the acquired data, making them useful by representing them by certain features, such as reference angles. The upper level is reached as this information is processed, *e.g.*, knowledge is acquired through pattern recognition techniques, allowing one to identify activities or poses. Gaining understanding from this knowledge, one steps up to the superior level, wisdom, where complex abstract concepts are elaborated, making it possible to provide a feedback to the patient about her/his performance.

In particular, the first step in this thesis has been focused, at the lowest level of abstraction, on the development of a prototypical wearable sensing system to capture human motion through accelerometer sensors. Designing a robust communication scheme and a data alignment algorithm has permitted the integration of five small wireless modules, to be worn by the subject, which can acquire data at high frequency, synchronized by an external master device. This system additionally includes the feature of video acquisition for providing visual feedback to the patient. Climbing up the DIKW pyramid, several artificial intelligence methods have been then examined for data interpretation.

Getting to the knowledge level, an initial approach to validate the sensing system has been aimed at classifying three activities, standing, sitting and walking, by using various standard classifiers implementing a supervised learning technique. Afterwards, human motion analysis has been focused on the Sun Salutation, a complex yoga exercise that has been chosen as case study. This sequence, which involves the movement of different parts of the body, is an interesting example of a phenomenon evolving in time and has important physical benefits, like improving the strength and flexibility of the muscles and the alignment of the vertebral column. Reaching the top level of wisdom, three different methods have been investigated for data analysis. The first one is based on the Memory Prediction Framework, a paradigm inspired on the working of the human brain, and studies a specific type of neural network. The second technique is based on the Computational Theory of Perceptions and aims to provide a linguistic description of the phenomenon, evaluating its quality by considering three particular features: symmetry, stability and rhythm. The last approach proposes a hybrid system for postural balance assessment, which merges the two previous schemes in order to join their advantages while compensating their drawbacks. All the methods compose a software suite that can provide a feedback to a subject performing a complex physical exercise using the hardware suite described above.

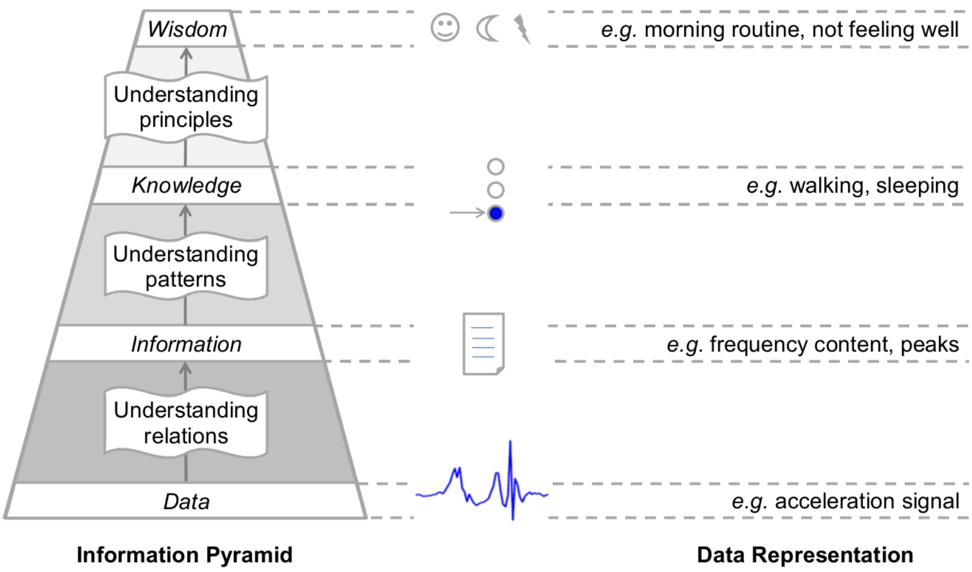

Figure 1.2: Data representation at different levels of abstraction [13].

1.3 Outline

The rest of the document is organized as follows. Chapter 2 introduces the current state of the art of systems for human motion acquisition and tracking and their application in rehabilitation. In Chapter 3, the development, implementation and validation of the proposed multimodal sensing system is described in detail. Chapter 4 is focused on three different methods for human motion data analysis. Finally, Chapter 5 draws some conclusions summarising the research performed in this thesis and introducing possible future research lines.

1.4 Publications

The research described in this thesis has produced the papers indicated below:

- Conference papers:

  "Wireless human motion acquisition system for rehabilitation assessment", Lara González-Villanueva, Lorenzo Chiesi and Luca Mussi, in Proceedings of the 25^{th} IEEE International Symposium on Computer-Based Medical Systems (CBMS), pp. 1–4, June 2012.

  "Computational model of human body motion performing a complex exercise by means of a Fuzzy Finite State Machine", Lara González-Villanueva, Alberto Alvarez-Alvarez, Luca Ascari and Gracian Trivino, in Proceedings of the International Conference on Medical Imaging using Bio-Inspired and Soft Computing (MIBISOC), pp. 245–251, May 2013.

  "A framework to extract readiness potential in single trials of EEG", Pouya Ahmadian, Saeid Sanei, Lara González-Villanueva, M. Alessandra Umiltà and Luca Ascari, in Proceedings of the International Conference on Medical Imaging using Bio-Inspired and Soft Computing (MIBISOC), pp. 261–266, May 2013.

- Journal papers:

  "Design of a wearable sensing system for human motion monitoring in physical rehabilitation", Lara González-Villanueva, Stefano Cagnoni and Luca Ascari, in Sensors, 13(6), pp. 7735–7755, June 2013.

  "Constrained blind source extraction of readiness potentials from EEG", Pouya Ahmadian, Saeid Sanei, Luca Ascari, Lara González-Villanueva and M. Alessandra Umiltà, in IEEE Transactions on Neural Systems and Rehabilitation Engineering, 21(4), pp. 567–575, July 2013.

  "A tool for linguistic assessment of rehabilitation exercises", Lara González-Villanueva, Alberto Alvarez-Alvarez, Luca Ascari and Gracian Trivino, in Applied Soft Computing, Volume 14, Part A, pp. 120–131, January 2014.

Chapter 2

State of the art

The greatest enemy of knowledge is not ignorance,
it is the illusion of knowledge.

Daniel J. Boorstin

2.1 Human motion tracking for rehabilitation

After suffering from a serious injury, illness or surgery, a patient typically must undergo a long and critical physical rehabilitation program to recover her/his former strength, mobility and fitness. Procedures for monitoring patients' movements are widely used in this context and are mainly aimed at identifying and maximizing life quality and movement potential. Many rehabilitation centres rely on classical treatments based on physiotherapy, which requires trained specialists and their precious experience. Sometimes, these treatments lack standardized and objective information that would be necessary for a proper evaluation of patients' performances. Along with the increased number of patients who suffer from motor function disability, this is the main reason why, since the 1980s, human motion tracking for rehabilitation has been an active research topic [5].

Stroke is considered the most common neurological disorder and has a high mortality risk. It is caused by the interruption of the blood supply to the brain, usually because a blood vessel bursts or is blocked by a clot. This cuts off the supply of oxygen and nutrients, causing damage to the brain tissue [14]. According to the World Health Report published in 2002, 15 million people suffer stroke worldwide each year. Of these, 5 million die and another 5 million are permanently disabled. The World Health Organization estimated in 2008 the world average incidence of the disease in about 200 new cases per 100.000 inhabitants [15]. In [16] it is estimated that its incidence in Spain is between 200 and 250 cases per 100.000 inhabitants, while a more detailed study published in [17] estimates its incidence between 120 and 350 annual cases per 100.000 inhabitants. This would be lower in women (169/100.000) than in men (183-364/100.000), and it is 10 times higher in the population over 70 years. In a similar direction, a study done by the Italian Longitudinal Study on Ageing (ILSA) shows that, in the age group between 65 and 84 years, the prevalence rate in the Italian population is of 6.5%, being the rate of the male subjects slightly greater (7.4% with respect to 5.9%) [18].

People who suffer a stroke require intense rehabilitative treatments during their stay in the hospital and afterwards, when they are dismissed. Treatments focused on high-intensity and repetitive task-specific practice do show promise for improving motor recovery after stroke [19]. In [20] strong evidence was found that patients with stroke benefit from therapeutic exercise programmes, when the exercise training was applied intensively and started as soon as possible after stroke occurred.

Physical rehabilitation is heavily based on the monitoring of body motion patterns. The objective of human motion tracking is to provide data that allows to obtain the related information about the pose of the human body, or part of it. Later analysis of these data may contribute significantly to the diagnostic process by processing the motion patterns. There are several ways to perform human motion acquisition and tracking [21]. The ones found in the literature can be divided mainly into three different groups:

Non-visual tracking systems are based on the use of sensors attached to the body in order to acquire human motion data. The sensors can be of several types as inertial –accelerometers, gyroscopes–, magnetic or acoustic, among others.

Visual tracking systems are based on the use of cameras to estimate the position. The systems in this category can be visual marker-based or marker-free, depending on whether they use or not markers attached to the body. When talking about visual marker-based tracking systems, it must be pointed out that "Vicon" [22], and "Optotrack" [23], are considered the golden standards due to their reduced error for the position information, their high cost being their main drawback.

Robot-aided tracking systems make use of therapeutic robots for specific tasks in neuro-rehabilitation, actively engaging the patients for relearning the movements.

[5] makes a performance comparison between the different groups of motion tracking systems. According to it, the most efficient kind of tracking systems from a computational point of view are the non-visual tracking ones, which have also the lowest cost, being additionally highly compact and accurate when using inertial sensors. For this reason, the rest of this chapter will be focused on the use of sensors for monitoring, while the part related to data analysis will be discussed in its corresponding chapter.

2.2 Using sensors for monitoring

Motion sensors technology makes it possible to accurately identify, track and analyse movement. The data that can be acquired using such devices support the diagnosis and the rehabilitation process [24] by allowing therapists to precisely assess the impact of clinical interventions on the patients' everyday life and recovery [25]. Among the many different sensors that can be used for monitoring patients during rehabilitation, MEMS (*Micro-Electro-Mechanical Systems*) inertial sensors have been shown to have great potentials. The progress of miniaturization and their decreasing cost allow to incorporate them in compact, non-obtrusive continuous monitoring devices easily attachable to the body [26], empowering the development of Wireless Body Area Networks (WBANs) [27, 28]. In particular, accelerometers can provide reliable information as well as objective and quantitative measurements when placed on different parts of the body [29]. For this reason, several studies about their use for body motion capture have been published recently.

In [30] it is stated that the use of accelerometers offers a practical and low-cost method for monitoring human movements, while providing objective and reliable measurements, including assessment of physical activity level and classification of the movements performed by subjects. In their review of the state of the art, the authors have found out that tri-axial accelerometers are able to provide valid and stable measurements of physical activity levels when compared to other indicators of functional capacity. For this reason, accelerometers have been used to study physical activity in many different experiments. One important application of this kind of sensors is within the tests of postural sway, which usually need to be set up and conducted by an external observer, different from the patient, where these sensors have shown to be a reliable tool for measuring balance while standing and walking. Even more, the studies that have been undertaken demonstrated their utility for monitoring human movements and quantitatively measuring important parameters of movement in an unsupervised home environment. This implies some technical requirements, as their usability, power supply and trustworthy wireless communications, for example.

[31] confirms that accelerometers have been widely accepted as useful and practical sensors for wearable devices to measure and assess physical activity. It concludes that sensor-based measurement of human activities can provide quantitative assessment of physical activity. The main advantage is that using these techniques enables automatic, continuous and long-term activity measurement of subjects in a free-living environment.

[32] makes use of a tri-axial accelerometer for posture sensing to be used in activity recognition. Experiments were done for eight different activities –standing, walking, running, climbing up stairs, climbing down stairs, sit-ups, vacuuming and brushing teeth– showing that these can be recognized with fairly high accuracy. Anyway, as expected, some of the activities, like brushing teeth, were comparatively harder to recognize than others due to the fact that there was just one accelerometer and that it was worn near the waist. In [33] an accelerometer attached to a belt,

centered in the back of the person, is used for body posture recognition, while in [34] vital body signals as posture, respiration rate, and body activities like walking and running, are monitored by placing one of them in a t-shirt.

Due to the potential use of accelerometers in a clinical setting and considering their reliability and low cost, the research performed in [35] is related to gait analysis and balance evaluation for elderly people. Being able to assess the risk of falls thanks to the quantitative measures of the gait provided by the accelerometers, the 24-hour ambulatory activity levels can be objectively quantified. Human gait modelling for helping in the diagnosis of walking and movement disorders or rehabilitation programs is also approached in [36] and [37]. The work presented in [38] goes in a similar direction. It consists on a wearable platform intended for long-term ambulatory health monitoring with real-time data streaming and context classification. For fall detection and the classification of other body movements, [39] and [40] use a small module which contains a high resolution accelerometer. They demonstrate its advantages for acquiring motion information due to its precision and size, as it is not intrusive for the subject.

As said in [41], a significant application area is remote monitoring, more specifically home-based rehabilitation monitoring systems, already introduced by [5], both for elderly people who live alone and are in need of additional support, and for people with physical disabilities. It could allow to check whether the patient is able to perform her/his physical therapy exercises in the correct and most efficient manner, and provide feedback to enable proper performance of the exercises. A portable patient-monitoring system might facilitate patient rehabilitation out of the hospital environment, enabling faster recovery and decreasing number of injuries. Even more, having a system that allows to bring the rehabilitation into their own house, might help the patients to perform exercises much more comfortably in a known environment, preventing them from getting stressed while being monitored in a rehabilitation centre or similar.

In this direction, [42] proposes a portable physical rehabilitation monitoring system for hip-and-knee-replacement rehabilitation, which makes use of accelerometers for sensing the patient's movements. It allows one to visualize selected data in real time on a PDA screen and to archive relevant data for later analysis by a specialist. [43] proposes a prototypical WBAN implementation for computer-assisted physical rehabilitation applications and ambulatory monitoring which provides guidance and feedback to the user, by generating warnings based on the user's state, level of activity, and environmental conditions in real time. On the other hand, the purpose of the study in [44] is to develop a motion tracking device that can be integrated within a home-based rehabilitation system for stroke patients. In particular, it integrates the measurements from the accelerometers and gyroscopes for acquiring the data related to the upper limb movements in real time. This work has afterwards been extended in [2], which presents an upper limb motion tracking system with two sensors near the wrist and elbow joints which shows promising results in view of its integration in a rehabilitation platform for describing the upper limb movements of a patient.

2.3 Summary of the reviewed systems

With the aim to sum up and be able to compare the characteristics of the specific systems that have been proposed in the literature cited above, Table 2.1 contains a relation with the principal features of each of them. It must be pointed out that not in all the cases information, such as the range or the sampling frequency of the accelerometers used, was provided.

Reference	Main characteristics
[2]	- Two wearable inertial sensors placed near the wrist and the elbow. - Each sensor contains a three-axial accelerometer, a three-axial gyroscope and a three-axial magnetometer (not used). - Gyroscopes improve accuracy of the estimates by accelerometers. - Sampling frequency: 25 Hz. - The modules are big, and for the elbow a wide band is needed. - The battery, encapsulated in a big package, is worn in the waist. - There are interconnection cables between the components.

Reference	Main characteristics
[29]	- One accelerometer attached on the front of the leg, near the ankle, using the elastic medical bandages. - Range: $\pm$2g, sampling frequency: 32Hz. - Tested for five different activities: standing, walking, running, climbing down stairs and climbing up stairs.
[32]	- Single three-axial accelerometer worn near the pelvic region. - Range: $\pm$4g, sampling frequency: 50Hz. - The data generated by the accelerometer was transmitted to an HP iPAQ, carried by the subject, wirelessly over Bluetooth. - Used for the recognition of eight activities.
[33, 36, 37]	- One three-axial accelerometer attached to a belt, centred in the back of the person. - Sampling frequency: 100Hz. - Bluetooth capabilities for data transmission.
[34]	- Wearable t-shirt with one accelerometer placed on the chest. - Range: $\pm$2g. - The sensor, battery and other electronic components are mounted with velcro on the t-shirt, including interconnection cables. - Detection of walking and running activities.
[38]	- One three-axial accelerometer. - It includes interconnection cables, bands, batteries and a PDA.
[39, 40]	- One three-axial accelerometer worn on the chest. - Range: $\pm$2g, sampling frequency: 160Hz. - Used for fall detection.
[42]	- Individual two-axial accelerometer sensor worn on the leg. - Range: $\pm$2g. - Used for thresholding preventing over-exercising and injuries.

Reference	Main characteristics
[43]	- Two two-axial accelerometers. - It includes a bio-amplifier for ECG monitoring.
[44]	- Two three-axial accelerometers and gyroscopes. - The sensors are attached to the elbow and the wrist. - Bluetooth communication. - It includes several interconnection cables and batteries.

Table 2.1: Main characteristics of the most relevant systems proposed in the literature.

Some of the mentioned works make use of commercial systems, being the most referenced ones those provided by XSens [45] and Inertia Technology [46]. The features of their main products are summarized in Table 2.2.

Feature	**Xsens**				**Inertia**
	[9]	[47]	[48]	[49]	[50]
Cordless power	No	Yes	No	Yes	Yes
Wireless data transmission	No	Yes	No	Yes	Yes
Usability	Low	High	Low	High	Medium
Cost	High	High	Very high	Very high	Medium
Data analysis & feedback	No	No	No	No	No

Table 2.2: Feature comparison of available commercial systems for human motion monitoring.

As can be seen, their main inconvenient, apart from their cost, is that they do not provide a complete solution, including data analysis, that can be directly used by clinicians and patients. For this reason, other studies and companies are focused completely on data analysis, using sensing systems provided by third parties. This is the case of [51], a software for analysis and rehabilitation, which makes use of a MEMS-based motion-sensing system provided by [52]. In addition to accurate motion analysis, this tool includes visual feedback, so that the range and quality of movement can be checked and worked on with feedback. Similarly, the main contribution of [53] has been the design of a gaming interface to support the physical rehabilitation of orthopaedics patients.

2.4 Importance of feedback

As pointed out before, it is important to consider the role of feedback in rehabilitation therapies. Providing information to the patient in response to the performance of the exercises could definitely influence the treatment progress. Performance feedback is generally accepted to be necessary for the learning process that underlies rehabilitation [54]. Depending on the application, this feedback could be provided in graded or absolute forms, *e.g.*, indicating a score or just if the exercise has been done well or not. In the same way, the information can be presented via different sensory modalities, as audio, visual or tactile.

Several studies demonstrate the impact of feedback in physical therapies. Providing feedback on performance is among the recommendations for treatments given by [19] for the alleviation of motor impairment and restoration of motor function after a stroke. In [55] it is suggested to provide people engage in a novel exercise with external feedback during training to ensure the highest level of performance is attained during practice sessions.

In particular, visual feedback is widely reported as useful in this kind of therapies. The study done in [56] shows that interacting with a game incorporating simple visual feedback results in improved accuracy when performing therapeutic exercises. Moreover, [57] reviews the potential use of visual feedback, in particular mirror visual feedback, for the treatment of many chronic neurological disorders, concluding that it can accelerate recovery of function from several disorders, such as phantom pain, hemiparesis from stroke or other brain injury or lesion. In the same direction, [58] illustrates a case report, in which a person with a stroke demonstrated clinical improvements after treatment with an exercise program, including balance activities and postural control exercises, with visual feedback utilizing a mirror. On the other side, in [59] visual feedback manipulation is used in robotic therapies for hand rehabilitation. [60] presents another application of visual feedback training, related to the improvement of postural control in patients with chronic mechanical back pain. One important field where to use visual feedback is balance training. In [61] it is concluded that individuals with incomplete spinal cord injury improved substantially the balance performance while training using visual feedback. Finally, the results of the study done in [62] suggest that balance training with visual feedback, including weight-shifting tasks when standing, might be successfully used in children with hemiplegia as the training improved gait symmetry and the tasks that were practised during quiet and dynamical standing.

2.5 Summary

Although many publications describe effective body motion data collection systems that rely on various multi-modal sensors, most of the proposed hardware devices or tracking systems include sensor/peripheral interconnection cables, not always flexible, and other components that have to be worn. Because of this, such systems are usually not so comfortably or easily wearable and hamper the patient's movements, making them unsuitable for certain types of activities, such as the training programs in sports rehabilitation. While these inconveniences might be solved by some of the current commercial systems, their cost made them unavailable for many rehabilitation centres and home-based therapies. Moreover, none of the reported systems provide a complete solution, which includes both a sensing system with vision, and a motion data analysis platform for providing a feedback to the clinicians and the patient.

Chapter 3

Sensing system

Never mistake motion for action.

Ernest Hemingway

3.1 System development

As has been previously mentioned, one of the main aims of this thesis is to develop a system for human motion acquisition and tracking, in order to use it in physical rehabilitation therapies. From the study of the state of the art, it has been stated that, when designing a system of these characteristics, it is necessary to take into account several requirements, as low cost, reduced size and weight, and easy use, among others. Therefore, the research has been aimed at developing a wearable sensing system that is comfortable to wear, easy to use, apply and re-apply, as well as non-limiting for the body movements and acceptable to clinicians. Such a system has a wide range of applications in various fields. As a result, a prototypical system composed by wearable sensors and a vision device, which has the following features, is proposed:

- *Wireless communications*: the IEEE 802.15.4 standard is used to transfer the raw data from the sensors to the receiver.
- *Easy manipulation*: the sensors are easy to use and to apply and re-apply on the body using elastic bands.

- *Correctness of data*: the system represents the real situation with high measurement accuracy.
- *Operation*: an analysis of sensors' data can be performed to provide the patient with an immediate feedback.
- *Visual feedback*: the system performs video acquisition and provides, additionally to the sensor's data, a visual feedback to the patient.
- *Automation*: the system collects and stores the patient's motion data automatically.
- *Friendly Graphical User Interface (GUI)*: the system includes an intuitive and simple user interface that makes it easy to use and displays the graphs of the data that are being acquired in real time.
- *Portability*: the system components have limited size and weight, while being robust and allowing good mobility. This is particularly important, especially in the case of home-based therapies.

Figure 3.1 shows the architecture proposed for the system. It includes six low-cost universal modules, one acting as a master and five as slaves. Considering the great potential of inertial sensors, especially the accelerometers in this field, it was decided to design a system formed by small electronic boards including this kind of MEMS for tracking patients and monitoring their movements. In the scheme shown in Figure 3.1, the slave modules are used to monitor the patient's knees, being placed one above and one below each knee, while the fifth module is placed on the back waist of the patient, near the centre of mass, to provide additional information about the patient's movement. Thin elastic bands are used to fix them to the body for easy wearability. Thanks to the system's flexibility, any other part of the body, *e.g.*, the upper limbs, could be monitored just by changing the placement of the modules. The slave modules transmit their data wirelessly to the master module, whose main function is to keep the system synchronized while receiving the accelerometer data from the slaves and to store them into a computer or a monitoring station via a USB connection. The system is completed by using Kinect, the video device developed by Microsoft, which includes both a RGB camera and a depth sensor, to be used for providing visual feedback to the patient. A software application featuring a friendly

GUI to control the sensing system has also been developed and can run under both Windows and Linux.

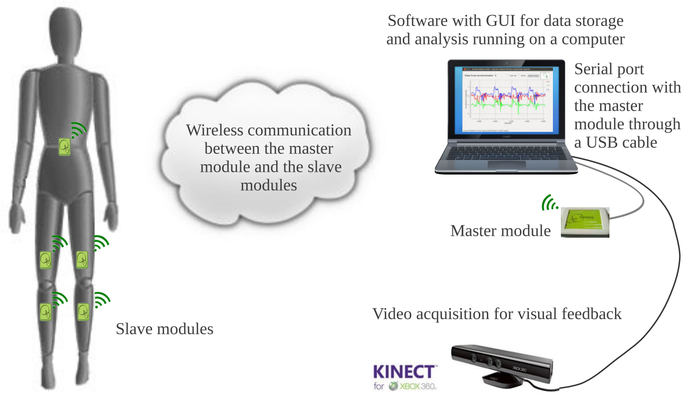

Figure 3.1: Proposed system architecture for human motion monitoring.

It must be pointed out that for establishing the requirements of the sensing system the Isokinetic Rehabilitation Centre of Milan [63] has collaborated allowing to meet their doctors and physiotherapists in order to know how to fulfil the specific field needs.

3.1.1 WiModule board

One of the products of Henesis S.r.l., the company with which collaboration this PhD thesis has been developed, is the WiModule, shown in Figure 3.2, a small low cost universal module that operates as a component of IEEE 802.15.4 wireless sensor networks and which contains a high-performance three-axial precision accelerometer [64]. It also includes digital buses and analog lines, allowing for future addition of new external sensors. Taking into consideration the requirements cited above, it was considered that using this board as the base of the architecture would allow to reach the proposed objectives.

The dimensions of the board are 60 $\times$ 39 $\times$ 11 mm, which makes it a small wearable module, as can be seen in Figure 3.3(a). Figure 3.3(b) shows how the electronic

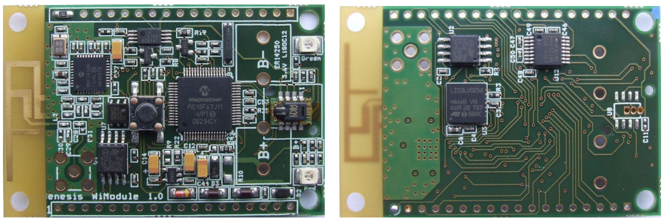

(a) Front side. (b) Rear side.

Figure 3.2: Henesis WiModule.

board has been packaged for applications in rehabilitation, in order to easily attach it to an elastic band using a rear clip. It should be noticed that all modules are based on the same hardware, and may be programmed to act either as master or slave.

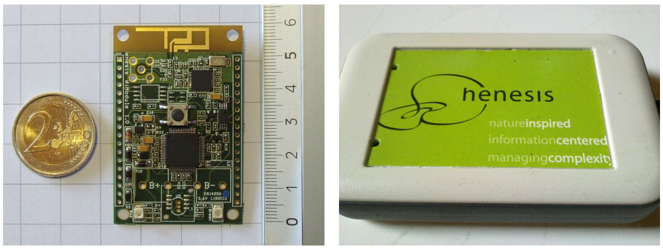

(a) Size comparison. (b) Example of packaging.

Figure 3.3: Details of the Henesis WiModule.

The components of the Henesis WiModule that are more relevant to this work are the high-performance three-axial accelerometer, a RF transceiver and an 8-bit PIC microcontroller. Programming correctly the device and interconnecting these components appropriately is critical for the final performance of the system. Figure 3.4 shows the generic architecture of the Henesis WiModule, with a basic interconnection between these three components.

The accelerometer used is the LIS3LV02DQ from ST Microelectronics [65]. It is a three-axial digital output low voltage linear accelerometer. It has a user selectable full scale of ± 2g / ± 6g and it is capable of measuring acceleration over a bandwidth of 640Hz for all axes. The small size and weight of its package make it ideal

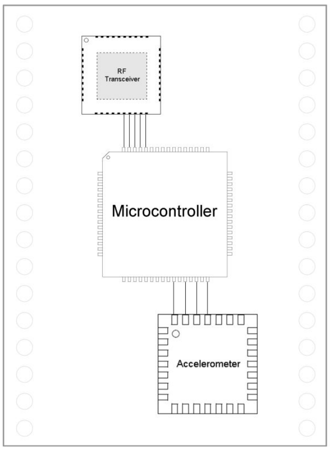

Figure 3.4: Generic architecture of the Henesis WiModule.

for handheld portable applications where size, weight and package performance are required.

It is important to know how acceleration is measured. The accelerometer provides the data using the g-force (gravitational force). One "g" is the acceleration due to gravity at the Earth's surface and it corresponds to the standard gravity (symbol: g_n), defined as $9.80665 m/s^2$. A three-axial accelerometer will output zero-g on all three axes if it is dropped or otherwise put into a ballistic trajectory, also known as an inertial trajectory, so that it experiences "free fall".

In Figure 3.5 the direction of the detectable accelerations is shown with respect to the encapsulated package, as provided by the manufacturer. These directions must be taken into account when interpreting the data that has been sampled. Each sample is composed by 6 bytes, *i.e.*, 2 bytes for each one of the three accelerometer axis: x, y and z.

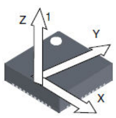

Figure 3.5: Direction of the detectable accelerations.

The RF transceiver used in the system is the MRF24J40 from Microchip [66]. Its main characteristics are the following ones:

- General features:
  - IEEE 802.15.4 2.4 GHz standard compliant RF transceiver.
  - Small, 40-Pin Leadless QFN 6×6 mm^2 package.
  - Integrated 20 MHz and 32.768 kHz crystal oscillator circuitry.
  - Supports ZigBee, MiWi, MiWi P2P and proprietary wireless networking protocols.
  - Low-current consumption: typical values of 19 mA in RX mode, 23 mA in TX and 2 μA in sleep mode.
- RF/Analog features:
  - ISM band 2.405-2.48 GHz operation.
  - Data rate: 250 kbps.
  - -95 dBm typical sensitivity with +5 dBm maximum input level.
  - +0 dBm typical output power with 36 dB TX power control range.
  - Differential RF input/output with integrated TX/RX switch.
- MAC/Baseband Features:
  - Hardware CSMA-CA (*Carrier Sense Multiple Access – Collision Avoidance*) mechanism, automatic acknowledgement response and FCS check.
  - Independent beacon, transmit and GTS FIFO.
  - Automatic packet retransmit capability.

Finally, the microcontroller mounted on the board corresponds to the Microchip PIC18F87J11 family [67]. Specifically, the PIC used is the 18F67J11, a 64-Pin TQFP, with the following characteristics:

- Device flash program memory: 128 kB.
- SRAM data memory: 3930 bytes.
- 29 interrupt sources.
- I/O ports: A, B, C, D, E, F, G.
- 10-bit Analog-to-Digital module: 11 input channels.
- 2 Capture/Compare/PWM modules.
- 3 Enhanced Capture/Compare/PWM modules.

- 2 MSSP for serial communications, with SPI and Master I^2C.
- 2 EUSART (Enhanced USART) for serial communications.
- 2 Comparators.
- 2 8-bit timers and 3 16-bit timers.
- No external bus.
- PMP/EPSP (Parallel Master Port/Enhanced Parallel Slave Port for parallel communications).

The power consumption of the Henesis WiModule specified on its datasheet is the following:

- 1 μA in sleep mode with external-trigger awakening.
- 19 μA in sleep mode with user-defined precise time awakening.
- 25 mA in active TX/RX modes.

The reported range of the wireless transmissions is up to 100 m outdoor, being in line-of-sight, and up to 20 m under typical indoor conditions.

3.1.2 Configuration of the system

The clock frequency of the system, for both the master and the slaves, has been set to the maximum allowed, *i.e.*, 32 MHz by using a 8 MHz oscillator and a Phase Lock Loop (PLL) frequency multiplier configured with a value of $4\times$.

A Transistor-Transistor Logic (TTL) level serial port is used for transmitting the data from the master module to the computer; its transfer rate has been set to a high value, 460,800 bauds. On the other side, for the communications with the console for debugging, the RS232 level serial port has been used. The console speed has been set to 19,200 bauds, although it has been tested that the maximum value that works is 576,000 bauds. Even if this is the maximum value, the most common programs do not allow to reach it, so the value of 19,200 bauds has been used for debugging.

The wireless communication section conforms the IEEE 802.15.4 standard [68]. It makes 16 channels available in the 2.4 GHz band, numbered from 11 to 26. Each of them has a bandwidth of 2 MHz and a channel separation of 5 MHz. Channel 26 was selected for the system's transmissions, as it is affected by fewer interferences than the others.

The accelerometer is capacitive since it guarantees higher stability than piezo-electric ones and it is therefore more suitable for measuring human motion [69]. According to the application's requirements and the clinicians' recommendations, 30 Hz is an adequate sampling rate. In fact, many of the products presented in [31] have this configuration. However, in order to have more data for posterior analysis, and considering the available bandwidth, a higher frequency of 160 Hz has been selected. The scale has been set to $\pm 6g$ as the results of the first tests demonstrated that the range $\pm 2g$ was not wide enough for measuring motion in activities like running. This can be considered an adequate configuration according to [70], where it is shown that, for assessing daily physical activity, accelerometers should be able to measure accelerations up to $\pm 6g$. At the same time, this configuration extends the range reported by similar systems for human activity recognition [32] and health monitoring [71].

Structure of the data packet

The structure of the data packet has been defined in compliance with the IEEE 802.15.4 standard. The latter defines four frame types, acknowledgement (ACK), data, beacon and MAC command frame, along with two modes of operation, beacon-enabled network (beacon-mode) or non-beacon-enabled network (non beacon-mode). In a beacon-enabled network, beacons are transmitted periodically by the Personal Area Network (PAN) coordinator and are mainly used to provide synchronization services between all the devices in the PAN. Instead, a network that is non-beacon-enabled does not transmit a beacon unless it receives a beacon request [66]. In order to have more flexibility in the design, it was chosen to define a proprietary wireless networking protocol using the non-beacon-enabled network and implementing later the beacon internally.

Figure 3.6 shows the structure of the data packet as provided to the transceiver of the module. The first byte indicates the packet length, including the header and the payload. The header length is 21 bytes: two bytes for the IEEE-compliant frame header that indicates, among other details, the type of packet; one byte for the sequence number; two bytes for the destination PAN; finally eight bytes for the destination address and eight more bytes for the source address.

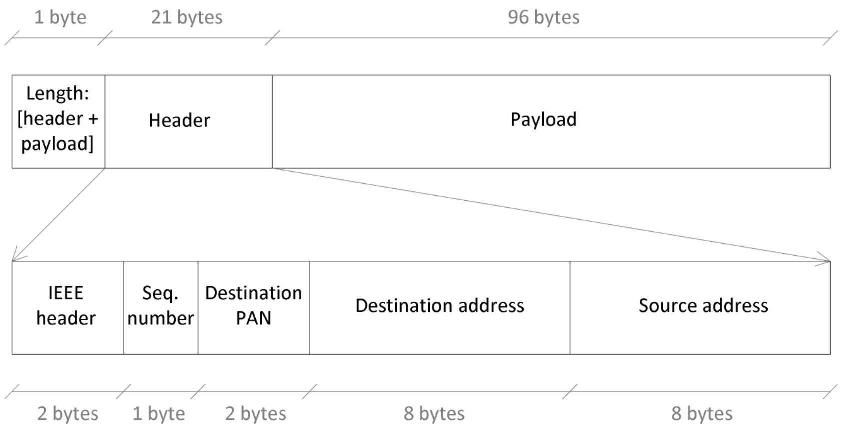

Figure 3.6: Structure of the data packet.

The payload includes sixteen samples of the accelerometer to take full advantage of the packet size (filling the payload as much as possible reduces the protocol overhead). Each accelerometer sample is formed by 6 bytes, two for each of the three accelerometer axes: x, y and z. Therefore, the payload length is 96 bytes, and the packet that reaches the transceiver is composed by a total of 118 bytes. The transceiver adds one byte at the beginning that specifies the header length, and two additional bytes at the end specifying the Frame Check Sequence (FCS) by using the Cyclic Redundancy Check (CRC). This final size of 121 bytes ensures the compliance with the IEEE 802.15.4 standard, which allows the payload of the MAC Protocol Data Unit (PDU) to be variable, with the limitation that a complete MAC frame cannot exceed 127 bytes. As mentioned previously, the beacon is implemented internally by using a MAC command frame (specified in the IEEE frame header) with no payload, having a size of 23 bytes. On the other hand, the ACK frame, which is sent automatically by the transceiver if requested, has a size of 5 bytes.

In the reception, the transceiver gets a packet with this structure plus 4 additional bytes at the end: two of them for the CRC, one for the Link Quality Indication (LQI), which is a characterization of strength or quality of a received packet, and the last one for the Received Signal Strength Indicator (RSSI).

3.1.3 Communication protocol

Taking the transmission medium into consideration, there would be high chances of losing packets or having collisions between them in the absence of a protocol that defines the system's behaviour. Bearing in mind the target application, it is very important that the monitoring station receives all slave boards' data packets and in the correct order. The custom communication protocol that has been designed, which follows a Time Division Multiple Access (TDMA) approach and where data is sent upon request, is described below. For better clarity, the diagram of the implemented protocol is shown in Figure 3.7.

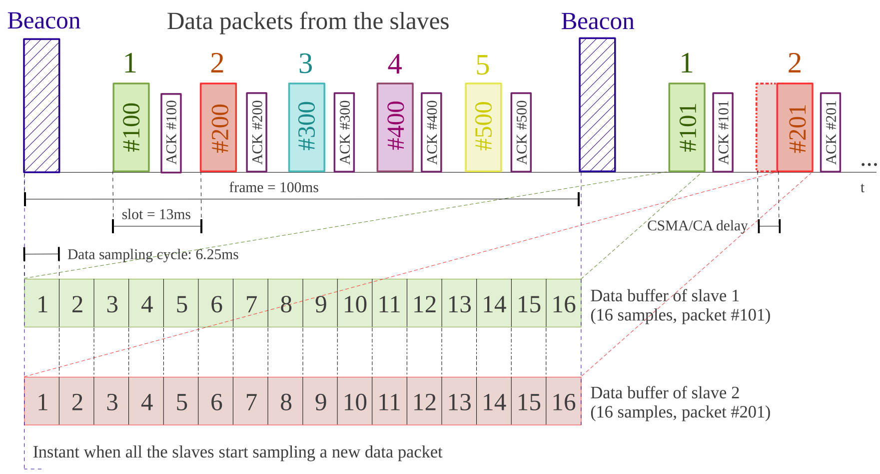

Figure 3.7: Communication protocol with data synchronization.

The synchronization between the different modules is one of the relevant features of the system, whose structure, based on distributed sensors for data acquisition, brings up to a design where no implicit synchronization of the sensor nodes is present, as all nodes have independent clock sources [72]. A traditional synchronization scheme such as the *Network Time Protocol* (NTP) cannot be used because it is not suitable for sensor networks due to computing limitations and energy issues [73]. The protocol developed and proposed here is inspired by the *Reference-Broadcast*

Synchronization (RBS), first published in [74]. As opposed to traditional protocols in which senders synchronize with receivers, in the RBS scheme nodes send reference beacons to their neighbours, synchronizing a set of receivers with one another. Its fundamental property is that this reference broadcast does not contain an explicit timestamp; instead, receivers use its arrival time as a point of reference for comparing their clocks. The protocol proposed in this thesis merges both strategies, using beacons for synchronizing implicitly the receivers among them and with the sender, the master module. It is therefore the master module the one in charge of sending the reference beacon to the slave modules. Unlike the RBS, in this proposal the receivers, *i.e.*, the slave modules, use the beacon arrival time not to compare or readjust their clocks, but to start sampling a new data packet synchronously. As mentioned before, the beacon mode is implemented internally, so the master board sends periodically a beacon packet to the slaves to request their accelerometer data. The period is mainly determined by the number of data samples included in a data packet. Considering that there are sixteen samples in the packet and that the sampling frequency has been set to 160 Hz, the beacon will be sent approximately every 100 ms, depending on the jitter of the system, which will require a later study [75]. It must be pointed out that both the master and the slaves use the same transmission channel. Their transceivers have reception filters set, so that the master receives only data packets addressed to it, and the slaves receive only command or ACK packets from the master.

The protocol described in Figure 3.7, represented also in Figure 3.8, operates as follows: the master board sends a beacon packet, which is received by all the slaves at the same time. At that moment, each slave gets ready to send its data packet and starts acquiring a new one. If all the slaves started transmitting their data packets when they receive the beacon, collisions would occur. To avoid this situation, a TDMA scheduling algorithm has been implemented to share the transmission medium in time, so each slave is assigned an ID number, which is used to distinguish and allocate them to a determined time slot to send their packets. During these time slots, the slaves send their data packets and wait till an ACK packet from the master is received. Having the ACK request configured allows to assure data reception and increases the robustness of the system. Another mechanism that has been implemented for this same reason is the Carrier Sense Multiple Access with Collision Avoidance (CSMA-CA), which avoids data collision when accessing the communication channel and improves communications reliability [76].

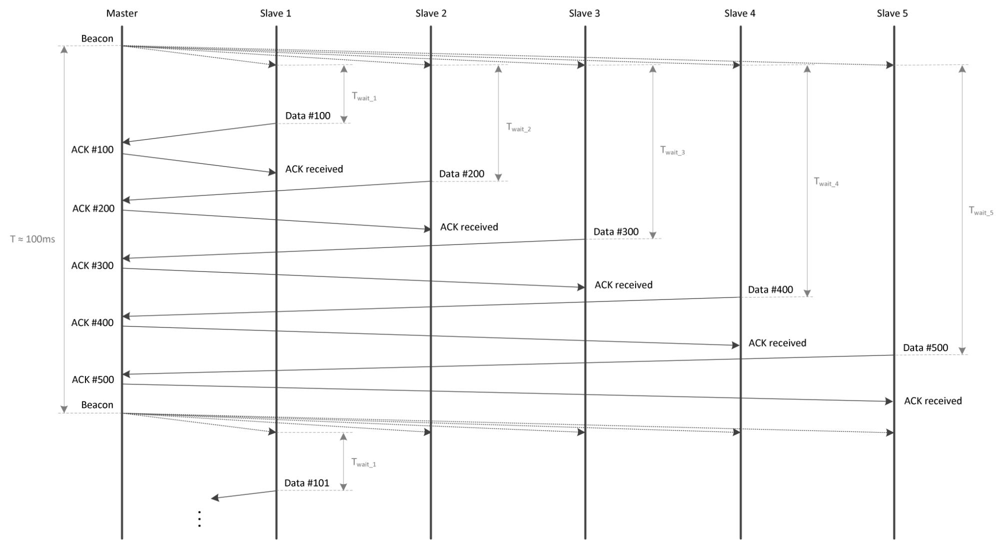

Figure 3.8: Communication protocol in normal conditions.

On the other side, when the master receives a data packet from a slave, it sends it the corresponding ACK packet and sends the data to the monitoring station through the serial port, so that the accelerometer samples are stored there. If the slave does not receive this ACK, it tries to send the same data packet for up to three trials, which is a native capability of the transceiver for packet retransmission. So, during the 100 ms interval between beacons (termed frame), each slave sends its data packet, waits for the ACK or retransmits the packet again if it has not been received. Anyway, to reach this stable situation, the system has to be synchronized first. For further comprehension, Figure 3.9 represents the communication considering just one slave module.

Two screenshoots of the 4-channels oscilloscope taken while testing the system are shown in Figure 3.10. In Figure 3.10(a), the master sends a beacon, represented as the rising edge which gets to the highest peak in yellow, and when the three slaves

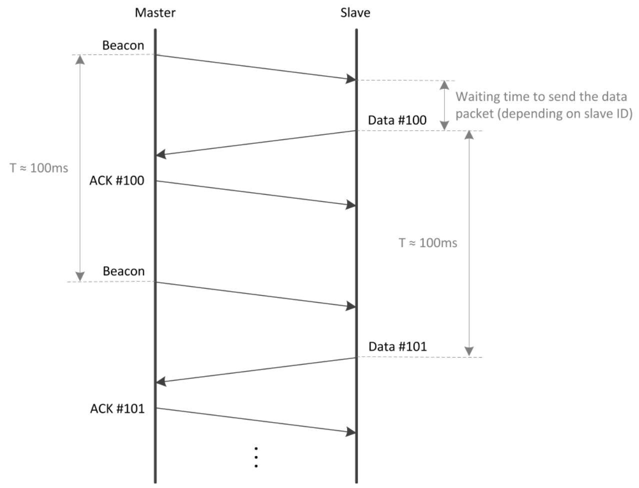

Figure 3.9: Communication protocol in a normal situation with one slave.

receive it (smaller rising edges), they wait a certain amount of time depending on their ID to send their data packets (corresponding falling edges), which, as can be seen, are equally spaced between them. Figure 3.10(b) represents the same situation with four slaves, and without the master, with more details.

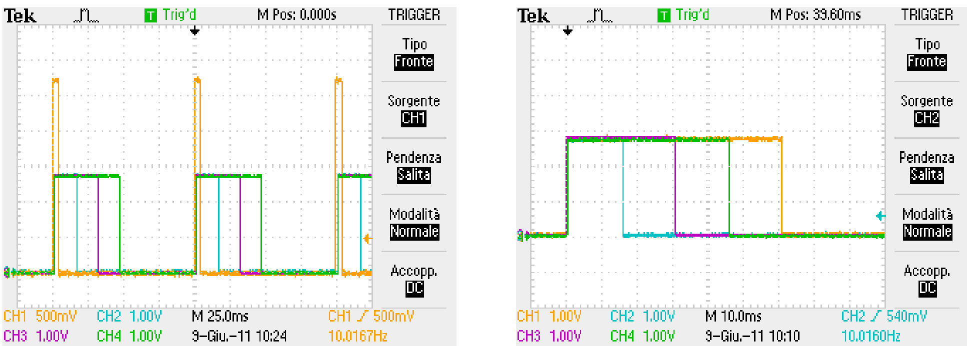

(a) Beacon and data packets.

(b) Synchronization of the slaves.

Figure 3.10: Beacon and data packets on the oscilloscope.

Master module synchronization

When the system is first powered, the master starts an internal synchronization process to set the ideal timing interval for sending the beacon packets. Initially this was done directly every time it acquired 16 samples from its own on-board accelerometer. However, this was not very precise and introduced an undesired deviation of the period (jitter) in the system. To reduce it, a different strategy was implemented. During synchronization, the master module calculates how much time it takes on average to fill a data packet by using the accelerometer Interrupt Service Routine (ISR). When this process finishes, it uses the value obtained to program a timer and enters the normal operation mode. The ISR of this timer is responsible for sending the beacon packet periodically. This strategy reduces the jitter in this part of the system, as the hardware used to generate the time base for the timer, a crystal quartz, is very precise. For a further explanation see Figure 3.11, where a comparison between both situations is shown. Figure 3.11(a) shows the beacon jitter when the packet has been sent after acquiring sixteen samples from the master board's accelerometer. On the other side, Figure 3.11(b) shows the jitter when the beacon is sent considering the timer set during the synchronization process.

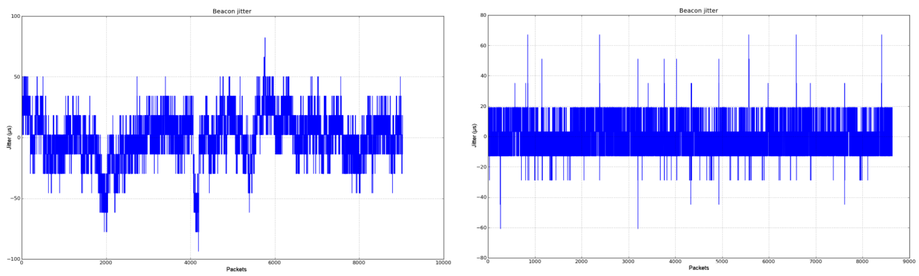

(a) Using accelerometer timing. (b) Using programmed timer.

Figure 3.11: Beacon jitter with two different configurations.

Table 3.1.3 shows the standard deviation of the jitter and its maximum value for both configurations. It can be observed that, when the programmed timer is used, the standard deviation is reduced by almost 50%.

Configuration	$jitter_{\sigma}$ (μs)	$jitter_{\max}$ (μs)
Using accelerometer timing	20.76	93.67
Using programmed timer	11.70	67.17

Table 3.1: Standard deviation and maximum value of the beacon jitter with two different configurations.

Slave modules synchronization and specific situations

On the slaves' side, when one receives a beacon packet for the first time, it also starts its own synchronization process, which is shown in Figure 3.12. This requires that a certain number of consecutive beacon packets are received, so that the slave can estimate the average time between them. When the required number of beacon packets is received, the synchronization process finishes and the calculated average is used for setting a timer to start saving the data acquired from the accelerometer. The main goal of this approach is to synchronize the instant when all slaves start sampling data for a new packet.

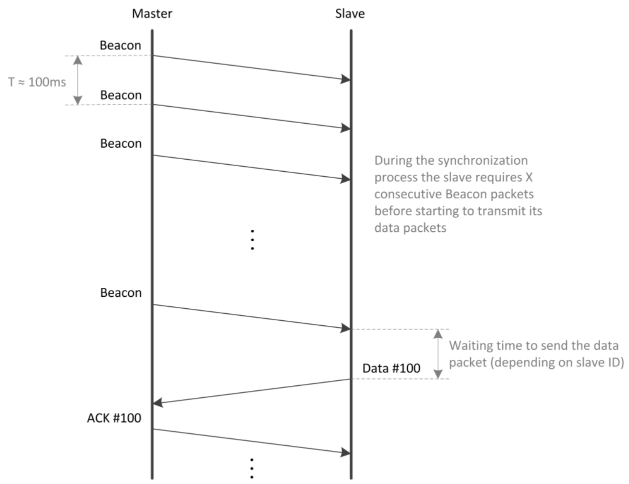

Figure 3.12: Communication protocol during the slave synchronization process.

The accelerometer ISR is programmed with high-priority to work independently, acquiring a sample every time one is ready, and keeping the mentioned timer in charge of copying the last sample acquired from the accelerometer into the data buffer. It is important to implement a buffering mechanism to avoid losing the samples that are to be sent with the next packet while transmitting the current one. To solve this problem, a double-buffer structure has been implemented, which makes it possible to use one buffer for sending a full packet while new data are being stored into the other buffer. To maintain data consistency it has also been specifically determined how to exchange the buffers. In this flow, the possible loss of beacon packets must also be checked. This is another task performed by the timer mentioned before. In case the beacon has been lost, or if there is an unexpectedly long delay, and the data buffer is full, this timer is responsible for exchanging the buffers and indicating that the packet is ready to be sent. If not, this is normally done by the transceiver routine when a beacon is received.

It is necessary to differentiate between the situations where a beacon is lost, but the master is still awake (and, therefore, keeps receiving and saving data), or when it has been powered off. To take this into account, the slaves feature an embedded energy-saving mechanism that allows them to keep on sending their data packets only until a threshold number of lost beacons is reached. If this happens, they enter into the synchronization mode again, which requires that they receive a certain number of beacons before they can start sending new data to the master.

If, instead, only one beacon has been lost, as shown in Figure 3.13, the slaves check that the beacon has not arrived when it should have, send directly the data packet that is ready and start sampling data for a new one. The possibility that the beacon arrives with a delay just after the data packet has been sent is also considered. In this case, and to maintain data synchronization, the samples that may have been acquired up to then are discarded, and the creation of a new packet is started.

On the other hand, in Figure 3.14 the protocol when several beacons are lost is shown. As has been said, this process continues till the maximum number of lost beacons is reached.

Regarding the situations in which a packet is retransmitted, this might happen because of two different events: the former occurs when the packet does not reach

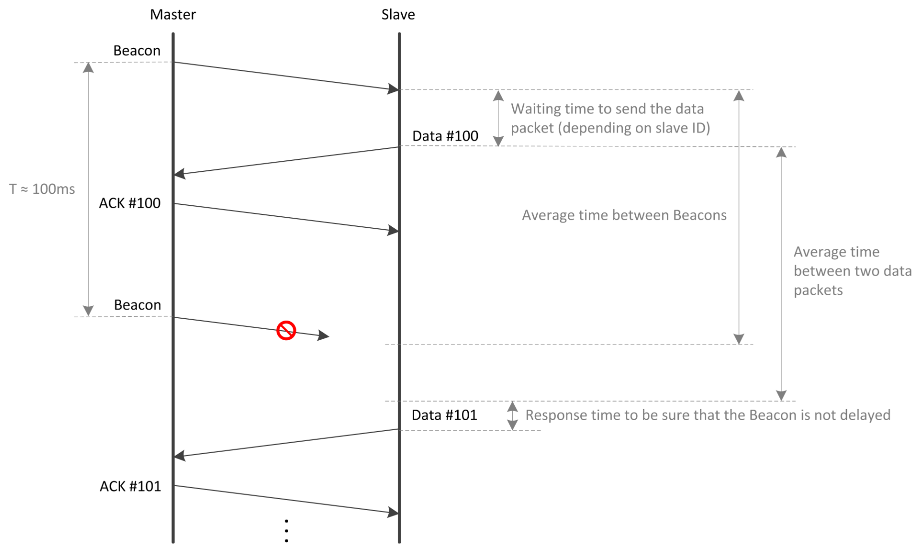

Figure 3.13: Communication protocol when a beacon is lost.

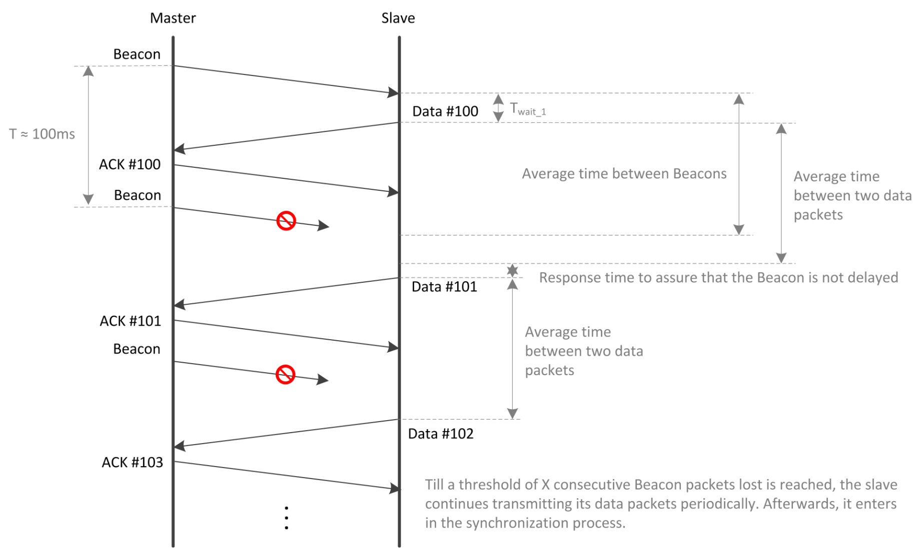

Figure 3.14: Communication protocol when several beacons are lost.

the master, as shown in Figure 3.15 while the latter occurs when the master receives the data packet, but the ACK is lost, as reflected in Figure 3.16. In both cases, which the slave cannot distinguish, it will retransmit the data packet.

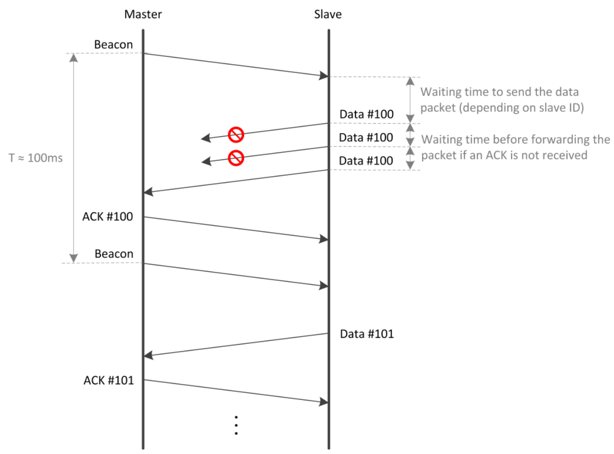

Figure 3.15: Communication protocol when a packet is lost.

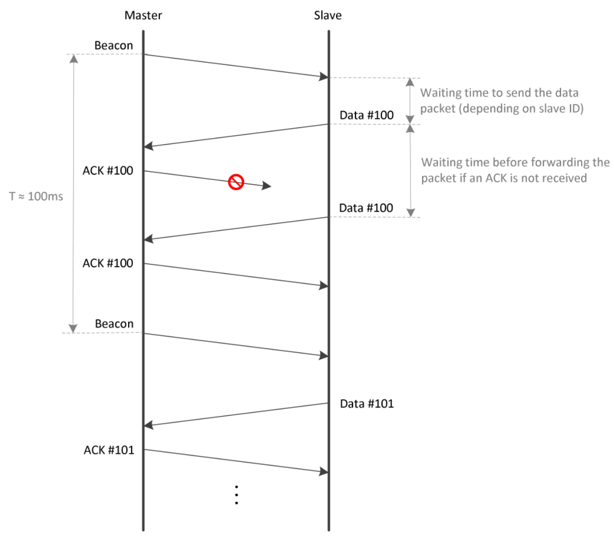

Figure 3.16: Communication protocol when an ACK is lost.

3.1.4 Data alignment

The previous section has explained how the communication of all the slave modules is synchronized and how the time is set when the sampling of a new data packet is started. The master module, just after receiving a data packet from a slave, transmits it to the monitoring station sequentially. In order to minimize the chances of transmission errors, or of an incorrect separation of a packet from the next one in the computer, start and stop delimiters are sent, too. Each of them is formed by 5 bytes and correspond to the sequences `TXSTR` and `TXEND`, respectively. The data contained in the packet is finally decoded and saved into the monitoring station. However, synchronization issues arise again when merging the data from different sensors. Different algorithms were designed but they all show situations in which their performance is not adequate. Finally, a robust algorithm, described in Algorithm 1, was designed and implemented in order to deal with all possible situations, as when beacon or data packets are lost, when a packet arrives with delay, or when a slave module is temporarily in synchronization mode. The main goal is to align the data from different accelerometers, to establish an exact correspondence between each of their packets. To facilitate the alignment task, every time a beacon is sent to the slave modules, the master device sends also a small packet to the computer through the serial port, which is detected thanks to the initial delimiter `TXMST`. This packet helps to divide the time into frames and to fuse the data of multiple sensors.

The combination of two different algorithms for time and data synchronization, named Multi-Data-Packaging and Slot-Data-Synchronization, is also used in the system-based design described in [77]. As their Slot-Data-Synchronization algorithm, the data alignment algorithm proposed here is implemented in the monitoring station. This choice allows to reduce the computational load of the master module while keeping the time synchronization through the beacon reference as its main task.

Algorithm 1 Data alignment.

```
Initialization;
while not at end of the received data do
  Read current packet;
  if it is a beacon then
    if previous frame is not completed then
      Set a missing packet for each slave that missed it;
    end if
    Start a new frame;
  else
    Extract the source (slave ID) and the sequence number;
    if received source != expected source then
      Set a missing packet for the expected source;
    end if
    if received sequence number != expected one then
      {At least one packet from this slave was lost before}
      Cancel the missing packet if the current frame has already been filled;
    else
      if the frame has just been filled then
        Cancel the missing packet as the right one has arrived late;
      end if
    end if
    if there is a new packet but its current frame has already been filled with real data
    then
      {The packet corresponds to a new frame}
      if previous frame is not completed then
        Set a missing packet for each slave that missed it;
      end if
      Start a new frame;
    end if
    Include the data packet in the frame and set it filled;
    Update the expected source and sequence number;
  end if
end while
```

3.1.5 Flowcharts

In this part, the flowcharts corresponding to the code developed both for the master and the slave modules are shown and explained.

Master device

As can be seen in Figure 3.17, the master board does not have a proper main function, which means that it is totally controlled by the programmed interrupts. After the configuration of the system, including the transceiver, timers, accelerometer and so on, it just updates the state of the green LED to show whether it is in the synchronization process or not.

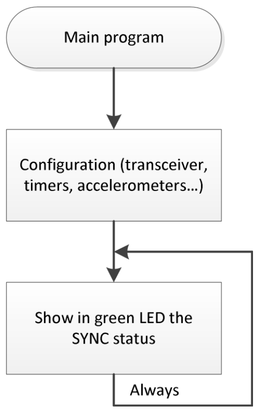

Figure 3.17: Master's main function.

Figure 3.18 shows how the transceiver interrupt service routine works. It is configured as a low-priority interrupt, as its frequency is not very high, because it just happens when a packet is received. When the system enters this routine, it first sets a variable to indicate that the transceiver is being used, so that other routines will not try to use it at the same time. Then, it checks if a packet has been received and, if this is the case, it gets the incoming packet and sends the data through the serial port. After finishing the transmission, the red LED blinks and the transceiver state is reset to "not in use".

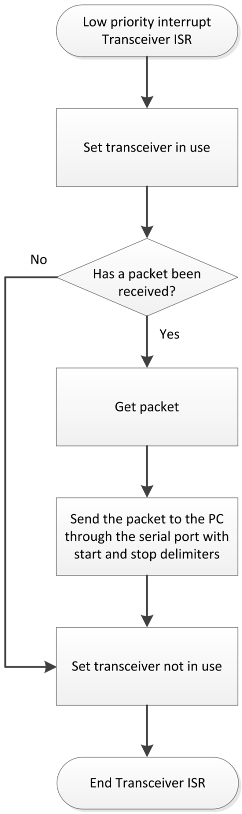

Figure 3.18: Master's transceiver function.

The accelerometer interrupt service routine, shown in Figure 3.19, is quite complex, as it controls the synchronization process. It is set as a high-priority interrupt, as the accelerometer sampling frequency is set to 160 Hz and, consequently, it will produce an interrupt every 6.25 ms, which is a high frequency, specially considering the frequencies of the other interrupts of the system. When the program enters the ISR, it is first checked if, considering the actual sample, the packet is full and the synchronization mode is ON. If they are not, then the sample from the accelerometer is read, which is a requirement of the sensor, even if afterwards it is not going to be used, and then the ISR finishes. In the other case, using the timer 0, the timing since the last sample is taken and it is reset again. This timing is used to update the average value of the time related to the acquisition of sixteen samples.

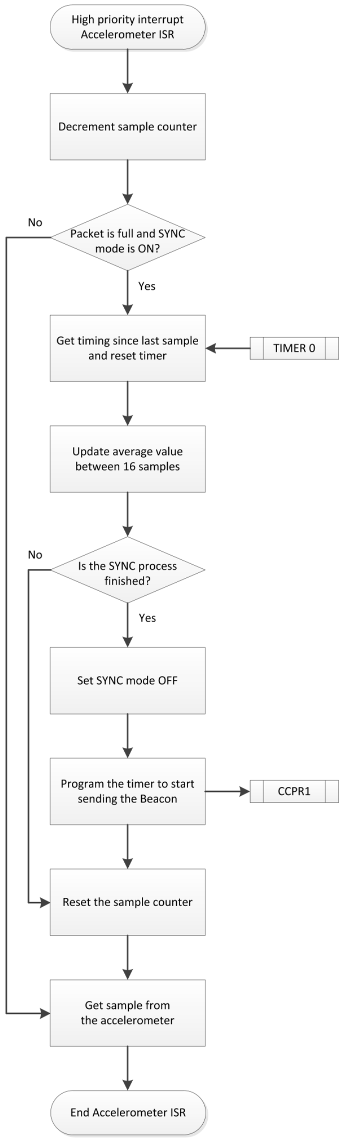

Figure 3.19: Master's accelerometer ISR.

If the synchronization process has finished after this step, the synchronization mode is set to OFF, and then the CCPR1 is programmed for sending the beacon packet. After that, or if the synchronization process has not finished, the sample counter is reset to start counting for sixteen new samples for the next packet.

The CCPR1 is a capture-and-compare timer which is used as a high-priority interrupt to count sixteen times in order to send the beacon packet to the slaves. Its period, 6.25 ms, is the reason why it has been configured as a high-priority interrupt –see Figure 3.20–.

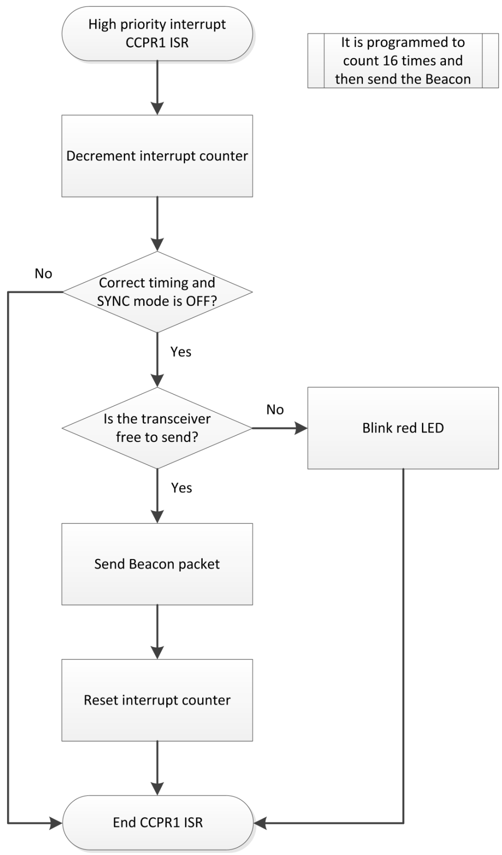

Figure 3.20: Master’s CCPR1 ISR.

On the other side, the timer 0 is used to count how many milliseconds are there between sixteen samples of the accelerometer during the synchronization process. In this case it has been configured as a low-priority interrupt, as can be seen in Figure 3.21.

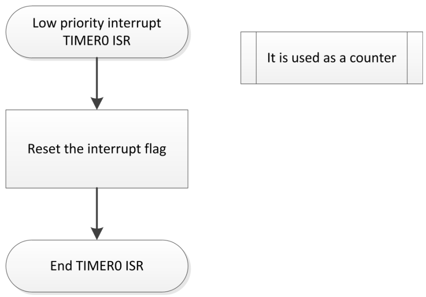

Figure 3.21: Master's timer 0 ISR.

Slave device

As shown in Figure 3.22, the main function of the slave also starts with the configuration of the different parts of the system: timers, accelerometer, etc. Then, it enters a loop waiting for the packet to be completed. Once it is filled with all the sixteen samples, it programs timer 3 in order to wait till its assigned time slot. At that moment, it encodes the data and sends the packet using the transceiver. When the slave is sending the packet, a variable indicates whether CSMA-CA is to be used or not, and the acknowledge for the packet is requested. In the main program, the state of the green LED is always updated to show if it is in the synchronization process or following the normal execution.

Figure 3.23 shows the RF transceiver ISR, which is configured as a low-priority interrupt, because it is supposed to be activated approximately every 100 ms, when receiving a beacon. As mentioned before, a reception filter has been configured at the transceiver in order to just receive the packets from the master module inside the defined PAN. In the ISR, when a beacon packet has been received, the time that has elapsed since the last beacon packet is saved using timer 0, whose ISR is shown in

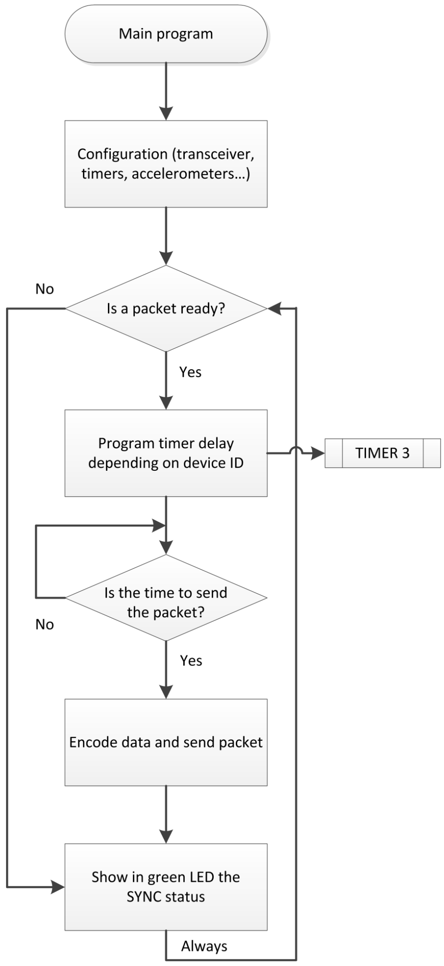

Figure 3.22: Slave's main function.

Figure 3.24. A variable is set to indicate that it has been received, so there can be a track of received beacons which can be used by the other ISRs. Then, it checks if a beacon has been lost immediately before. If there was not a lost beacon before, it updates the average value of the timing between beacon packets. If the synchronization mode is ON, the beacon counter is increased and it is checked if the threshold has been reached. In this case, the synchronization process has finished and the capture-

and-compare timer, CCPR1, is programmed to allow to start acquiring data from the accelerometer. In the case there was not a lost beacon before, it is checked again if the synchronization mode is ON. If it is not ON, *i.e.*, the system is in normal function, it is checked if the buffers need to switched, and it is set that the packet is ready to be sent. Then, the timer of CCPR1 is reset for the acquisition of the following samples. The next packet is started by saving the last sample acquired from the accelerometer on the buffer. Finally, a variable that indicates that a beacon has been lost is set to False and the ISR finishes.

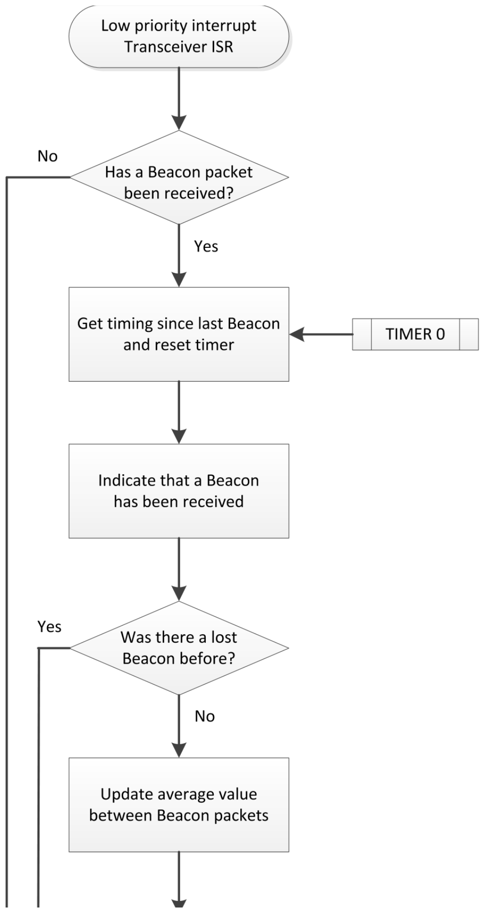

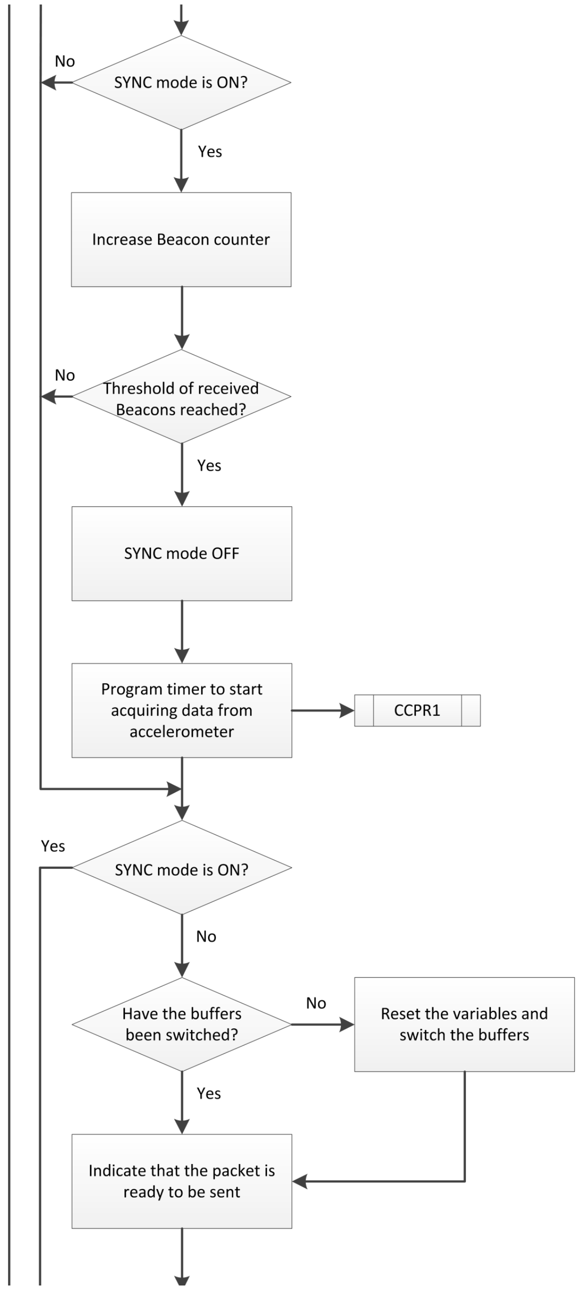
No
SYNC mode is ON?
Yes
Increase Beacon counter
No
Threshold of received Beacons reached?
Yes
SYNC mode OFF
Program timer to start acquiring data from accelerometer
CCPR1
Yes
SYNC mode is ON?
No
Have the buffers been switched?
No
Reset the variables and switch the buffers
Yes
Indicate that the packet is ready to be sent

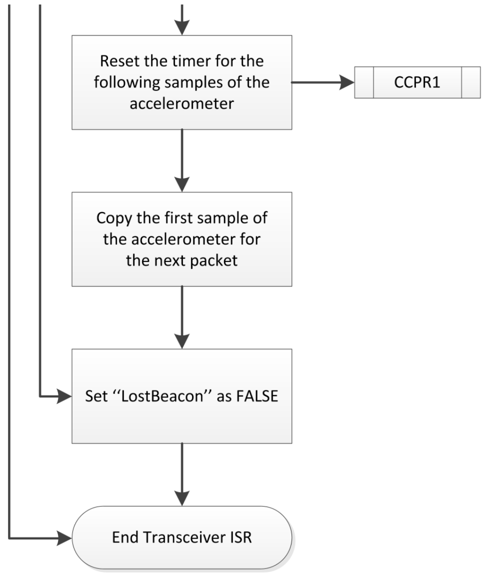

Figure 3.23: Slave's transceiver ISR.

The ISR corresponding to timer 0 is shown in Figure 3.24. As just said, it is used as a counter for lost beacons. It is also responsible for switching to the synchronization mode when the threshold established for lost beacons has been reached.

After switching to normal mode, CCPR1, whose ISR flowchart can be seen in Figure 3.25, is programmed with the average time that it takes to acquire two accelerometer samples and becomes active. When the program enters this ISR, defined as a high-priority interrupt, it updates the value of the timer and copies the last sample of the accelerometer in the buffer. In order to control the exchange of the data buffers, it checks if a beacon has just been lost or has not been received in time. And, in this case, if the packet has been completed, it is indicated that it is ready to be sent after exchanging the buffers.

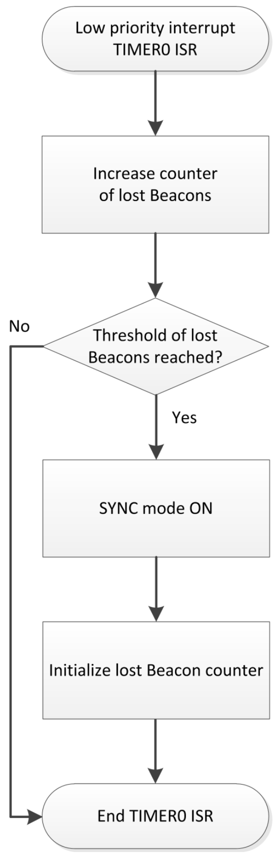

Figure 3.24: Slave's timer 0 ISR.

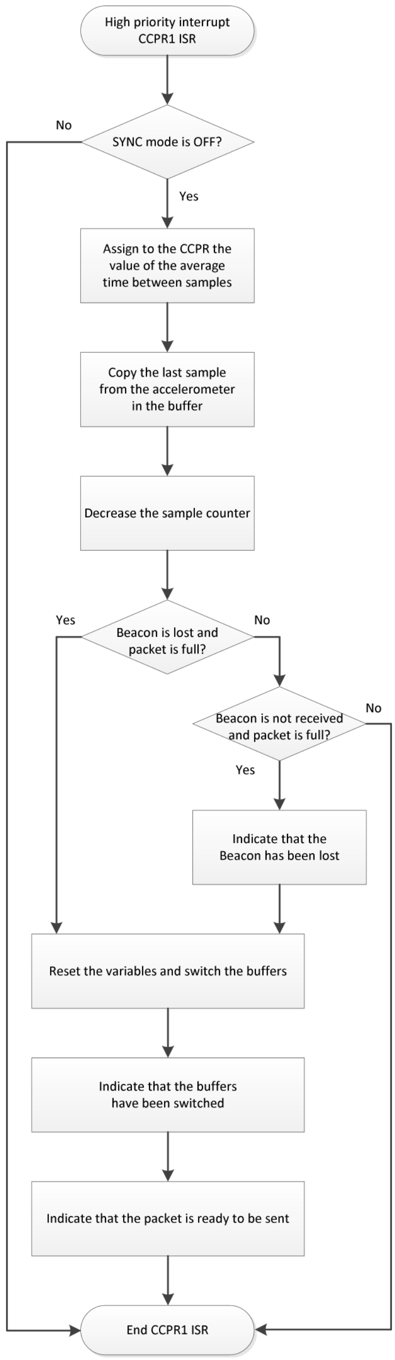

Figure 3.25: Slave's CCPR1 ISR.

Figure 3.26 corresponds to the accelerometer ISR, which just gets the sample from the accelerometer and saves it into a buffer. As the sampling frequency has been set to 160 Hz, this interrupt takes place every 6.25 ms, being defined as a high-priority interrupt.

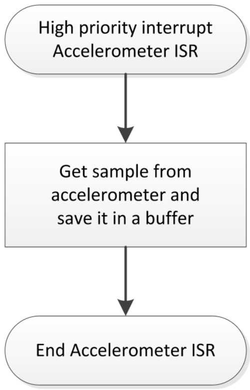

Figure 3.26: Slave's accelerometer ISR.

Timer 3 is used for each slave to know when to send its data packet after receiving the beacon. This time depends on its ID, so it is programmed differently for each slave. Its corresponding ISR is shown in Figure 3.27.

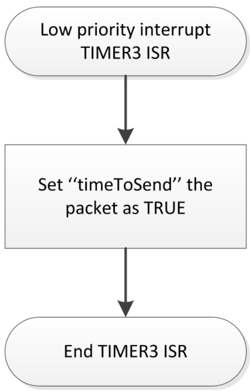

Figure 3.27: Slave's timer 3 ISR.

As the Henesis WiModule includes a push button, its functionality was implemented in the slaves as an ON/OFF button in order to save energy while the system is not being used. This was done by using the Port B Interrupt-On-Change, whose ISR is shown in Figure 3.28. The value of the port is masked in order to know if the button has been pressed or released. In case it has been pressed, it checks if the system is ON. If it is, it turns it OFF by disabling the interrupts of the transceiver, the accelerometer and the timers, and it puts the transceiver, the accelerometer and the microcontroller in sleep mode. If the system is OFF, the microcontroller is awaken automatically. It finishes turning the system ON completely by awaking the transceiver and the accelerometer, resetting the variables of the system to the initial state and enabling the corresponding interrupts.

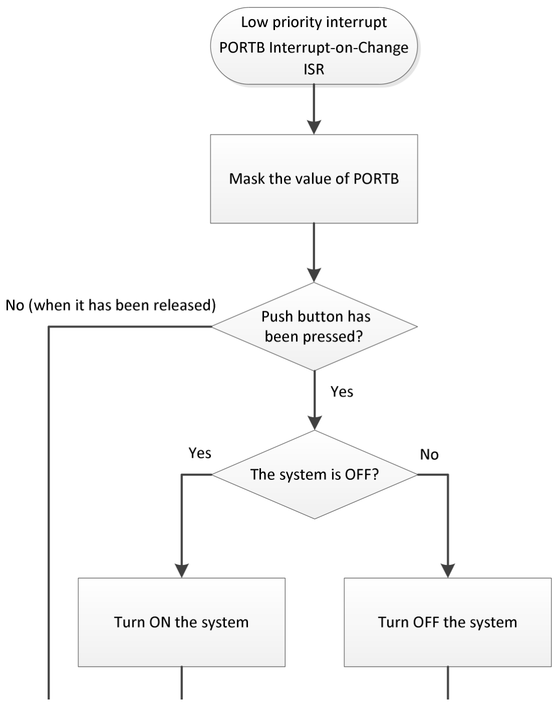

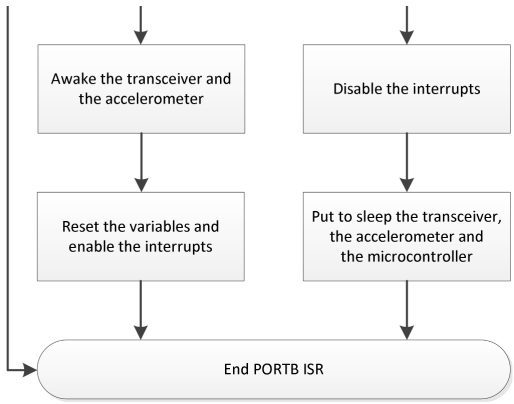

Figure 3.28: Slave's PORTB Interrupt-On-Change ISR.

3.1.6 Slave's batteries issues

K. Kunze, when giving an inspiring talk in the 3^{rd} PerAda Summer School on Adaptive Socio-technical Pervasive Systems about the work presented in [78], everyday activities recognition by using accelerometers, explained very clearly the problem of the batteries when using wearable sensors. In Figure 3.29 two real examples of his wearable system are shown. As can be seen, it includes, apart from several wires, a quite big module on the waist which contains the system's battery. The woman in the left is K. Kunze's grandmother. And, in his opinion, it was not acceptable that she had to wear such a heavy and big module for the power supply when performing the activities.

This has been taken into account when thinking about the design of the batteries in the system. At the beginning, small 3.6V Li-$SOCI^2$ disposable batteries were used, as shown in Figure 3.30(a). However, they have some main inconveniences: their size requires a bigger encapsulation module than expected, and the module has to be opened every time the batteries are discharged to replace them with new ones, so they are also not very environment-friendly. This is the reason why, afterwards, it was decided to use 3.6V Li-Ion rechargeable batteries. They are much lighter and thinner than the others, so they also allowed a smaller encapsulation, seen in Figure 3.30(b),

Figure 3.29: Real examples of a wearable system [78].

which is more comfortable to wear. To enable their recharge with a standard mobile phone charger, the board was modified to include a connector for it.

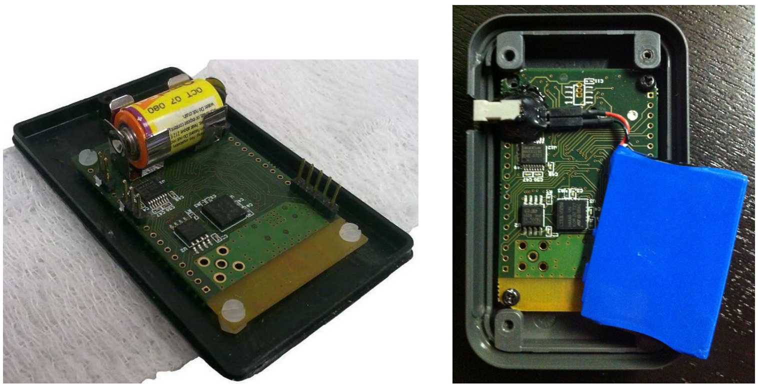

(a) Module with the 3.6V Li-SOCI^2 disposable battery.

(b) Module with the 3.6V Li-Ion rechargeable battery.

Figure 3.30: Modules with two different kinds of batteries.

3.1.7 Including vision

Due to the importance of visual feedback in rehabilitation therapies, already discussed in the previous chapter in Section 2.4, it was decided to add vision to the proposed system. This has been done by using Kinect, a motion sensing input device developed by Microsoft for the Xbox 360 video game console, which includes both a RGB camera and a depth sensor. The choice of using this device allowed to evaluate the present proposal, providing visual feedback within the suite, while maintaining a low-cost scheme.

Although instantaneous visual feedback may contribute to improved error reduction during task performance, it may be detrimental to learning, as subjects fail to attend to intrinsic information in favour of the more concrete external information [79]. For this reason, video is recorded during the exercise session, but it is provided to the subject afterwards.

Kinect calibration

Before proceeding to the video acquisition it is necessary to calibrate both cameras, the RGB and the depth one, in order to enable a mapping between their outputs. This calibration aims to improve the one provided by the device firmware.

The RGB camera intrinsics are calibrated using standard chessboard recognition, as shown in Figure 3.31. In order to get a good calibration it is necessary to move the chessboard around in the camera frame, especially checking for coverage of the corners and edges of the field of view, detecting the chessboard at various angles with respect to the camera, filling the entire field of view and tilted to the left, right, top and bottom. On the other hand, to calibrate the depth camera intrinsics, the corners of the chessboard on the depth images are extracted manually and saved. Finally, this is also done on the colour images so that a standard stereo calibration can be performed.

Limitations

Initially, it was considered that Kinect could support the calibration of the wearable sensors with respect to their position on the body, by recognizing a pattern, a small

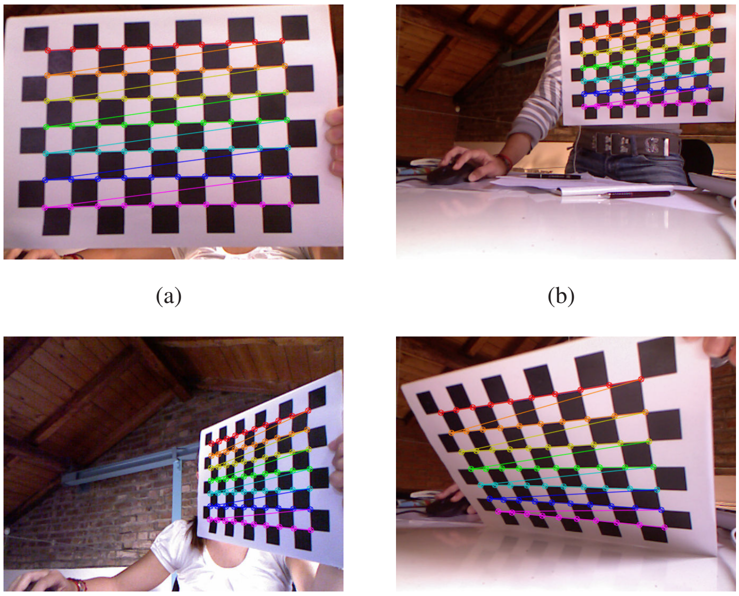

(a) (b)

(c) (d)

Figure 3.31: Calibration process for Kinect RGB camera intrinsics.

chessboard, attached to the front part of the modules packaging. Several dimensions of chessboard were tested, as shown in Table 3.2. The second chessboard, with larger edge length, was the one which gave better results.

Chessboard ID	**Squares**	**Internal corners**	**Edge length**
1	5×3	4×2	1.05 cm
2	5×3	4×2	1.50 cm
3	6×4	5×3	0.75 cm
4	7×4	6×3	0.90 cm
5	7×4	6×3	0.95 cm
6	10×6	9×5	0.50 cm

Table 3.2: Modules calibration chessboards.

Figure 3.32 shows how the module with the chessboard on it appears both on the colour and the depth views. Also, it shows how it was recognized on the window "Result". Several algorithms were tested for detecting the pattern, using the Harris corner detection and Hough transform for line detection, among other techniques. However, the tests made it clear that Kinect was not appropriate for calibrating the position of the on-body sensors. This limitation was due to the size of the pattern, which could not be increased due to the packaging size, and the distance needed between the Kinect device and the user in order to cover all the scene while the subject is performing the exercises.

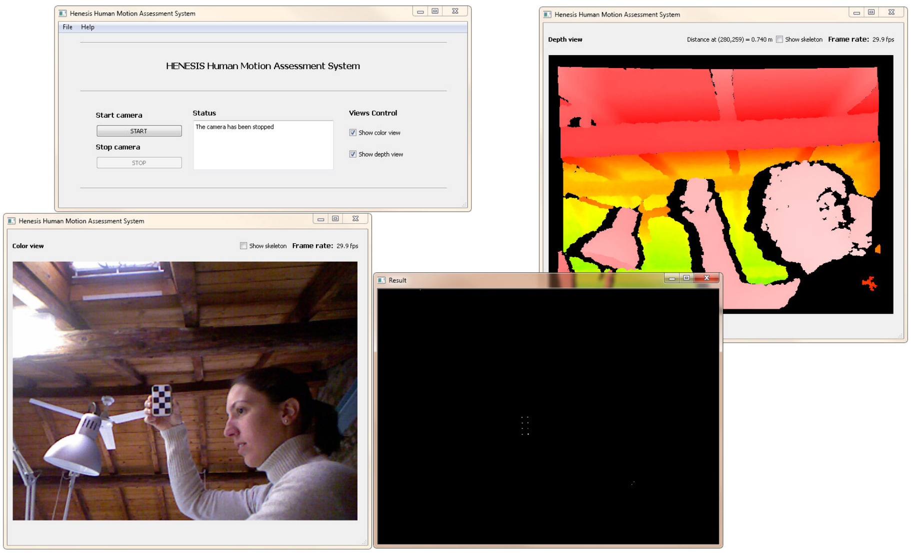

Figure 3.32: Using Kinect to identify a pattern on the sensors.

Another feature that was tested was the skeleton tracking, as shown in Figure 3.33, but it brought up several problems, not just in case of truncation and occlusion, but also due to the required distance between the subject and the camera (between 1.5 m and 2.0 m) and because the system did not show as much accuracy as required. For example, from the leg, the following joints can be obtained: hip, knee and ankle. If the lengths of the two segments of the leg (upper and lower part) are extracted from these points, their values vary in the centimetre range while the subject is moving, which is not adequate for the application considered.

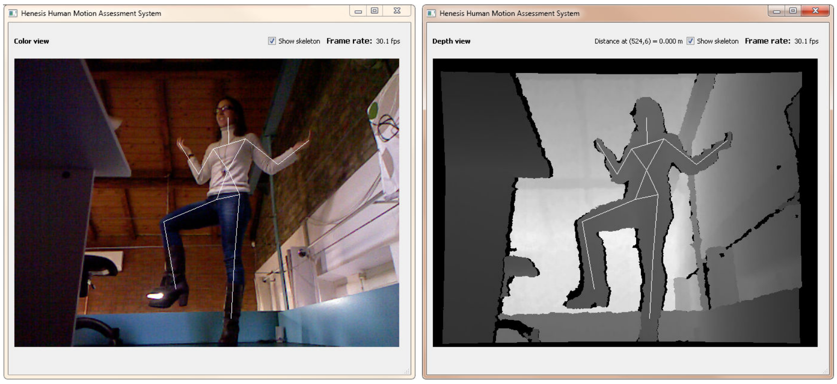

Figure 3.33: Skeleton tracking.

3.2 Graphical User Interface

A GUI (Graphical User Interface) has been developed in order to facilitate the use the system, especially considering that it has been conceived to be used by doctors and physiotherapists or directly by patients performing home-based rehabilitation therapy. This GUI can run under both Windows and Linux.

The main windows of the GUI are shown in Figure 3.34. Figure 3.34(a) represents the part concerning the accelerometer sensor system. In the upper part of the window, the type of experiment can be selected among several tags as running or jumping. The central part allows to start or stop the acquisition and includes a status window to inform the user about the task that is currently being developed. Below, the displays indicate the accelerometers that are active at each moment. The lowest part is composed by the plotting controls, that allow the user to show the graph with the data that is being acquired at the moment, clear it, or reproduce the last session. Figure 3.34(b) shows the window which allows to manage the Kinect device, including the views control, for both the colour and the depth cameras.

It is also possible to show independently any other saved accelerometer data session or to obtain the statistics of a session in terms of lost and forwarded packets,

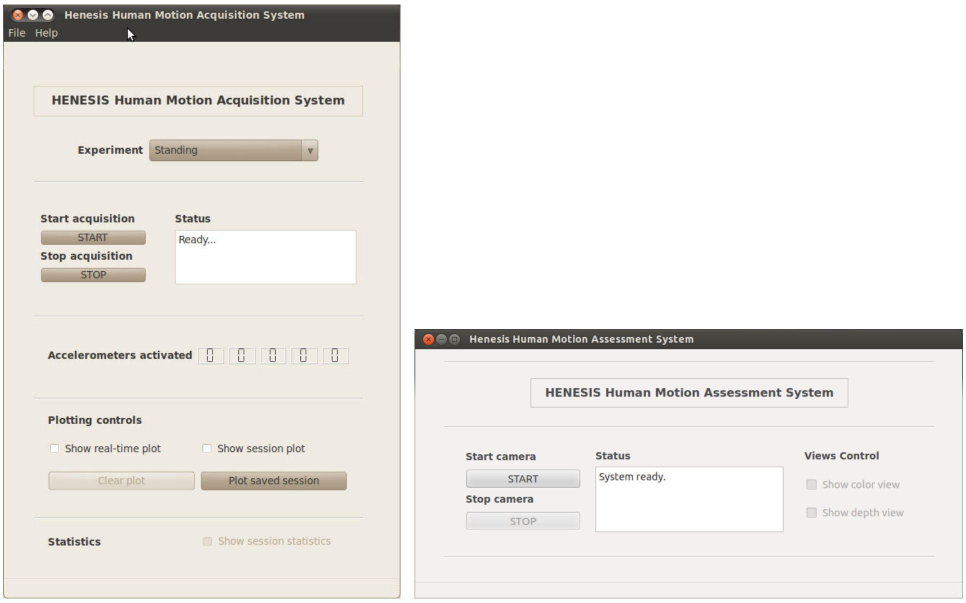

(a) Window for the accelerometer system. (b) Window for Kinect.

Figure 3.34: Main windows of the GUI.

as shown in Figure 3.35, to perform the calibration or a basic data analysis, among other options.

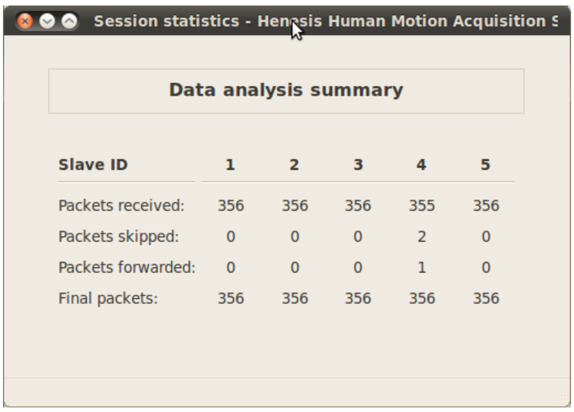

Figure 3.35: Window with the session statistics.

The accelerometer data are shown in separated windows, one for each of the sensors. The plot corresponding to one of them is shown in Figure 3.36, with a graph where the three axes are represented, with the samples in the x axis and the amplitude, the acceleration measured in g, in the y axis. In the upper right corner of the window there is a zoom button, which allows to perform both zoom in and zoom out. It is also possible to reset the zoom to get back to the initial state of the graph, or move it: *panning movement*. One interesting feature is that the system allows to synchronize the plots of all the accelerometers. So, if one selects the check box "Sync all", any zoom or panning that is made in one of the plots will be replicated on the other ones. This is of particular interest when representing in detail a certain temporal window in a session.

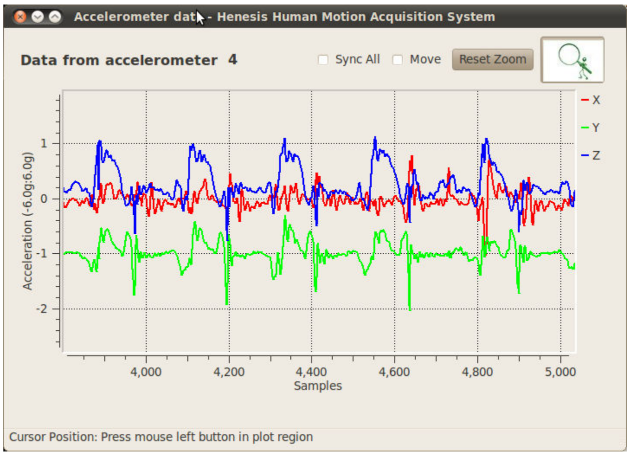

Figure 3.36: Plotting window of a single accelerometer sensor.

3.2.1 Calibration

The GUI includes a menu that controls the calibration of the sensors position. To proceed with the calibration process, it asks the user to pose for some seconds in four different pre-established postures. Considering how the accelerometer is mounted –see in Figure 3.37 the coordinate system of the accelerometer with respect to the human body reference axes– the system has the raw values of every axis and accelerometer in those postures saved internally.

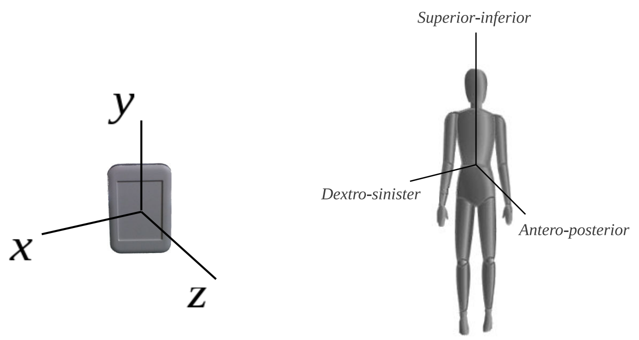

(a) Sensor coordinate system.

(b) Human body reference axes.

Figure 3.37: Coordinate reference system.

After the acquisition, the results obtained are compared with the expected ones. This information can be used to determine the position of the accelerometers when being worn and to correct it, if necessary, before starting the exercises. Figure 3.38 shows the window for the system calibration, after finishing this procedure.

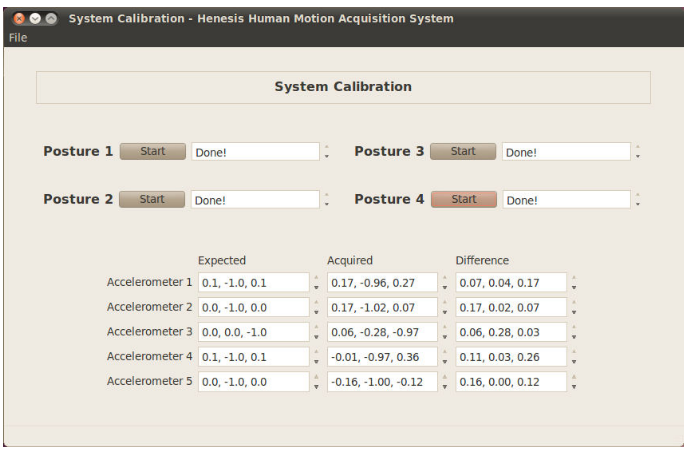

Figure 3.38: Calibration window for the sensors.

Figure 3.39 shows the window that controls the calibration of the Kinect device, which offers the possibility to load a file with the data from a previously performed calibration.

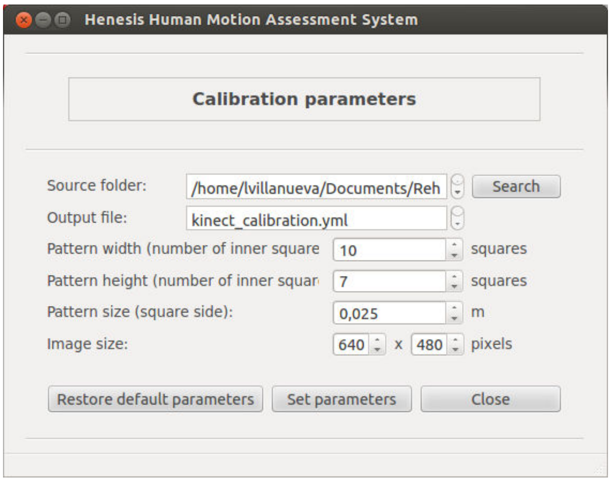

Figure 3.39: Calibration window for Kinect.

3.3 System validation

During the development of the system, before getting to the final version, it was necessary to start testing and validating it in order to know if more modifications on the architecture or the configuration were needed, or to choose the best approach among different possibilities. This is the reason why here the results are presented separately for two different configurations of the system. At the beginning, it was formed just by four slaves instead of five, placed on the legs of the patient, and its performance was tested with this configuration. The results obtained in this case allowed to decide a particular feature of the system configuration, that is, if the slaves should implement the Carrier Sense Multiple Access with Collision Avoidance (CSMA-CA) mechanism or not. This mechanism avoids data collision when accessing the communication channel and improves communications reliability [76]. This first version of the system, which is described in detail below, has been published in [80], while the final version including the five slave modules has been published in [81].

The validation process takes mainly into account three different aspects: data synchronization, data loss and jitter. As pointed out before, synchronization is a key aspect of the proposed system for later data analysis. To assess it, the so called "wooden bar experiment" was performed. The slave boards were fixed next to each other on a wooden bar with the purpose of assuring rigid mechanical connection. Afterwards, the bar was hit with a hammer with the aim to simulate a δ impulse. The main goal was to detect the start of the vibration produced by the hammer and check that it was consistently sensed by all modules. In Figure 3.40 the setup of the experiment can be seen.

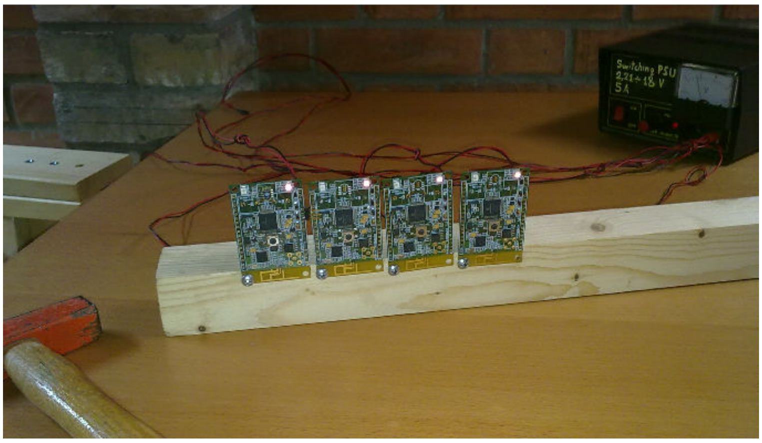

Figure 3.40: Experiment setup to check data synchronization.

Another important factor to be studied during the experiments was the number of lost packets, which corresponds to the number of time intervals with no data when reconstructing a sequence. As has been said, to assure the best performance of the system, in its first version, with four slaves, the experiments were performed with and without CSMA-CA in order to later choose the best configuration based on the experimental results.

The other experiments were focused on the data packets transmission for measuring the time jitter, both with and without CSMA-CA in the first version. While for the first two aspects, data synchronization and data loss, the analysis considered the information stored in the computer by the master board containing all the data packets received from the slaves, for the jitter measurements the data were analysed from a different point of view, by using an external device, a packet sniffer, which is illustrated below. Using this double-check mechanism gives the possibility of acquiring data from different sources and therefore using more available information about the system performance.

The ZENA tool, shown in Figure 3.41, is a wireless network analyser that graphically displays wireless network traffic following the IEEE 802.15.4 specifications on the 2.4GHz band [82]. In this case, it has been used for a non beacon-enabled network, as explained in Section 3.1.2. Zena uses a USB mini-B cable to connect to the PC and to power it, while a PCB trace antenna receives the packets on a specified channel and sends the information over the USB to the PC.

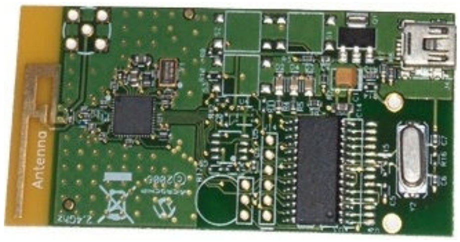

Figure 3.41: Zena Analyser from Microchip.

Figure 3.42 shows the standard scenario seen with Zena's GUI. The first packet corresponds to the beacon, which is sent in order to let the slaves to start sending their data packets and to start acquiring and creating a new packet. Afterwards, each slave sends its own data packet and receives the corresponding ACK from the master. At the end of the process, a new beacon is sent.

After performing an experiment, the data can be saved with Zena, that creates a binary file with extension `.zna`. For later analysis it was necessary to write a small script to read the data and transform it into a file with the information organized as shown in Figure 3.43 (it represents the same situation shown before in Figure 3.42).

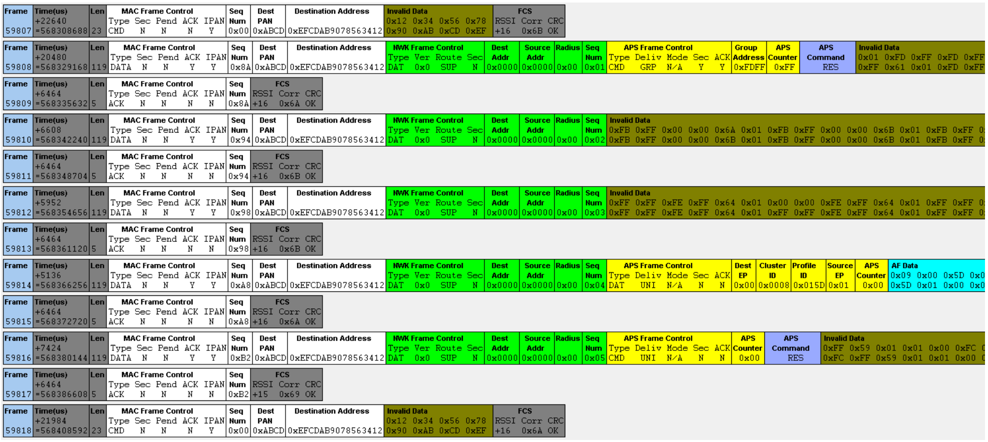

Figure 3.42: Scenario represented by Zena.

Frame	Time (us)	Type	Seq number	Source
1	454304	1	0	0
2	474464	2	31	1
3	480928	0	31	0
4	487008	2	4	2
5	493472	0	4	0
6	500416	2	61	3
7	506880	0	61	0
8	511520	2	51	4
9	518000	0	51	0
10	526432	2	35	5
11	532896	0	35	0
12	555504	1	0	0

Figure 3.43: File with Zena's information decoded.

Zena assigns a frame number to the packets in order of arrival. The time, in μs, is the absolute time of arrival of a packet. The type of packet is an internal parameter that has been set during the development for differentiating between the beacon (type 1), a data packet (type 2) and an ACK (type 3). The sequence number corresponds to the one encoded by the board when it sent the packet. In case of a beacon, it is always 0, the data packets have the sequence number set by the slave when sending them, and the ACK has always the sequence number corresponding to the data packet which is being acknowledged. Finally, the source permits to identify unequivocally each board. Number 0 corresponds to the master, and the numbers from 1 to 5 define each slave ID. Once the information from Zena has been decoded as explained, it is analysed to get the timing measurements.

3.3.1 Tests performed using four slave modules

This section includes the tests performed in the previous phase using four slave modules. These preliminary tests allowed to check how the system performs using CSMA-CA and without it. Considering the target application and the kind and duration of the exercises that are performed in a rehabilitation centre, the experiments carried out for data acquisition had a duration of 15 minutes, which corresponds to the transmission of approximately 100,000 packets, considering beacon, ACK and data packets.

Data synchronization

After performing the "wooden bar experiment", the data was plotted and analysed. The data sequence in Figure 3.44 –just the z axis, for the sake of clarity– shows the beginning of the vibration produced by the hammer, sampled by all slave boards at the same time. It was also checked that the maximum de-synchronization among the four modules was one data sample, *i.e.*, 6.25 ms.

Data loss

To assess data loss and timing measurements ten experiments have been performed, five with each configuration, with and without CSMA-CA. The statistics are calculated taking into consideration all the data available. For example, in the case of the lost packets, the average of all data received from all the slaves in all the experiments was computed.

The statistics about data loss for each type of configuration are shown in Table 3.3. They were measured by counting the time slots skipped, considering them as

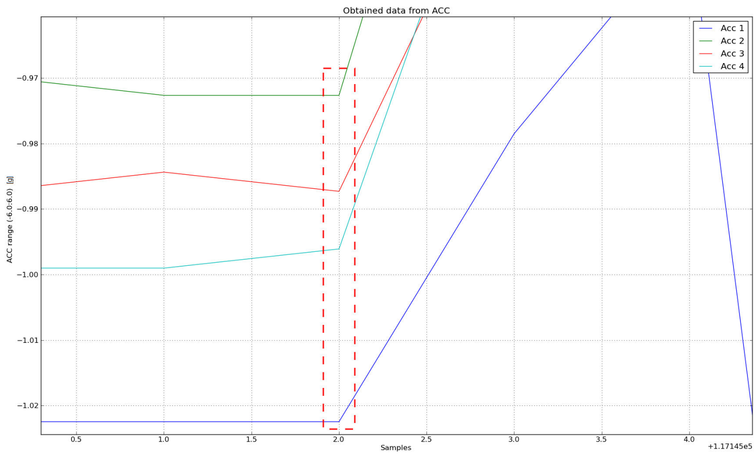

Figure 3.44: Zero sample difference with 4 slaves.

lost data packets, as there is a missing sample at a certain moment which cannot be recovered. Comparing both cases, it can be seen that using CSMA-CA reduces drastically the amount of lost packets, therefore helping to increase the system robustness.

Statistic	Without CSMA-CA	With CSMA-CA
Average	0.12%	0.00%
Median	0.00%	0.00%
σ	0.23%	0.00%

Table 3.3: Lost packets.

Timing measurements

The last experiments were focused on studying the performance of the data transmission in the network.

Average time between packets Table 3.4 shows the statistics related to the measurement of the timing between packets. In particular, for the master, the timings related to the beacon are shown, while for the slaves the one corresponding to their data packets. As before, the results are shown for both configurations, using CSMA-CA and not using it. The columns of the table display the average time between packets for each module and the corresponding standard deviation. The rows indicate the statistic used for all of the experiments.

Board	**Statistic**	**Without CSMA-CA**		**With CSMA-CA**	
		Δ_{packet} (μs)	σ_{packet} (μs)	Δ_{packet} (μs)	σ_{packet} (μs)
Master	*Average*	99918.61	12.74	99929.44	13.02
	Median	99919.44	12.74	99924.57	13.25
	σ	7.77	0.46	11.14	0.38
Slaves	*Average*	99900.45	461.17	99926.51	1059.14
	Median	99914.01	313.95	99923.85	1049.28
	σ	46.71	399.57	10.94	23.46

Table 3.4: Average time between packets.

To make things clearer, it is necessary to provide an explanation: for each experiment and for each slave, the average time and the standard deviation between the data packets corresponding to that slave were calculated. Afterwards, considering the results obtained by the other slaves the average, the median and the standard deviation of those values were calculated and shown in the table.

As can be seen in Table 3.4, the master does not show any significant difference between the two type of experiments. This was expected, as these configurations were applied to the slaves and do not influence the master's performance. On the other hand, for the slaves, it is seen that, while the average time between packets does not show a big difference, the standard deviation increments when using CSMA-CA. Both for the master and for the slaves, the average time between packets is approximately 100 ms, which corresponds to the acquisition of sixteen samples from the accelerometer, that is, the number of samples included in a data packet.

Jitter measurements The time jitter of the beacon and data packets, both with and without CSMA-CA, was also measured. The measurements are shown in Table 3.5.

The average jitter is zero, which means that, in general, the packets were sent when expected. $jitter_{\sigma}$ represents the deviation from the expected value of the timing between the packets, while $jitter_{\max}$ corresponds to the maximum jitter. Both data help to infer the minimum possible duration of a time slot and, hence, the maximum number of slaves in the system. Allowing for a wide safety margin (the maximum jitter plus two times the standard deviation), that is having a time slot of approximately 13 ms, sets the maximum number of slaves that can be included in the system to five, as proposed. It can also be seen that the jitter is minimal in the case of the master, which validates the choice made for its configuration when sending the beacon packet.

Board	**Statistic**	**Without CSMA-CA**		**With CSMA-CA**	
		σ_{jitter} (%)	$jitter_{\mathbf{max}}$ (%)	σ_{jitter} (%)	$jitter_{\mathbf{max}}$ (%)
Master	*Average*	0.01	0.08	0.01	0.08
	Median	0.01	0.08	0.01	0.08
	σ	0.00	0.01	0.00	0.01
Slaves	*Average*	0.41	9.70	1.05	8.65
	Median	0.40	8.69	1.05	7.79
	σ	0.27	6.43	0.02	3.87

Table 3.5: Jitter measurements.

Figures 3.45(a) and 3.45(b) show a comparison between two different configurations for the transmission from the slaves to the master, with respect to the use of the CSMA-CA technique. Figure 3.45(a) shows the data jitter with the first configuration. In this case, the standard deviation of the jitter is 1017.37 μs while the maximum is up to 7284.86 μs. On the other side, Figure 3.45(b) shows the data jitter when not using CSMA-CA. Due to the direct implications of this approach, the standard deviation of the jitter is reduced to 149.78 μs, while the maximum jitter is still quite high, 6403.69 μs.

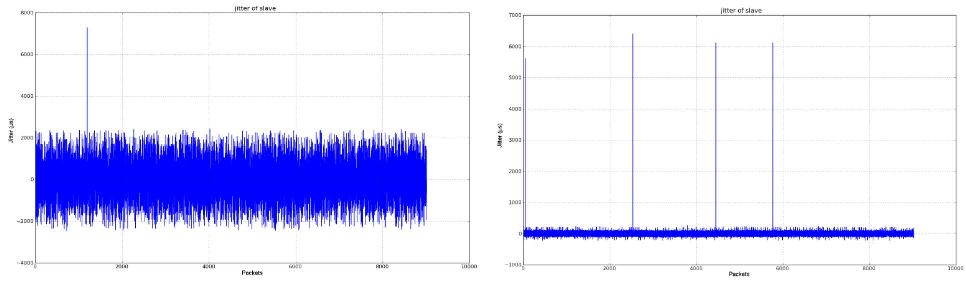

(a) Using CSMA-CA.

(b) Not using CSMA-CA.

Figure 3.45: Data jitter with two different configurations.

Evaluation of the results

A considerable amount of results has been presented with different kind of statistics for both methods, using CSMA-CA or not using it. However, for helping to decide which system configuration is best, the Wilcoxon signed-rank test has been applied [83]. It is a non-parametric statistical hypothesis test that permits to compare two related samples or repeated measurements on a single sample to assess whether their population medians differ. It does not assume that the population is normally distributed, as the paired Student's t-test does.

It has been applied to the maximum jitter and its standard deviation, to select the method with the smallest ones. The test has been performed with a typical significance level $\alpha = 0.05$ and for the null hypothesis "the median difference between pairs of observations is zero". The Wilcoxon signed-rank test returns a p-value, a probability, which is compared with α in order to see if the null hypothesis is to be rejected. The results are shown in Table 3.6. The null hypothesis was not rejected, as expected, for the master. This happens because the choice of the slaves configuration does not affect its performance. In the case of the slaves, the null hypothesis has neither been rejected for the maximum jitter, *i.e.*, it does not matter which method is used because the difference between them is not significant. However, it was rejected for the standard deviation of the jitter.

To decide which method is the best, it is necessary to check the medians of the

	Board	p-value	Rejection of the null hypothesis
$jitter_{\mathbf{max}}$	**Master**	6.25e^{-1}	0
	Slaves	6.27e^{-1}	0
σ_{jitter}	**Master**	1.88e^{-1}	0
	Slaves	2.19e^{-4}	1

Table 3.6: Applying Wilcoxon signed-rank test.

standard deviation, which have already been shown in Table 3.5. For the sake of clarity, only these values of interest are shown again in Table 3.7. As can be seen, the lowest median corresponds to the configuration without using CSMA-CA. This means that when not using it in the communication protocol, the packets would be placed more precisely in their time slot. However, it also has to be considered that, since the approach followed in the communication protocol consists in dividing the time in slots, so that each slave knows exactly when to send its packet, it is not expected that the channel is occupied in that moment. Even if this is not relevant for data synchronization, which is governed by the master's beacon, it could be interesting in other schemes, fitting more slaves in the configuration but getting worse data loss statistics.

	Without CSMA-CA	With CSMA-CA
Median of σ_{jitter} (%)	0.40	1.05

Table 3.7: Comparison of the median of the standard deviation of the jitter.

Taken into account the results related to data loss, shown in Table 3.3, it must be pointed out that when using CSMA-CA there were no lost packets. And, as pointed out before, it is very important for this application to receive all of the data packets, or at least, as many as possible. For this main reason, in order to assure data correctness, the configuration with CSMA-CA was selected to be used in the communication protocol.

3.3.2 Final results using five slave modules

Once the system was developed to its final configuration, using five slave modules, it was necessary to repeat the test sessions in order to verify its performance. The assessment of the communication performance takes into account four different aspects: data synchronization, data loss, timing measurements and battery life. As in the previous part, the experiments carried out for data acquisition to assess data loss and timing measurements had a duration of 15 minutes.

Data synchronization

Figure 3.46 shows the accelerations along the y axis of the five slave modules, for the sake of clarity, acquired while performing the "wooden bar experiment". The *peaks* on the data correspond to the moments in which the bar was hit with the hammer with the aim to create these δ impulses.

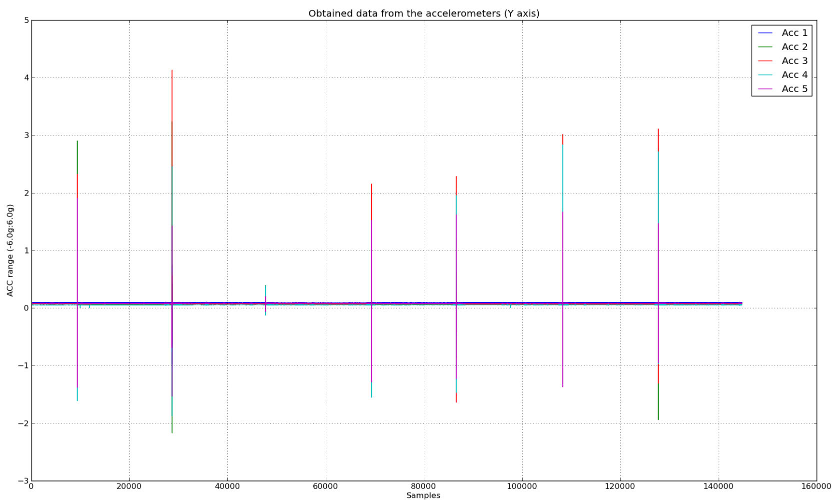

Figure 3.46: Data of the whole experiment for the synchronization test.

Figure 3.47(a) shows the data when zooming into one of these peaks. It can be seen see that the beginning of the impulse is sampled simultaneously by all the accelerometers. The maximum de-synchronization among the modules corresponds to two data samples, *i.e.*, 12.5 ms, as shown in Figure 3.47(b). This was expected since the accelerometer sampling process relies on its own internal clock, which cannot be synchronized with the board's clock signal. This result represents an improvement with respect to the maximum error for data synchronization of a similar system made up of three sensors, proposed in [77], which was 24 ms.

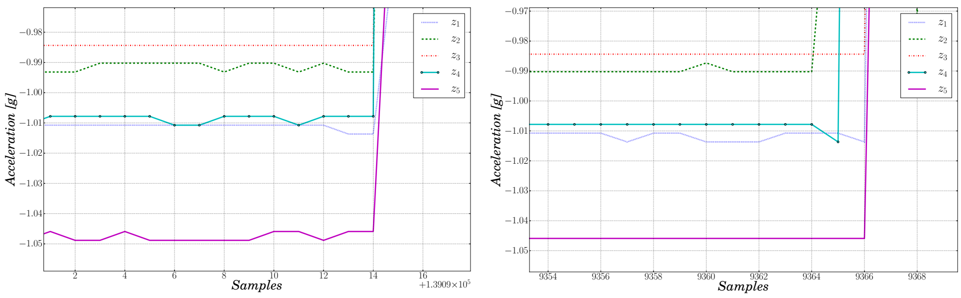

(a) Best case: perfect synchronization.

(b) Worst case: de-synchronization of two data samples.

Figure 3.47: Zoom of the data for the synchronization test.

Data loss

Table 3.8 shows the performance related to data loss (average, median and standard deviation) in two different environments, considering both ideal conditions in the lab (15 experiments) and real experiments while wearing the sensors (48 acquisitions from 10 different people). Although the number of lost packets increases in free-living environments, the high sampling frequency used allows to interpolate the missing information in the monitoring station without any noticeable degradation in the signal.

Timing measurements

The last results are focused on the study of the performance of the data transmission in the network.

Environment	Statistic	Lost packets
Lab-controlled	*Average*	0.000 %
	Median	0.000 %
	σ	0.001 %
Free-living	*Average*	3.160 %
	Median	3.380 %
	σ	1.580 %

Table 3.8: Performance related to data loss in the final system.

Average time between packets Table 3.9 shows the experimental results corresponding to the time between packets, beacon in the case of the master, and data packets in the case of the slaves. As can be seen, the average time is approximately 100 ms and the standard deviation has minimum values for the master board and acceptable ones for the slaves having the CSMA-CA configuration.

Board	Statistic	Δ_{packet} (μs)	σ_{packet} (μs)
Master	*Average*	101203.33	12.58
	Median	101202.32	12.61
	σ	5.57	0.40
Slaves	*Average*	101196.89	1101.80
	Median	101199.25	1079.73
	σ	11.94	75.09

Table 3.9: Average time between packets in the final system.

Jitter measurements Finally, Table 3.10 shows the results of the jitter measurements. The experimental values obtained confirm the ones calculated previously for the initial system with four slaves. It should be mentioned that using the CSMA-CA mechanism slightly increases the jitter on the slaves, as explained in [80], while, on the other hand, it reduces data loss significantly.

Board	Statistic	σ_{jitter} (%)	$jitter_{\mathbf{max}}$ (%)
Master	*Average*	0.01	0.07
	Median	0.01	0.08
	σ	0.00	0.01
Slaves	*Average*	1.09	8.56
	Median	1.07	8.83
	σ	0.07	2.65

Table 3.10: Jitter measurements in the final system.

Battery life

The battery life of the 3.6V Li-Ion rechargeable batteries used in the slave modules was also tested. Experiments have shown that they allow up to 12 hours of continuous operation, which is adequate for daily monitoring, improving additionally the 3-4 hours of operating time reported by [9, 47, 48, 49].

3.3.3 Use of the proposed system

The prototypical hardware setup corresponding to the accelerometer sensing system is shown in Figure 3.48. In the upper part of the image, there are the five slaves to be worn (as can be seen, in one of them there is a clip in the back part of the package that permits to attach the module to the elastic band shown below) and the master module, which is the one with the USB connection cable.

The size of the master module, once it has been packaged, is 90 $\times$ 55 $\times$ 22 mm, while the size of the slave modules is 84 $\times$ 52 $\times$ 16 mm. The package chosen for the slave modules made it possible to include light 3.6 V lithium ion rechargeable batteries, making them small self-powered and comfortably wearable modules. The weight of the slave modules, including battery, is 60 g. This solution overcomes the inconvenience of other systems, which require wearing a larger additional module on the waist containing the battery as well as several wires connected to the sensors, as described in [78]. This approach is also used in the commercial sys-

Figure 3.48: Hardware corresponding to the accelerometer sensing system.

tem described in [9]. The Xbus Master is a portable device, worn on the waist, which connects up to 10 inertial sensors and supplies power to them. Its size is $110 \times 150 \times 40$ mm and its weight is 330 g, including batteries. On the other hand, this scheme allows the sensors to be smaller ($38 \times 53 \times 21$ mm) and lighter (30 g).

The images in Figure 3.49 show a person wearing the slave modules as proposed in Figure 3.1. The IDs of the sensors help to place them always in the same position of the body, which is very important for data analysis. Sensor 1 is placed in the upper part of the right leg, while sensor 2 is placed below the knee. Sensor 3 is placed above the knee of the left leg and sensor 4 below it. As an example, Figure 3.50 shows the GUI with the graph of the waveforms corresponding to the three axes of the four modules on the legs, acquired while the subject was walking: one can see that there is a pattern in the movement performed, as expected.

On the other hand, Figure 3.51 shows the computer with the whole system acquiring data while a person is performing an exercise. On right part of the monitor there is the window corresponding to the accelerometer acquisition, where it can be seen

(a) (b)

Figure 3.49: Subject wearing the sensors.

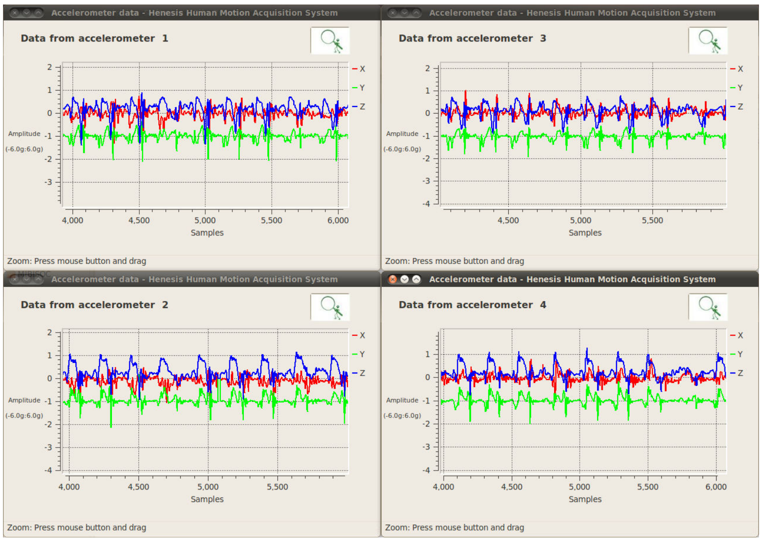

Figure 3.50: Plot of the four slaves on the legs while walking.

that all five sensors are active. On the left part, it is shown that Kinect is also capturing the scene for providing afterwards a visual feedback. The figures shown in this section demonstrate the use of the system in a real environment, the wireless connectivity between the slaves and the master module and how this kind of sensors makes it possible to capture body motion while Kinect is acquiring simultaneously the scene while the subject is performing an exercise, so that both sources of data can afterwards be analysed together.

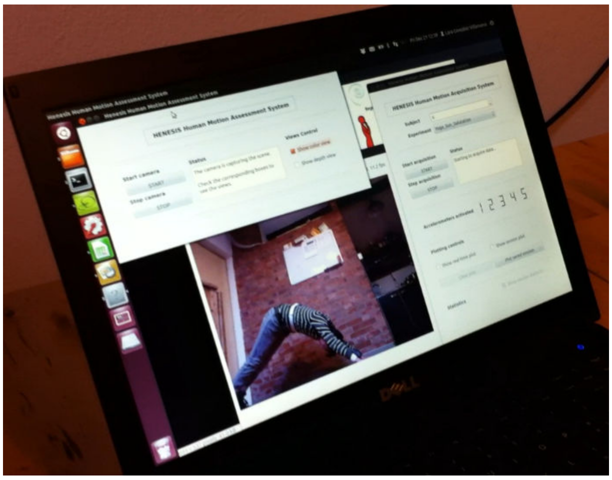

Figure 3.51: Computer display while the system is acquiring data.

Validation of the system for classification

The aim of this experiment was to demonstrate that the data obtained from the proposed system were meaningful. One person was asked to wear the slave modules as shown in Figure 3.49 and perform three different activities for 45 minutes: standing, sitting and walking. The acquired data was then separated into a training and a test set (60% and 40%, respectively). Afterwards, various classifiers were trained with the corresponding training set. Weka [84], a collection of machine learning algorithms for data mining tasks, was chosen for the analysis of the data. The supervised methods selected for validating the system are: *J48*, a decision tree classifier [85], *SMO* (Sequential Minimal Optimization), a non-probabilistic linear binary classifier [86], and a probabilistic classifier, *Naive Bayes* [87]. All the classifiers implement a supervised learning algorithm. In this technique, the training samples are formed by the input data and their labels, that must be associated to them. When analysing these data, the algorithm deduces a function which allows it to correctly determine afterwards the class labels corresponding to unseen instances.

It was necessary to take into account the system altogether, so the information obtained, without being pre-processed, was considered as a whole, *i.e.*, the classifiers were fed with all 15 channels, 3 axes for each of the 5 accelerometers, at the same time. The data saved in the computer by the master was transformed to the format required by Weka, `.arff` files. with information organized as indicated in Figure 3.52, where only one sample of the data is shown, for simplicity.

The results on the test set (over a total of 52,616 instances) are shown in Table 3.11. They demonstrate that the data obtained by the different sensors are meaningful and can be effectively used for activity classification.

Combining the system with EEG

Many of everyday human works and actions are considered voluntary. There are evidences from Electroencephalography (EEG) data which show that the human brain is active even before the beginning of the voluntary movement. One of the changes seen in these data preceding human voluntary movement is a cortical potential called Readiness Potential (RP). Detection of this potential can benefit researchers in clinical neurosciences for rehabilitation of malfunctioning brain and those working on brain computer interfacing to develop a suitable mechanism to detect the intention of movement.

The objective of the research published in [88] is to determine whether this brain potential exists in single trials of the EEG. With that aim an experiment setup was designed including the necessary software and hardware to evoke the RP in EEG of the subjects. In this experiment, the subjects were asked to move their hands and press a button on the pad whenever they wanted; no specific cues were given and the subject had complete freedom for the movement time. After data acquisition, first,

```
@relation 'Accelerometer_data_for_training'

@attribute source_1 numeric
@attribute x_axis_1 numeric
@attribute y_axis_1 numeric
@attribute z_axis_1 numeric
@attribute source_2 numeric
@attribute x_axis_2 numeric
@attribute y_axis_2 numeric
@attribute z_axis_2 numeric
@attribute source_3 numeric
@attribute x_axis_3 numeric
@attribute y_axis_3 numeric
@attribute z_axis_3 numeric
@attribute source_4 numeric
@attribute x_axis_4 numeric
@attribute y_axis_4 numeric
@attribute z_axis_4 numeric
@attribute source_5 numeric
@attribute x_axis_5 numeric
@attribute y_axis_5 numeric
@attribute z_axis_5 numeric

@attribute activity {Sitting,Standing,Walking}

@data
1,0.087890625,-0.3896484375,-0.9404296875,
2,-0.12890625,-1.001953125,0.140625,
3,0.0,-0.41015625,-0.9052734375,
4,0.052734375,-1.0078125,0.140625,
5,-0.0556640625,-1.0224609375,-0.0849609375,Sitting
```

Figure 3.52: File for data analysis with Weka.

the EEG data needed to be segmented based on the start of hand movement.

The acquisition framework used E-Prime and EGI's NetStation software to acquire EEG data from a 128-channel Sensor Net (Electrical Geodesic, Eugene, USA) helmet, shown in Figure 3.53, where one of the subjects is being prepared to participate in the experiment. The E-Prime software was used for experimental paradigm and stimuli delivery. The main feature of this setup was the possibility to mark on-line

J48		**Predicted activity (%)**			**Total accuracy**
		Standing	*Sitting*	*Walking*	
Actual activity	*Standing*	100.00	0.00	0.00	99.98%
	Sitting	0.00	100.00	0.00	
	Walking	0.09	0.00	99.91	

SMO		**Predicted activity (%)**			**Total accuracy**
		Standing	*Sitting*	*Walking*	
Actual activity	*Standing*	100.00	0.00	0.00	99.89%
	Sitting	0.00	100.00	0.00	
	Walking	0.57	0.00	99.43	

Naive Bayes		**Predicted activity (%)**			**Total accuracy**
		Standing	*Sitting*	*Walking*	
Actual activity	*Standing*	98.77	0.00	1.23	99.49%
	Sitting	0.00	99.98	0.02	
	Walking	0.00	0.00	100.00	

Table 3.11: Activity classification results on the test set.

the beginning of the hand movement, which made it possible, after data acquisition, to segment the EEG data before processing it. This was allowed by the use of one of the sensor modules, which was configured for this specific situation, both regarding hardware and software.

The module was attached to the hand of subjects during the experiment, so it was internally programmed to detect the beginning of the movement. An algorithm based on thresholding and the Exponential Moving Average (EMA) was implemented. Using this technique in time series smooths out the short-term fluctuations and highlights longer-term trends. For each sample of the accelerometer, the energy is calculated considering the data in its three axis. Afterwards, it is filtered, giving more weight to the latest data. This filtered value is the one compared with the set thres-

Figure 3.53: Subject being prepared for EEG experiment

hold. When a small hand movement is done, e.g. just when the subject starts to rise his/her hand, the given threshold is exceeded and the module triggers an event sending a signal through a wired connection to E-Prime, the workstation where EEG data is being recorded, allowing to mark these data. Choosing the correct threshold is of the utmost importance because, if it is too low, any minimal movement done by the subject would be caught while, if it is too high, the beginning of the movement would not be marked properly, but later in the data sequence. Several experiments were carried out by different subjects in order to choose the correct threshold for the given movement, "raising the hand and pressing a button on a pad".

The work accomplished showed that using an ad-hoc modified part of the proposed sensing system for complementing the EEG acquisition was useful and necessary for marking the EEG data online, enabling later analysis for detection of RP, as described in [89].

3.4 Summary

In this chapter, the prototypical system developed for human motion monitoring, which can be used in rehabilitation therapy, has been described. The integration of five small wireless modules, worn by the subject, which can acquire accelerometer data at high frequency, synchronized by an external master device, makes the system ideal for patient monitoring, since it is easily wearable and does not interfere with the movements. Furthermore, it provides significant flexibility, allowing monitoring different parts of the body with the same modules by just changing the placement of the elastic bands. Some exercises, such as monitoring a single arm during rehabilitation therapy, could require fewer modules, which makes it possible to use the system in a simpler configuration without affecting its capabilities. In addition, it includes Kinect for providing visual feedback to the user, which is of great importance in physical therapies.

The resulting system operates in real time and in a wireless network, guaranteeing data correctness while being portable and easy to manipulate, which are crucial factors for the target application. A software with a GUI for easy management of the sessions is also provided.

The successful working of the system has been demonstrated during the experiments carried out to assess the communication performance, which have been focused on data synchronization, data loss, jitter measurements and battery life. Furthermore, the system functionality has been tested analysing the data acquired with it in the task of activity classification by using three different standard classifiers and in combination with an EEG data acquisition machine for marking on-line the beginning of the hand movement. The results obtained show the potential of using the proposed system for human motion monitoring in rehabilitation.

Chapter 4

Data analysis

It is a capital mistake to theorize before one has data.

Sherlock Holmes, Arthur Conan Doyle

4.1 Introduction

In this chapter, human motion analysis is performed by modelling a complex physical exercise. One of the oldest yoga exercises, the Sun Salutation (see Fig. 4.1), with physical benefits as improving the strength and flexibility of the muscles and the alignment of the spinal column, is taken as an example of a rehabilitation exercise. It is a sequence formed by twelve postures, each of them counteracting the preceding one, producing a balance between flexion and extension. The reason for choosing this practice is that it provides a very well established sequence of movements, involving different parts of the body, which can be performed by any person in a limited frame of time and space without needing any additional equipment. The work done can however be extended to any other activity or exercise.

Empirical studies show the beneficial effects of yoga poses, not just by improving muscular strength and flexibility through stretching, but also on psychological conditions including anxiety and depression, and on pain syndromes and cardiovascular conditions, through, *e.g.*, body-and-breath control [90, 91]. Other studies are focused on the potential use of yoga in rehabilitation programs [92, 93, 94], and more speci-

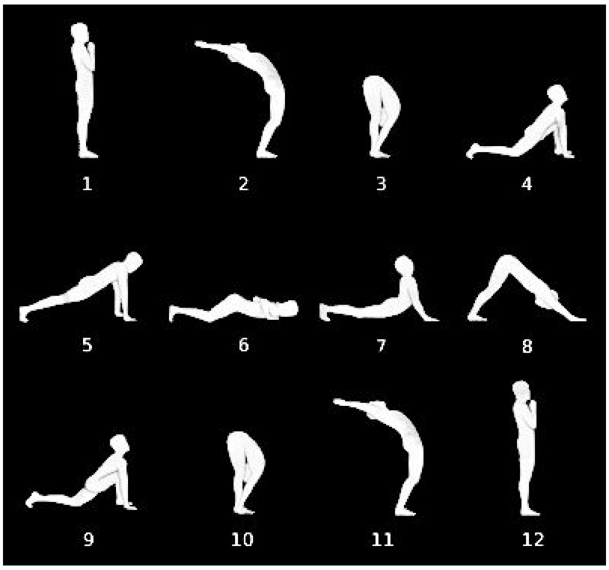

Figure 4.1: The twelve poses of the Sun Salutation sequence.

fically in physical therapies [95, 96], where the effects of practising yoga on motor variability, *i.e.*, strength, steadiness and balance, are assessed.

Some work has already been done regarding motion analysis of the Sun Salutation. In [97] a study, afterwards extended in [98], was made on the transition phase during motion of such an exercise in terms of grace and consistency by using one sensor attached to the lower back, but without providing a feedback to the user about how the exercise had been performed. This work was complemented in [99] studying the effects on specific joints during this practice. This particular sequence has also been used in [100, 101] for testing a virtual rehabilitation system which guides the user through a therapeutic exercise program. In [100] feedback on performance is provided in terms of scores. Based on these results, [101] is able to provide corrective advices stating the part of the body needing adjustment to achieve the pose. At the physical level, the main inconvenient of these systems is the use of a motion tracking suit which includes several wires. At the level of text generation, there is a clear necessity of new computational systems able to generate performance reports and linguistic advice more complex than the current ones.

For this thesis, the temporal series of measures that contains a numerical description of this exercise have been obtained by using the sensing system proposed in the previous chapter, as shown in Figure 4.2.

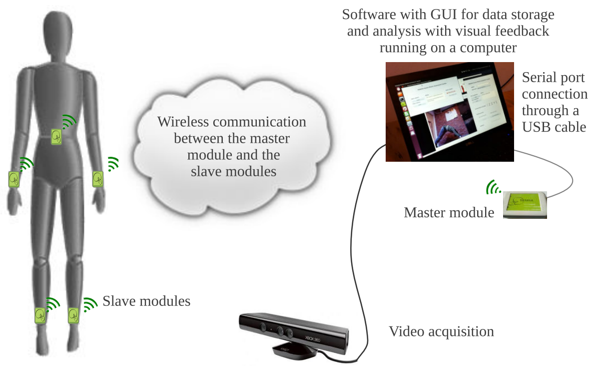

Figure 4.2: System architecture for the Sun Salutation motion acquisition.

In order to acquire meaningful data to model the movement appropriately, the postures assumed during the Sun Salutation were taken into consideration. The sensors were therefore placed as follows:

- Sensor 1: on the right forearm, above the hand.
- Sensor 2: on the left forearm, above the hand.
- Sensor 3: on the back waist, near to the centre of mass of the body.
- Sensor 4: on the right lower part of the calf, over the Achilles tendon.
- Sensor 5: on the left lower part of the calf, over the Achilles tendon.

The selected locations allow, in addition, to avoid the problems related to placing the sensors and the influence of the user's height. As the accelerometers provide measurements with a sampling frequency $f_s = 160$Hz, for each time instant, *i.e.*, every 6.25 ms, the record contains the following information: $(x_1, y_1, z_1, x_2, y_2, z_2, x_3, y_3, z_3, x_4, y_4, z_4, x_5, y_5, z_5)$, fifteen channels which correspond to the three axes of each of the five slave modules.

During the Sun Salutation, the movements of the body mainly occur along the antero-posterior and superior-inferior axes, as shown in Figure 4.3(a). Considering how the exercises are performed in space, it was realized that the movements could be modelled by considering the angle of the sensors with respect to the vertical axis as a relevant feature. Therefore, it was decided to switch from the Cartesian to the spherical coordinate system (see Figure 4.3(b)), obtaining the vector representation of each accelerometer and then extracting the angle, θ, with respect to the vertical axis, Z. This angle proves to be a relevant attribute with an adequate resolution degree to describe the human body movements while performing this sequence of poses. Analysing the data within this reference frame allowed to reduce their dimensionality, decreasing the record to five channels related to the angles: $(\theta_1, \theta_2, \theta_3, \theta_4, \theta_5)$. In addition, in order to recognize the transitions between the different poses of the exercise more accurately, five extra signals were considered, corresponding to the derivatives of the angles: $\left({}^{d\theta_1}/_{dt}, {}^{d\theta_2}/_{dt}, {}^{d\theta_3}/_{dt}, {}^{d\theta_4}/_{dt}, {}^{d\theta_5}/_{dt} \right)$. Each of these channels allows one to know if the corresponding angle is decreasing, increasing or constant at each instant of time.

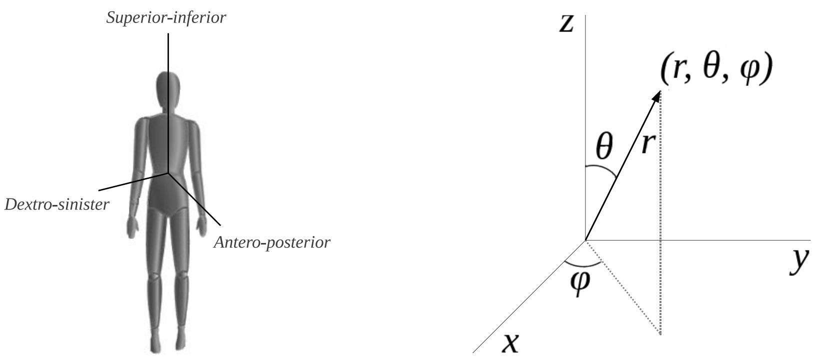

(a) Human body reference axes. (b) Spherical coordinate system.

Figure 4.3: Reference coordinate system.

For this specific application, a custom calibration method was defined to align the axes of the accelerometers to the coordinate reference system, shown in Figure 4.3. At the beginning of the exercise, once the sensors are worn, the subject must stay in a pre-defined position, just standing with the arms in a relaxed position along the body and the legs aligned together, for a few seconds. In the proposed convention, the Z axis is aligned with the gravity and is positive in the upper half-plane. Computing the corresponding rotation matrix and applying it to the data acquired, in this static position, all the accelerometers' vectors point to the floor, due to the gravity, with $\theta = 180^\circ$. These angles are referred afterwards to the horizontal plane, ranging from -90^{o} to 90^{o} (in the calibration pose).

In order to assess the quality of execution of the Sun Salutation exercise, the acceleration signals of a set of 10 healthy participants, who voluntarily took part in the evaluation, were collected. The subjects involved in the experiments were 7 men and 3 women with physical characteristics specified in Table 4.1. Each subject was asked to perform the Sun Salutation exercise 4 times, producing a total of 4 datasets per subject, except for the first subject who performed the exercise 10 times (where the additional six datasets were intensively used during the initial stage of interpretation of the data in order to be able to tune the model parameters appropriately).

Gender	**Age (years)**	**Height (cm)**	**Weight (kg)**	**Body Mass Index (kg/m^2)**
Male	27.86 (2.12)	182.71 (8.54)	82.71 (12.87)	24.69 (2.66)
Female	28.67 (2.08)	162.33 (9.24)	53.33 (2.31)	20.30 (1.38)

Table 4.1: Subject characteristics (mean and, in parenthesis, standard deviation).

The subjects were told to hold each position for 5 seconds while performing the exercise. The first two subjects had almost no external guidance, while the other ones were performing the exercise following an expert who was doing the same exercise and another person modulating the pose execution and cadence. At the same time, the scene was being captured by Kinect in order to provide them with visual feedback. Figure 4.4 shows one reference frame of each pose (both the RGB and depth views), acquired while Subject 6 was performing his first sequence.

(a) Pose 0

(b) Pose 1

(c) Pose 2

(d) Pose 3

(e) Pose 4

(f) Pose 5

(g) Pose 6

(h) Pose 7

(i) Pose 8

(j) Pose 9

(k) Pose 10

(l) Pose 11

(m) Pose 12

(n) Pose 0

Figure 4.4: Sun Salutation video acquisition with Kinect (RGB and depth views).

The next sections describe three different methods investigated for analysing these data. The first one is based on how the brain works and studies a specific type of neural network; the second one aims to provide a linguistic description of the exercise; and the last one proposes an hybrid system merging the two previous schemes in order to join their advantages while compensating their drawbacks.

4.2 Henesis Memory Prediction Framework (hMPF)

Mimicking the efficiency and robustness by which the human brain represents information has been a core challenge in artificial intelligence research for decades [102]. "hMPF" is the name given to the architecture developed within the research group of Henesis based on the Memory Prediction Framework (MPF), firstly proposed by Jeff Hawkins in [103]. The theory is based on how the brain works. In particular, most of the attention is focused on the neocortex, which is part of the brain of mammals, as it is stated that almost everything we think of as intelligence –perception, language, imagination, mathematics, art, music, and planning– occurs there. Two other brain regions which are considered within the theory are the thalamus and the hippocampus. The former is indispensable to normal living, receiving many axons from every part of the cortex and sending axons back to those same areas, while the latter is essential to the formation of new memories.

Hawkins' theory of intelligence is rooted in the assumptions of biology, but also makes sense from a computational point of view. It emphasizes the primacy of pattern recognition in the neocortex, able to both recognize invariant sequences in real time and elaborate feedback mechanisms that generate predictive patterns. The key to understanding the neocortex is understanding its hierarchical structure. Figure 4.5 shows a conceptual diagram of the cortical regions with different levels, being the lower related to various forms of perception (touch, audition and vision). The data sensed at this level, which might correspond to a spatial and/or temporal pattern, is processed and passed to the higher levels. While the pattern propagate through sensory regions, the system learns and forms invariant memories and predictions about it. The cortex takes the detailed, highly specific input and converts it to an invariant form, capturing the essence of relationships, not the details of the moment or object. Memory storage, memory recall, and memory recognition occur at the level of invariant forms.

[104] proposes a first implementation of this theory, new algorithms, named collectively Hierarchical Temporal Memory (HTM), that can be used to learn hierarchical-temporal models of data. It summarizes well the main points of the Memory

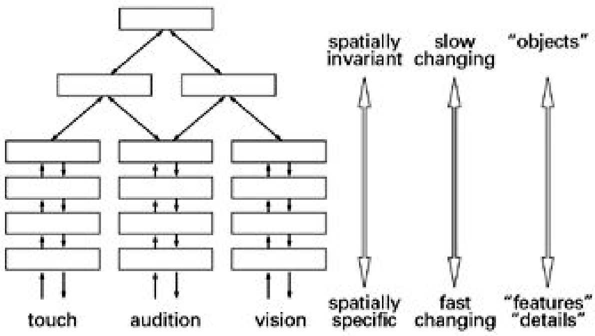

Figure 4.5: Forming invariant representations in the hierarchical structure.

Prediction Framework as follows:

1. The neocortex is constructing a model for the spatial and temporal patterns that it is exposed to. The goal of this model construction is the prediction of the next pattern on the input.

2. The cortex is constructed by replicating a basic computational unit known as the canonical cortical circuit. From a computational point of view, this canonical circuit can be treated as a node that is replicated several times.

3. The cortex is organized as a hierarchy. This means that the nodes, which are the basic computational units, are connected in a tree shaped hierarchy.

4. The function of the cortex is to model the world that it is exposed to. This model is built using a spatial and temporal hierarchy by memorizing patterns and sequences at every node of the hierarchy. This model is then used to make predictions about the input.

5. The neocortex builds its model of the world in an unsupervised manner.

6. Each node in the hierarchy stores a large number of patterns and sequences. The pattern recognition method employed by the cortex is largely based on storing lots of patterns.

7. The output of a node is in terms of the sequences of patterns it has learned.
8. Information is passed up and down in the hierarchy to recognize and disambiguate information and propagated forward in time to predict the next input pattern.

Whether it has been previously investigated the use of the Hierarchical Temporal Memories within the hMPF, their limitations, both during the learning and the inference phases, promoted the research on finding other algorithms for the implementation of the MPF theory [105]. Part of the data analysis of this thesis has been focused on the investigation of the use of neural gas algorithms, which will be explained in depth in the following sections, and their potential when analysing motion data.

4.2.1 State of the art of neural gas algorithms

Vector quantization, as a technique for data compression, is the process of modelling a probability density function using a distribution of discrete elements, often called codebook vectors, and a number of algorithms exist that perform this function [106]. One widely used is Kohonen's Self Organizing Map (SOM) [107], a type of neural network where, with no supervision, the neural units, which have certain neighbourhood relations to all other neural units, attempt to map their weights to conform to the given input data. However, it does not fulfilled two desirable capabilities: quantizing topologically heterogeneously structured manifolds and learning the similarity relationships among the input signals without the necessity of pre-specifying a network topology. [108], published in 1991, describes the first proposal of the *neural gas* (NG) as a neural network algorithm for vector quantization of topologically arbitrarily structured manifolds of input signals. This approach deals with the two aspects previously mentioned by presenting synaptic weights which are adapted independently of any topological arrangement of the neural units, also called neurons, within the net. Algorithm 2 describes the pseudo-code of the proposed algorithm.

The main parameters that influence the algorithm's performance are the number of neurons in the net; the adaptation step size, ε; λ, determining the neighbourhood

Algorithm 2 Neural Gas (NG)

Parameters initialization.
for *each given input vector* **do**
  Step 1: Update the internal parameters of the algorithm: the adaptation step size ε, the neighbourhood range λ and the maximum connection's age T.
  Step 2: Compute the distances of the neurons in the net, by considering their weights, to the given input vector and get the first and second winning neurons, *i.e.* the nearest ones.
  Step 3: Modify all the neurons in the net by adapting their weights.
  Step 4: Initialize or update the connection between the first and the second winning neurons.
  Step 5: Increase the age of all the other connections in the neighbourhood of the winning neuron.
  Step 6: Remove the lateral connections between the winning neuron and the neurons in its neighbourhood with age greater than the maximum connection's age, T.
end for

range, *i.e.* the number of neural units changing their synaptic weights with each adaptation step; and T, which defines the maximum connection's age. Both ε and λ are reduced as iterations increase. After sufficiently many adaptation steps the feature vectors cover the data space with minimum representation error. The resulting graph at the end of the training procedure represents the similarity, the neighbourhood relationship, among the input data. It can be considered that the main inconvenient of this approach is the need to pre-specify the network size, the number of neurons in it, without knowing if it will be sufficient for the current problem or if it will exceed the needs, being computationally very expensive to compute the distances of all the neurons in the net to each given input vector.

Some of the applications of neural gas include: clustering [109, 110], character recognition [111], fuzzy modelling [112], compression [113], segmentation [114, 115], classification [116] and robotics [117]. It has also been used in medical applications [118, 119, 120, 121], to guide the acquisition of deformable objects [122], to simplify the learning of a Self-Organizing Relationship (SOR) network [123] and for mapping high-dimensional data into a low-dimensional space [124, 125, 126, 127, 128], among others [129, 130, 131].

Having a great impact in the scientific field, several publications have been focused on a further study on the characteristics of the algorithm, as the the quality of quantization and visualization of vectors obtained with it [132], the importance of sorting [133] or the analysis of the learning dynamics [134, 135]. On the other hand, [136, 137] are focused on the hardware parallel implementation of NG, or a modified version of it [138]. Many studies have proposed improvements in the original algorithm [139, 140, 141, 142, 143, 144, 145, 146], from speeding it up [147, 148] to including modifications in the cost function [149] or developing a plastic model of it [129].

Many others publications propose modifications of NG which lead to new algorithms based on it. [150] first studies growing neural networks by using controlled growth process that also includes occasional removal of units, and then [151] proposes the “Growing Neural Gas” (GNG) algorithm, which will be described in detail later. Afterwards, [152] proposes an on-line criteria for removal of units which results in GNG-U (Growing Neural Gas with Utility criterion) for closely tracking of non stationary distributions. Other algorithms found on the literature are: “Recurrent Neural Gas” [153], “Hierarchical Overlapped Neural Gas” [154], “Recruiting Neural-Gas” [155], “Supervised Neural Gas” [156], “Neural Gas Attraction with EN” (Evolution strategy with Neighbourhood attraction) [157], “Robust Neural Gas” [158, 159], “ Supervised Relevance Neural Gas” [160, 161], “Kernel Neural Gas” [162], “Enhanced Neural Gas” [163], “Batch Neural Gas” and “Median Neural Gas” [164, 165], “Supervised Batch Neural Gas” [166], “Topographic Neural Gas” [167], “Evolutionary Neural Gas” [168], “Fusion-NG” [169], “Hierarchical HyperEllipsoidal Neural Gas” [170], “Sparse Coding Neural Gas” [171] afterwards used in [172, 173, 174, 175], “Energy Supervised Relevance Neural Gas” [176], “Matrix Neural Gas” [177], “Neural Gas based Cluster Ensemble Algorithm” [178], and the most recent “Contextual Neural Gas” [179].

Several studies are related with the extension of the neural gas vector quantization method to local Principal Component Analysis (PCA), named NG-PCA, PCA-

NG or NG-LPCA [180, 181, 182, 183]. And, similarly to what happened with the original NG, improvements were proposed to the modified versions of the algorithm [184, 185, 186, 187], *e.g.*, for "Batch Neural Gas" [188, 189] and "Median Neural Gas" [190].

[191, 192] compare the NG with SOM, while in [193] several algorithms are tested, including NG and GNG, for clustering, both with real and simulated data sets.

Growing Neural Gas, GNG

As mentioned previously, in order to overcome the main limitation of the NG approach, which is having a pre-determined size of the net, [151] proposes the "Growing Neural Gas" (GNG) algorithm, influenced also by the "Competitive Hebbian Learning" (CHL), deepened in [194], and Fritzke's previous work on growing cell structures [150]. Its main advantage over the NG is the incremental character of the model, having a dimensionality that depends on the input data and can vary locally [195]. The GNG algorithm starts with two neurons at random positions in the input space. Periodically new neurons are added by evaluating local statistical measures gathered during previous adaptation steps. The proposed insertion criterion is to introduce a new neuron every λ input samples between the neuron that has accumulated the highest local error and its neighbour with the highest error. Algorithm 3 shows the pseudo-code of the proposed GNG algorithm.

In this case, the parameters of interest are: the maximum number of neurons in the net, which could be considered as a stopping criterion; ε_b and ε_n, which affect the movement of the winning neuron and of its neighbourhood, respectively; T, the maximum connection's age; λ, parameter that defines the step that determines when it is possible to include a new neuron in the net; and α and d, constants that influence the decrement of the error variables. The adequate definition of their values determines the algorithm's performance.

Some of the applications of GNG are clustering [196, 197, 198, 199, 200, 201, 202, 203], even large amounts of data as air-photography data [204], classification [195, 205, 206, 207], modelling, representation and compression [208, 209, 210, 211, 212, 213, 214], and specifically hand modelling [215, 216], image segmenta-

Algorithm 3 Growing Neural Gas (GNG)

Parameters initialization. Start with two neurons at random positions in the space.
for *each given input vector* **do**
  Step 1: Compute the distances of the neuron weights in the net to the given input vector and get the first and second winning neurons, *i.e.*, the nearest ones.
  Step 2: Increase the age of all the connections emanating from the winning neuron.
  Step 3: Update the local accumulated error of the winning neuron.
  Step 4: Move the weights of the winning neuron and of its direct topological neighbours towards the given input vector considering ε_b and ε_n, respectively.
  Step 5: Initialize or update the connection between the first and the second winning neurons.
  Step 6: Remove the lateral connections between the winning neuron and the neurons in its neighbourhood with age greater than the maximum connection's age, T. In case a neuron remains without connections, remove it as well.
  if *it is a* λ *step* **then**
    Step 7: Add a new neuron between the neuron having the maximum accumulated error and its neighbour with the largest error. Update the connections among these three neurons and their error variables (multiplying them with a constant α).
  end if
  Step 8: Decrease all error variables (multiplying them with a constant d).
  if *a stopping criterion is not yet fulfilled* **then**
    Step 9: Go to **Step 1**.
  end if
end for

tion [217, 218, 219], automatic landmark extraction in medical images [220, 221], object categorization and recognition [222, 223], robotics [224, 225, 226, 227], learning the turbine characteristic surface torque versus wind speed and machine speed [228, 229, 230, 231, 232], or security-related applications [233, 234], among others [235, 236, 237, 238, 239, 240, 241, 106].

Some modifications proposed for the GNG regard the growing, update or stopping criteria [242, 243], the creation of a more biologically-plausible algorithm, an hybrid between NG and GNG [244], or a hierarchical extension [245] or overlapped architecture [246, 247] combining the unsupervised and supervised learning schemes in GNG.

New algorithms derived from the GNG are: “Double Growing Neural Gas” [248], “Self-Growing Neural Gas Network” [249], “Grow When Required” [250], “Robust Growing Neural Gas” [251], “Incremental Growing Neural Gas” [252] with posterior improvements [253, 254, 255], “TreeGNG” [256], “Adaptive Growing Neural Gas” [257], “Lifelong Growing Neural Gas” [258], “GNG with Post-Pruning” [259], “Supervised Growing Neural Gas algorithm” [260] used later in [261], “Growing Neural Gas Clustering” [262], “Meshing Growing Neural Gas” [263], “GNG with Targeting” [264], “GNG-UF” [265] and “fast Autonomous Growing Neural Gas” [266].

Some of the papers in the literature present a comparison of different algorithms [267]. [268], for example, studies the performance of three incremental neural network based algorithms: fuzzy ARTMAP (FAM), Growing Neural Gas (GNG) and growing cell structures, while [269] is focused on the study of different variations of GNG to quantify topology preservation. Some experiments are performed in [270] for comparing GNG, GNG with Utility and Supervised GNG, and [271] presents the implementation of the GNG algorithm on a GPU with CUDA.

Self-Growing and Self-Organized Neural Gas, SGONG

The “Self-Growing and Self-Organized Neural Gas”, also known as SGONG, was first presented in 2005 in [272, 273]. This approach combines the growing mechanism of the “Growing Neural Gas” and the learning adaptation mechanism of the Kohonen’s Self Organizing Map. The innovation introduced by the algorithm in the growing procedure is that, at the end of each epoch, three different criteria are applied to ensure the fast convergence of the neural network, detecting the isolated classes and automatically including or deleting neurons, determining adaptively the final number of neurons. With respect to the learning scheme, the learning rate and the radius of the neighbourhood of the winning neuron are monotonically decreased during the training procedure, each neuron having two learning rates: ε_{1_i} and ε_{2_i}. Additionally, a local counter is defined for each neuron, N_i, which depends on the number of input vectors that are classified through that neuron, that is incremented every time that it becomes the winning neuron. The pseudo-code corresponding to the SGONG algorithm is shown in Algorithm 4.

The parameters that mainly influence the algorithm's performance are indicated below:

- N_{idle}, threshold that determines the possibility of the local learning rates to update their values, when being compared with the local counter of the neuron N_i.
- ε_1: its initial and final values determine the learning rates of the winning neuron, as it is applied to its weights.
- r_{max} is referred to the maximum ratio between ε_1 and ε_2; ε_2 being the learning rate applied to the weights of the neurons that belong to the neighbourhood of the winning neuron.
- T defines the maximum connections' age.
- β defines the number of consecutive epochs that determine an inactive neuron.
- m_1 regulates new neurons' insertion.
- m_2 regulates neurons' removal.

The main advantage of this algorithm is that it automatically adapts the size of the network and its topology depending on the input data used during the training phase. This is done by applying three criteria that influence the growing of the output lattice of neurons and the final number of obtained classes, having a convergence speed comparable to the GNG and a stability comparable to that of the SOM. The procedure for removing inactive neurons can be considered as a memory function for the neural network, as the inactive neurons remain only for β consecutive epochs in the output lattice. On the other hand, new neurons are added just if they satisfy the condition for efficiently decreasing the sum of accumulated errors from one epoch to

Algorithm 4 Self-Growing and Self-Organized Neural Gas (SGONG)

Parameters initialization. Start with two neurons at random positions in the space.
for *each given input vector* **do**
  if *it is the beginning of an epoch* **then**
    Step 1: Set the accumulated errors of each neuron, $AE_i^{(1)}$ and $AE_i^{(2)}$, to zero.
  end if
  Step 2: Compute the distances of the neurons in the net to the given input vector and get the first and second winning neurons, *i.e.*, the nearest ones.
  Step 3: Update the local variables of the winning neuron: the accumulated errors $AE_{w1}^{(1)}$, $AE_{w2}^{(2)}$, and the local counter N_{w1}.
  Step 4:
  if $N_{w1} \leq N_{idle}$ **then**
    Update the local learning rates, $\varepsilon_{1_{w1}}$ and $\varepsilon_{2_{w1}}$, and the ratio r_{w1} of the winning neuron.
  end if
  Step 5: Update the weights of the winning neuron and its neighbourhood considering their respective learning rates.
  Step 6:
    · Update the connection between the first and the second winning neurons.
    · Increase the age of all the other connections in the neighbourhood of the winning neuron.
    · Remove the lateral connections between neurons with age greater than the maximum connections' age, T.
  if *it is the end of an epoch* **then**
    Step 7: Apply three criteria which might modify the number of output neurons:
      · Removing of inactive neurons, those that have not become the first winning neuron for a number of β consecutive epochs.
      · Check for adding a new neuron near the one with the maximum contribution in quantization error.
      · Check for removing the neuron which is close enough to its neighbours.
  end if
end for

another. Finally, the scope of the third criteria is to remove the classes that are closer to their neighbouring classes, while the isolated classes are retained.

The initial work done using SGONG was associated to colour reduction and estimation of the number of dominant colours in an image [274]. Afterwards, it was tested on hand gesture recognition [275], while later work is related to classifying video frames into clusters [276].

Time series analysis

Till now, the algorithms presented for data analysis consider just the spatial context of the input data. However, one important dimension to consider is the time, as the temporal evolution of a signal might be of the utmost importance in a vast number of applications, *e.g.*, when analysing human motion in rehabilitation therapies. The two main aims of time series analysis are the identification of the nature of the observed phenomenon and the prediction of future values.

In [277] a neural gas network is used to represent the attractor of the Mackey Glass equation and to predict its time series. However, in its original formulation, both NG and SOM have been proposed for processing real-valued vectors, not sequences. In the mentioned work, the temporal context within the time series is realized by means of a data window which considers the four past values of the input signal and the forecast is implemented iteratively. [278] investigates the "Merge Self-Organizing Map" (MSOM) approach for unsupervised sequence processing. The MSOM network is formed by neurons which are equipped with a tuple including a weight and a context, considered during the training process. When combining the context model with neural gas for accurate quantization the "Merge Neural Gas" (MNG) is obtained. This model approach is extended in [279] to an incremental network by using the GNG, proposing the "Merge Growing Neural Gas" (MGNG) as a recursive growing self-organized neural network for time series analysis which does not require any a-priori knowledge. In MGNG each neuron comprises a weight vector w_n representing the current time step and a context vector c_n representing all past time steps of a sequence. When calculating the distance between the neurons and the input sequence a parameter α allows to weight the importance of the current input signal over the past and also takes into consideration a global temporal context C_t, computed as a linear combination (merge) of both the weight and context vector of the winning neuron in the previous step. Moreover, in C_t the parameter β controls the influence of the far over the recent past, constituting an exponentially decayed sum of all past winning neurons' weight vectors beside the current. Experimental results demonstrated reduced time complexity while retaining accuracy in time series representation.

4.2.2 Experimentation

Different neural gas algorithms were selected to be included within the hMPF: the original "Neural Gas" (NG), the "Growing Neural Gas" (GNG), the "Double Growing Neural Gas" (DGNG), the "Growing Neural Gas with Utility" (GNG-U), the "Incremental Growing Neural Gas" (IGNG), the "Self-Growing and Self-Organized Neural Gas" (SGONG) and the "Merge Growing Neural Gas" (MGNG).

Several datasets have been used both for training and testing the different neural gas algorithms. With respect to the spatial algorithms, the dataset used in the first proposal of NG described in [108] has been used. The data manifold consists of a 3D, a 2D and a 1D subsets connected among them. A 2D spatial distribution known as "Circles and Squares" formed by several separated subsets and the Fundamental Clustering Problems Suite (FCPS) [280] have also been used. When analysing the performance of the temporal neural gas, the Mackey Glass time series and the Noisy Automata dataset have been considered.

After an initial experimental phase, the algorithms which have shown to be more relevant for this thesis are the GNG, the SGONG and the MGNG for its capacity of considering the temporal context. Figure 4.6 shows some different structures that have been considered to analyse the motion while performing the Sun Salutation sequence using neural gas algorithms within the hMPF hierarchy. Figure 4.6(a) shows how one single node with one of these algorithms on it (SS meaning Sun Salutation) analyses the input signals coming from all sensors, consisting on the angles related to the five on-body accelerometers $(\theta_1, \theta_2, \theta_3, \theta_4, \theta_5)$, as explained before. In Figure 4.6(b) each of these signals is analysed independently (RF meaning Right Forearm, LF for Left Forearm, BW for Back Waist, RC for Right Calf and LF for

Left Calf) and afterwards a top node collects and analyses their outputs for providing a higher level interpretation. Finally, in Figure 4.6(c) an intermediate level is included for a previous analysis of the information related to the forearms, the back waist and the calves before getting to the top level. Other options considered during this thesis included, additionally, the information related to the derivatives of the five angles. The architectural options shown consider, generally, that the nodes include spatial neural gas algorithms. However, these options have also been tested including a final top node with a temporal neural gas or even using the architecture with just one node following the approach shown in option 1.

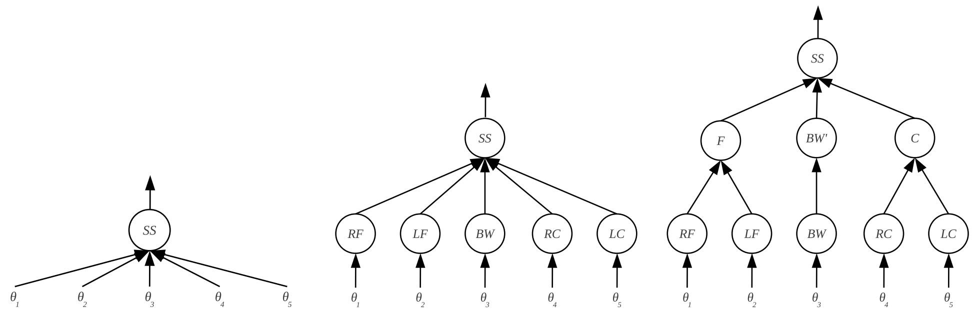

(a) Option 1. (b) Option 2. (c) Option 3.

Figure 4.6: Different hierarchical structures of the hMPF using neural gas algorithms.

It should be mentioned that the training process of the networks might be very expensive computationally and time consuming due to the fact that a large amount of data is needed for the algorithm to learn. This complexity, which increases when the network grows and has several levels or layers, is added to the difficulty of finding the right parametrization of the algorithms in order to boost their performance.

In order to provide an idea of the potential of using this kind of algorithms within the hMPF, here the three architectures tested which have provided the most significant results are shown. The initial experiments done using spatial neural gas algorithms were aimed at recognizing the poses forming the Sun Salutation sequence. Following the approach shown in Figure 4.6(a), a significantly reduced GNG network was trained to this purpose. For the training process, four datasets of the Sun Salutation performed adequately were selected, so that the network could learn how the sequence is correctly executed by being exposed intensively to these data. Figure 4.7 shows its topological graph along with the input data which is mapped during the test process, $(\theta_1, \theta_2, \theta_3, \theta_4, \theta_5)$. The topological graph shows the structure of the network, how the neurons are distributed in the space and how are they are connected to each other, aiming to closely reflect the topology of the data distribution.

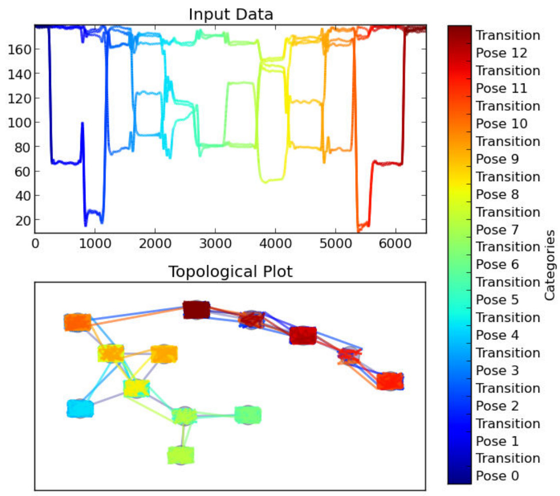

Figure 4.7: Topological graph of a GNG network trained for pose recognition.

Instead, Figure 4.8 shows the result produced by this network when exposed to the same input data during the inference process. “FF In” is the feedforward input signal to the network, while “FF Out” is the corresponding output in the feedforward direction. This output contains the degree of activation of each neuron in the network for each given input sample. The number in the upper part of the “FF Out” signals is the ID of the winner neuron, which also determines the colour of the vertical stripe for easy visual differentiation of the classification performed, which allows to recognize the pose at any time. As can be seen, the poses are recognized as follows:

- Pose 0 (calibration) $\leftrightarrow$ Neuron ID: 4.
- Poses 1 and 12 $\leftrightarrow$ Neuron ID: 9.
- Poses 2 and 11 $\leftrightarrow$ Neuron ID: 3.

- Poses 3 and 10 ↔ Neuron ID: 5.
- Pose 4 ↔ Neuron ID: 7.
- Pose 5 ↔ Neuron ID: 11.
- Pose 6 ↔ Neuron ID: 12.
- Pose 7 ↔ Neuron ID: 0.
- Pose 8 ↔ Neuron ID: 10.
- Pose 9 ↔ Neuron ID: 6.

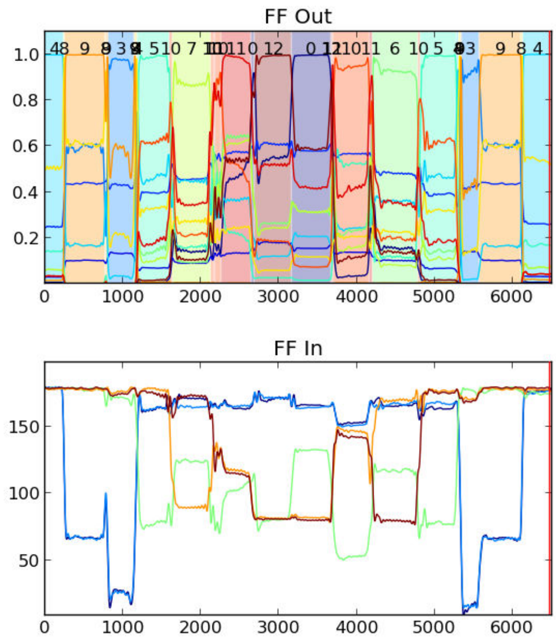

Figure 4.8: Pose recognition performed by using a GNG network.

One of the limitations of this model is that, not considering the temporal context, it is not able to differentiate between the poses that are the same, but being performed at the beginning and at the end of the Sun Salutation sequence. On the other side, it is not capable of analysing the transition phases between one pose and the next one.

Within the available GUI a feedback is given to the subject in form of a level bar which, considering the "coverage" of the input signal, *i.e.*, how well it can be represented or matched to a neuron or group of neurons in the network, changes its level and colour from green, in case of a good coverage (good performance of the current pose), to red, when the network is not able to map it due to a bad execution.

Afterwards, a node including a temporal gas network was added on top of the one corresponding to the GNG network for getting additional knowledge about the sequence and consider the temporal context. This algorithm has as input signals the outputs of the node below. Figure 4.9 shows the temporal graph corresponding to that network. Unlike the topological graph, the temporal graph takes into consideration the temporal context of each of the neurons, being the connections among them established depending on this criterion. This means that neurons adjacent in the temporal graph are activated in moments close in time. Therefore, neurons in a chain would be activated serially to describe data that follows a sequence.

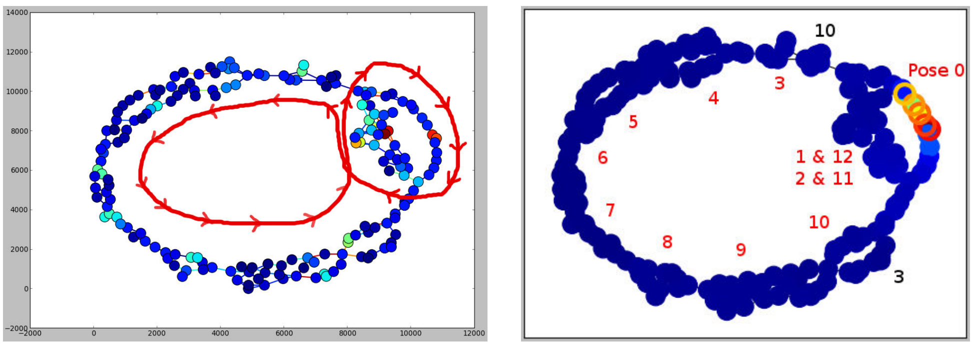

(a) Path followed in the temporal graph.

(b) Activations in the temporal graph.

Figure 4.9: Temporal graph of the top node of a hMPF hierarchy.

In Figure 4.9(a) the path that is followed while analysing the input signal of an unknown sequence is specified to show how and in which order the neurons are activated while seeing it. The image in Figure 4.9(b) illustrates to which pose each part of the path corresponds. As can be seen, poses 0, 4, 5, 6, 7, 8 and 9 are recognized unequivocally. Poses 3 and 10, which are at the beginning and at the end of the exercise, respectively, are also recognized appropriately, although there is some reminiscent activation of the other pose. On the other hand, poses 1 and 12 and poses 2 and 11 are found in the same zone of the graph due to the characteristics of the Sun Salutation sequence, that is, the *mountain* pose (which corresponds to 1 and 12) is at the beginning of the exercise before the *bending backward* pose (corresponding to 2 and 11), while it is after it at the end. The important feature of this architecture having the temporal node at the top is its capacity to recognize the sequence and, therefore, to anticipate which is the following pose that it expects to see, including some kind of prediction capability within its characteristics.

One interesting approach followed was using option 1 of the hMPF in Figure 4.6, an architecture with just one node, but including a temporal neural gas in this case. This neural gas was intensively trained with sequences of two different subjects, forming the temporal graph shown in Figure 4.10, where the different colours identify the poses, from dark red related to the calibration pose, to increasingly colder colours up to the last poses. The darkest blue has been used to identify the transitions among the poses. The graph allows to see how the network is well self-structured to differentiate between the poses of the sequence. It can also be seen how some poses, as the ones in light blue, need just few neurons to be recognized adequately, while others, as the previous ones in green, require many more neurons.

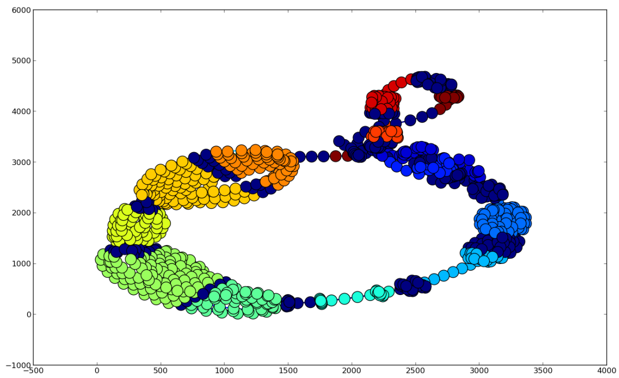

Figure 4.10: Temporal graph of a temporal node.

This could mean that the neural gas has not been able to generalize appropriately, which might be due to the need of seeing a larger amount of data during the training process. The GUI allows one to see if a neuron or a group are sufficiently generalized or not or to see which poses are associated to them or they are able to recognize. Figure 4.11 shows two different situations. In this case, on the x axis, poses are numbered from 0 to 13 (being poses 0 and 13 related to the calibration one), while the transitions are numbered from 14 to 26. Figure 4.11(a) shows neuron #90, which belongs to group #7, that gets active when seeing the input signal corresponding to transition 26 (the one between the last two poses of the sequence). As can be seen, the group also is activated practically just during this transition. Instead, Figure 4.11(b) shows the graphs corresponding to neuron #118, belonging to group #9. While the neuron correctly identifies pose 0, the corresponding groups are activated, not just by the input corresponding to this pose, but also by the following transition, 14.

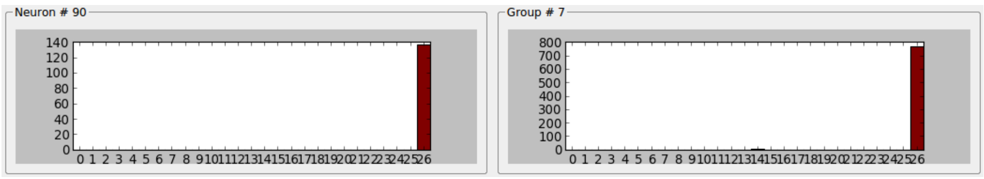

(a) Neuron and group specialized in recognizing the transition between the last two poses.

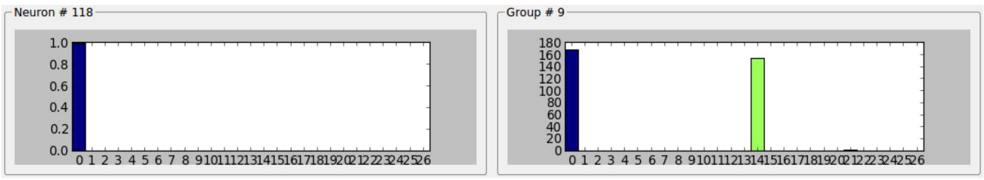

(b) Neuron specialized in Pose 0 and group recognizing also the following transition.

Figure 4.11: Neuron and belonging group associated to the pose and transition that they recognize.

The results obtained using this approach, which includes neural gas algorithms within the hMPF architecture, show that it can effectively be used for analysing motion data, both for classification in pose recognition and to include the temporal context for adding prediction capabilities. Additionally, an initial feedback is provided to the subject related to the performance of the exercise considering how well the current pose matches the pose learnt during the previous training process.

4.3 Linguistic modelling of complex phenomena

The main contribution to the quality analysis of the Sun Salutation exercise in this section is made by providing a new technique for modelling this type of phenomenon. A computational application which generates linguistic descriptions for assessing the subject's performance, after the analysis of the acquired data, has been developed and published in [281].

In order to face the complexity of the exercise, the Granular Linguistic Model of a Phenomenon (GLMP), including a Fuzzy Finite State Machine (FFSM), is used for modelling the different poses of the user and merging information from several sensors. First, the relevant poses of the Sun Salutation are identified based on the accelerations produced during the process, performing the analysis involving body parts. Once the poses are recognized by the FFSM, the symmetry, stability and rhythm of the movements produced are analysed for evaluating the Sun Salutation quality corresponding to a specific exercise. Finally, a method for producing a linguistic report about the quality of the execution, in terms of the relevant features, is used. This type of reports could be used to analyse the temporal evolution of the Sun Salutation exercise, *e.g.*, while learning and improving its execution during physical rehabilitation therapies.

The GLMP has demonstrated to be useful for implementing complex assessment criteria using inference systems based on linguistic rules [282]. This technique is based on fuzzy logic and the Computational Theory of Perceptions (CTP). This field was first introduced in Zadeh's seminal paper "From computing with numbers to computing with words – From manipulation of measurements to manipulation of perceptions" [283] and further developed in subsequent papers. The Computational Theory of Perceptions provides a framework to develop computational systems with the capacity of computing with the meaning of Natural Language (NL) expressions, *i.e.*, with the capacity of computing with imprecise descriptions of the world in a human-like way.

In the Computational Theory of Perceptions, a granule is a clump of elements which are drawn together according to criteria like indistinguishability, similarity, proximity or functionality [284]. The boundary of a granule is fuzzy, which allows one to model the way in which human concepts are formed, organized and manipulated in an environment characterized by imprecision, uncertainty, and partial truth [285]. A granule underlies the concept of a linguistic variable [286], *i.e.*, a variable whose values are words or sentences in NL [287, 288, 289].

The contributions to the field of quality assessment of rehabilitation exercises are both theoretical and practical and derive from the design and development of a tool for linguistic assessment of a physical rehabilitation exercise such as the Sun Salutation sequence. The tool includes a computational model able to describe the exercise execution at different levels of granularity by giving insights about its symmetry, stability and rhythm. The theoretical contribution consists of exploring the possibility of creating linguistic descriptions about how phenomena evolve in time. It is analysed not only the current state of phenomena, but also their intermediate states, to generate a new type of linguistic descriptions.

4.3.1 Linguistic description of phenomena evolving in time

The approach followed to define a computational model of phenomena is based on subjective perceptions of a domain expert, called from now on the “designer”. The more experienced the designer, with better understanding and use of NL in the application domain, the richer the model with more possibilities of achieving and responding to final users’ needs and expectations. The designer uses the available resources, *e.g.*, sensors, to acquire data about a phenomenon and uses her/his own experience to interpret these data and to model it. Then, the designer uses a computer to produce the needed linguistic utterances.

In the current project, the designer is a person experienced with the motion of the body while performing the Sun Salutation sequence, being able of modelling the exercise by using the data available from several on-body sensors. Furthermore, the designer takes into consideration the relevant information to be extracted during the analysis in order to provide a useful feedback for rehabilitation purposes.

In this section, the components of the Granular Linguistic Model of a Phenomenon (GLMP), the approach based on the Computational Theory of Perceptions followed for developing computational systems able to generate linguistic descriptions of phenomena [37, 290], are presented.

Computational perception (CP)

A *CP* is the computational model of a unit of information acquired by the designer about the phenomenon to be modelled. In general, *CP*s correspond to particular details of the phenomenon at certain degrees of granularity. A *CP* is a couple (A, W) where:

$A = (a_1, a_2, \ldots, a_n)$ is a vector of n linguistic expressions (words or sentences in NL) that represents the whole linguistic domain of the *CP*. Each a_i describes the value of the *CP* in each situation with specific granularity degree. These sentences can be either simple, *e.g.*, $a_i =$ *"The angle of the sensor is negative."* or more complex, *e.g.*, $a_i =$ *"The symmetry of the calves during the first pose is high."*.

$W = (w_1, w_2, \ldots, w_n)$ is a vector of validity degrees $w_i \in [0, 1]$ assigned to each a_i in the specific context. The concept of validity depends on the application, *e.g.*, it is a function of the truthfulness of each sentence in its context of use.

Perception mapping (PM)

*PM*s are used to create and aggregate *CP*s. A *PM* is a tuple (U, y, g, T) where:

U is a vector of input *CP*s, $U = (u_1, u_2, \ldots, u_n)$, where $u_i = (A_{u_i}, W_{u_i})$ and n is the number of input *CP*s. In the special case of first-order perception mappings (1-*PM*s), these are the inputs to the GLMP and they are values $z \in \mathbb{R}$ being provided either by sensors or obtained from a database.

y is the output *CP*, $y = (A_y, W_y)$.

g is an aggregation function employed to calculate the vector of validity degrees assigned to each element in y, $W_y = (w_1, w_2, ..., w_{n_y})$. It is an aggregation of input vectors, $W_y = g(W_{u_1}, W_{u_2}, ..., W_{u_n})$, where W_{u_i} are the degrees of validity of the input perceptions. In fuzzy logic, many different types of aggregation functions have been developed. For example, g might be implemented using a set of fuzzy rules. In the case of 1-*PMs*, g is built using a set of membership functions as follows:

$$W_y = (\mu_{a_1}(z), \mu_{a_2}(z), \ldots, \mu_{a_{n_y}}(z)) = (w_1, w_2, \ldots, w_{n_y})$$

where W_y is the vector of degrees of validity assigned to each a_y, and $z \in \mathbb{R}$ is the input data.

T is a text generation algorithm that allows generating the sentences in A_y. In simple cases, T is a linguistic template, *e.g.*, *"The calves symmetry is {low | medium | high}"*.

Granular Linguistic Model of a Phenomenon

The GLMP consists of a network of *PM*s. Each *PM* receives a set of input *CP*s and transmits upwards an output *CP*. It is said that each output *CP* is *explained* by the *PM* using a set of input *CP*s. In the network, each *CP* covers specific aspects of the phenomenon with a certain level of granularity. Figure 4.12 shows an example of a GLMP, where the phenomenon can be described at a very basic level in terms of two variables providing two values, z_1 and z_2, at a certain instant of time.

As mentioned above, *first-order perception mappings* (1-*PM*) are those which are input to the GLMP. These 1-*PM*s produce *first-order computational perceptions* (1-*CP*). On the other side, *PM*s whose inputs are *CP*s are called *second-order perception mappings* (2-*PM*) and their outputs are named 2-*CP*s.

Using different aggregation functions and linguistic expressions, the GLMP paradigm allows the designer to model computationally her/his perceptions. In the case of Figure 4.12, the second order perception mapping 2-PM_3 indicates that 2-CP_3 can be explained in terms of the first order computational perceptions 1-CP_1 and 1-CP_2, *i.e.*, how the validity of each item in 2-CP_3 is explained by those of 1-CP_1 and 1-CP_2. Finally, the highest-order description of the phenomenon is provided, at the highest

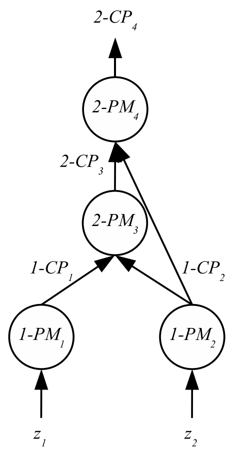

Figure 4.12: Example of a Granular Linguistic Model of a Phenomenon.

level of abstraction, by 2-CP_4, explained by 2-PM_4 in terms of 2-CP_3 and 1-CP_2. Notice that, by using this structure, one can provide not only a linguistic description of the phenomenon at a certain level, but an explanation in terms of linguistic expressions at a lower level.

Report generation

Once the GLMP is fed with input data, the aggregation functions are used to calculate the validity degrees corresponding to potentially hundreds of linguistic expressions. The input data depends on each particular application. In this case, it is motion data acquired by the proposed wearable sensing system. Now, the challenge consists of choosing the most adequate combination of these sentences to generate a useful linguistic description of the phenomenon evolution including the current state. The design of this report requires a deep analysis of the application domain of language and, therefore, the collaboration of an experienced final user.

For the proof of concept, here a simple report is used, made by choosing the linguistic expressions with the highest validity degree and including detailed explanations of a perception by using the conjunction “because”. In [291] other two different types of report templates are developed.

4.3.2 Linguistic assessment of the Sun Salutation exercise

Figure 4.13 shows the GLMP designed for the linguistic description of the Sun Salutation exercise quality. The grey speech bubbles show different examples of linguistic expressions associated to several *CP*s. Three main features to assess the patient's performance have been selected: the symmetry, the stability and the rhythm. People with disabilities, such as people who suffered a stroke, are generally affected by weakness or paralysis on one side of their bodies, which results in an asymmetrical posture. Working on postural symmetry in the early stages of rehabilitation creates awareness of body position. On the other hand, being able to stabilize the movement determines the postural balance control. Evaluation of postural stability is important for clinicians to diagnose balance problems early and to evaluate the effects of interventions to treat these problems [292]. Finally, the study of the rhythm reflects the pace of the movement of the patient, which is particularly relevant for Parkinson's disease patients [293].

The GLMP is organized into three levels. The lowest one corresponds to the time instant and it is divided into three different sub-levels (entry, pose elements, and pose recognition), the medium level is related to the pose and the highest one to the whole Sun Salutation sequence. It is worth noting that linguistic expressions can be generated for each level of granularity.

On the entry level, the angles related to the five accelerometers $(\theta_1, \theta_2, \theta_3, \theta_4, \theta_5)$ and their derivatives $\left({}^{d\theta_1}/_{dt}, {}^{d\theta_2}/_{dt}, {}^{d\theta_3}/_{dt}, {}^{d\theta_4}/_{dt}, {}^{d\theta_5}/_{dt}\right)$ are used to identify the poses and movements of the forearms, the back waist and the calves for the pose elements level. Afterwards, in the pose recognition level, the corresponding *CP*s allow to identify the pose that is being performed at each instant.

In the intermediate level related to the pose, the symmetry of the forearms and the calves is analysed for each pose, by considering the data provided by the accelerometers worn on them. The stability during each pose is also obtained by analysing how well it is maintained without trembling.

These measures are aggregated at the Sun Salutation sequence level to evaluate

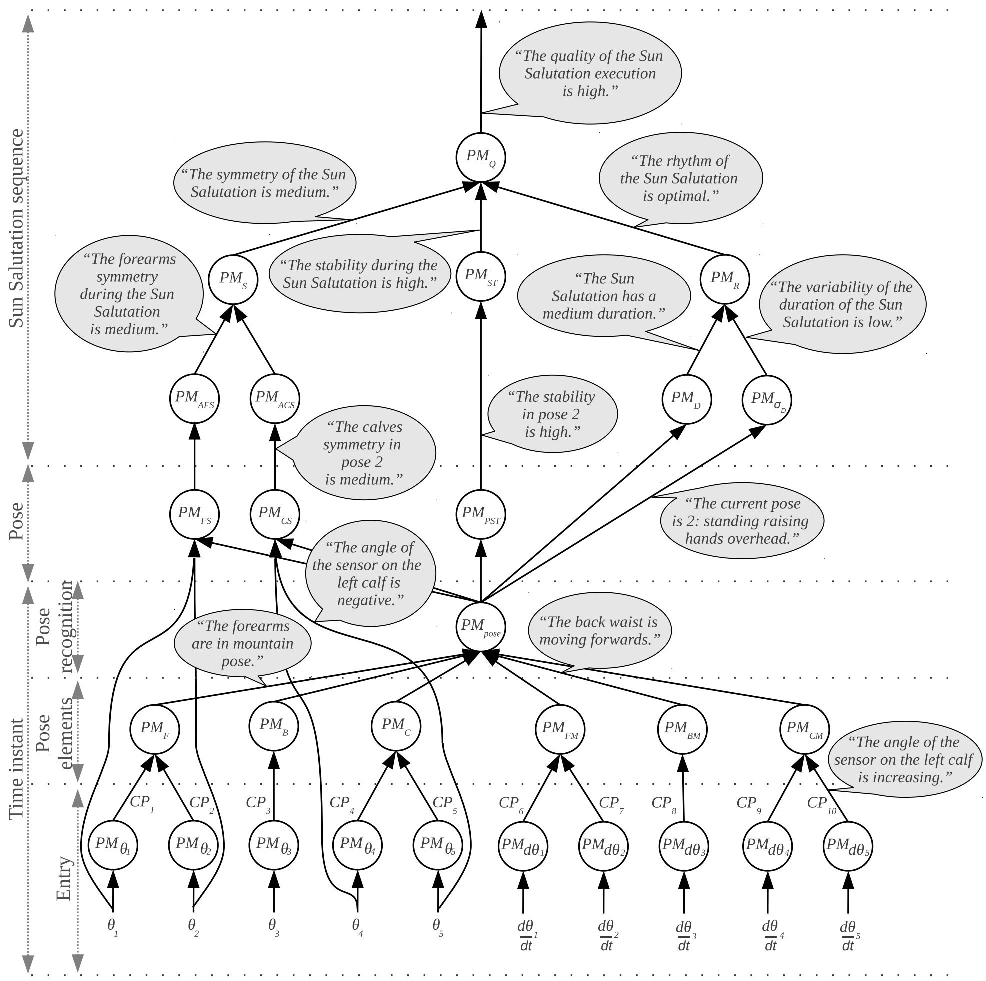

Figure 4.13: GLMP for the linguistic description of the Sun Salutation quality.

the symmetry and the stability during the whole exercise. Moreover, the duration of each pose and its variability are taken into account. These measures make it possible, afterwards, to evaluate the rhythm of the execution of the exercise. Finally, the total symmetry, stability and rhythm of the Sun Salutation execution are used to estimate its quality in order to provide a feedback to the patient and the clinicians by a linguistic description. "*The quality of the Sun Salutation execution is medium because the symmetry is medium, the stability is low and the rhythm is adequate*" could be an example of a final report.

In this section, each of the *PM*s is described. For the sake of simplicity, the set of poses of the Sun Salutation to be considered is reduced to the first three and the last two poses (which correspond to poses 1, 2, 3, 11 and 12 in Figure 4.1, respectively), including an additional one at the beginning and at the end for sensors calibration.

Time instant level – Entry level

The entry level is formed by 1-*PM*s which collect information directly from the sensors. They are of two different types: the former related to the angle of the sensors, and the latter related to the corresponding derivatives.

Angle of the sensor *(PM_{θ_i})* It is a 1-*PM* whose input is the numerical value of the angle formed by the vector given by the sensor i and the Z axis $(\theta_i \in [0^o, 180^o],$ $i \in [1,5])$. The output *CP* y_{θ_i}, gives a fuzzy description of the angle formed by the vector given by the sensor i and the horizontal plane $(\theta_i^{'} \in [-90^o, 90^o],\ i \in [1,5])$. It includes the following set of NL sentences:

$a_{1_{\theta_i}} \rightarrow$ *"The angle of the sensor 'i' is very negative."*
$a_{2_{\theta_i}} \rightarrow$ *"The angle of the sensor 'i' is negative."*
$a_{3_{\theta_i}} \rightarrow$ *"The angle of the sensor 'i' is zero."*
$a_{4_{\theta_i}} \rightarrow$ *"The angle of the sensor 'i' is positive."*
$a_{5_{\theta_i}} \rightarrow$ *"The angle of the sensor 'i' is very positive."*

which can be described by the following template:

$a_{[1:5]_{\theta_i}} \rightarrow$ *"The angle of the sensor 'i' is {very negative | negative | zero | positive |very positive}."*

The validity degrees are obtained from trapezoidal membership functions (see Figure 4.14) that were designed empirically after an important experimental effort, and were tuned according to the criteria of the specific final application. The same happened for the definition of the most suitable set of sentences for describing each *CP*.

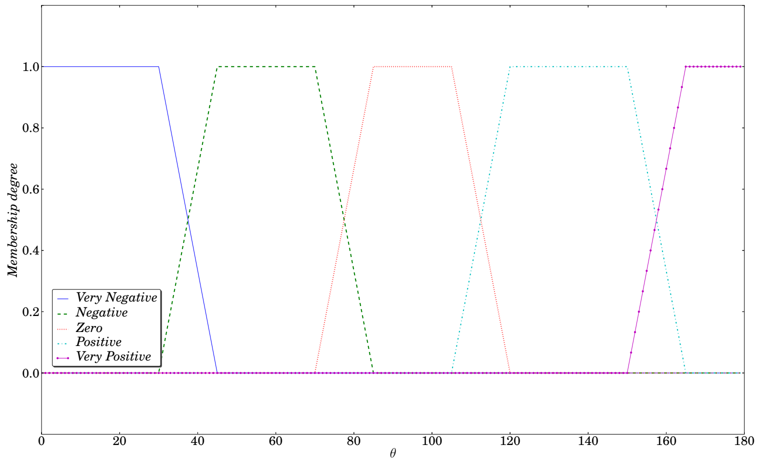

Figure 4.14: Trapezoidal membership function used to calculate the validity degree of the angles.

Derivative of the angle of the sensor $(PM_{d\theta_i})$ It is a 1-*PM* whose input is the numerical value of the derivative of the angle θ_i of the sensor i: ${}^{d\theta_i}/_{dt}$, which is negative when the angle is decreasing, positive when it is increasing and zero when it is kept constant. The output *CP* $y_{d\theta_i}$ gives information about this derivative. The corresponding set of NL sentences is described by the following template:

$a_{[1:3]\frac{d\theta_i}{dt}} \rightarrow$ *"The angle of the sensor 'i' is {decreasing | not varying | increasing}."*

The validity degrees are also calculated by means of trapezoidal membership functions, shown in Figure 4.15.

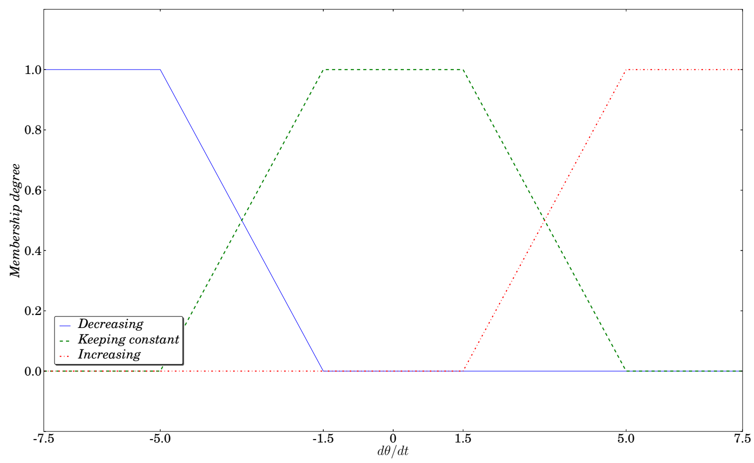

Figure 4.15: Trapezoidal membership functions used to calculate the validity degree of the derivative of the angles.

Time instant level – Pose elements level

It was decided to aggregate the information from the sensors in such a way that the pose of different parts of the body (forearms, back waist and calves) and their movement could be described. This level is formed by 2-PMs whose inputs are the outputs of the 1-PMs of the level below: CP_{θ_1}, CP_{θ_2}, CP_{θ_3}, CP_{θ_4}, CP_{θ_5}, $CP_{d\theta_1}$, $CP_{d\theta_2}$, $CP_{d\theta_3}$, $CP_{d\theta_4}$ and $CP_{d\theta_5}$. In particular, PM_F, PM_B and PM_C use the CPs related to the angles to describe the poses of the forearms, the back waist and the calves. On the other side, PM_{FM}, PM_{BM} and PM_{CM} have as inputs the CPs related to the derivatives of the angles of the sensors to describe the movements of these parts of the body. These PMs allow to specify intermediate fuzzy variables that will simplify later the rules of the FFSM in the upper level.

***Forearms pose** (PM_F)* The PM_F has two inputs: the two CPs corresponding to the angles of the sensors on both forearms which provide an output CP y_F with information about the forearms pose, as shown in Table 4.2. Next to each NL description, the associated variable is indicated.

Sentence	Forearms pose	Associated variables
a_{1_F}	*Straight*	$a_{5_{\theta_1}}$ AND $a_{5_{\theta_2}}$
a_{2_F}	*Mountain*	$a_{2_{\theta_1}}$ AND $a_{2_{\theta_2}}$
a_{3_F}	*Overhead*	$(a_{1_{\theta_1}}$ OR $a_{2_{\theta_1}})$ AND $(a_{1_{\theta_2}}$ OR $a_{2_{\theta_2}})$

Table 4.2: Forearms poses for the output CP y_F and related variables.

These conditions result in the following set of sentences:

$a_{1_F} \rightarrow$ *"The forearms are in straight pose."*
$a_{2_F} \rightarrow$ *"The forearms are in mountain pose."*
$a_{3_F} \rightarrow$ *"The forearms are in overhead pose."*

Being the associated template:

$a_{[1:3]_F} \rightarrow$ *"The forearms are in {straight | mountain | overhead} pose."*

Figure 4.16 shows the space where the forearms poses are defined considering the membership functions of the angles of sensors 1 and 2.

***Back waist pose** (PM_B)* The PM_B has just one input, the CP corresponding to the angle of the sensor in the back waist. Its main purpose is to provide a more descriptive output, CP y_F, indicating the back waist pose, as shown in Table 4.3. The corresponding set of NL sentences is described by the following template:

$a_{[1:3]_B} \rightarrow$ *"The back waist is in {straight | bending backward | bending forward} pose."*

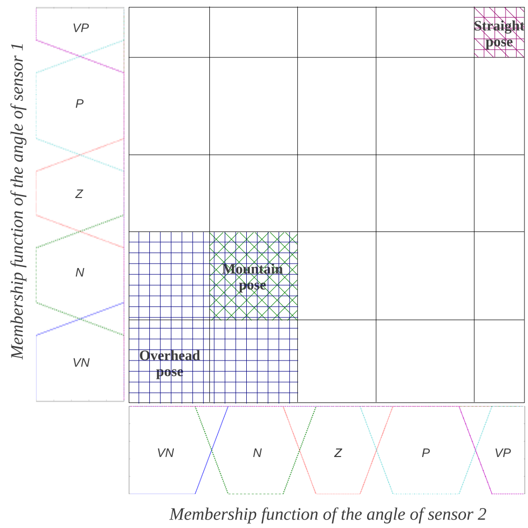

Figure 4.16: Space where the forearms poses are defined.

Sentence	Back waist pose	Associated variables
a_{1_B}	*Straight*	$a_{5_{\theta_3}}$
a_{2_B}	*Bending backward*	$a_{4_{\theta_3}}$ OR $a_{5_{\theta_3}}$
a_{3_B}	*Bending forward*	$a_{2_{\theta_3}}$ OR $a_{3_{\theta_3}}$

Table 4.3: Back waist poses for the output CP y_B and related variables.

***Calves pose** (PM_C)* Table 4.4 shows the NL description of the calves pose and the corresponding intermediate variables, provided by the PM_C by using the CPs corresponding to the angles of the sensors on both calves.
The associated template for its NL sentences is the following one:

$a_{[1:2]_C} \rightarrow$ *"The calves are in {straight | bending backward} pose."*

***Forearms movement** (PM_{FM})* By combining the information of the derivatives of the angles corresponding to the sensors of the forearms, PM_{FM} provides an output CP describing their movement, as shown in Table 4.5.

Sentence	Calves pose	Associated variables
a_{1_C}	*Straight*	$a_{5_{\theta_4}}$ AND $a_{5_{\theta_5}}$
a_{2_C}	*Bending backward*	$(a_{4_{\theta_4}}$ OR $a_{5_{\theta_4}})$ AND $(a_{4_{\theta_5}}$ OR $a_{5_{\theta_5}})$

Table 4.4: Calves poses for the output *CP* y_C and related variables.

Sentence	Forearms movement	Associated variables
$a_{1_{FM}}$	*Not moving*	$a_{2_{d\theta_1}}$ AND $a_{2_{d\theta_2}}$
$a_{2_{FM}}$	*Moving up*	$a_{1_{d\theta_1}}$ AND $a_{1_{d\theta_2}}$
$a_{3_{FM}}$	*Moving down*	$a_{3_{d\theta_1}}$ AND $a_{3_{d\theta_2}}$

Table 4.5: Forearms movement for the output *CP* y_{FM} and related variables.

Its template for the NL sentences is:

$a_{[1:3]_{FM}} \rightarrow$ *"The forearms are {not moving | moving up | moving down}."*

Back waist movement (PM_{BM}) PM_{BM} provides a description of the movement of the back waist by interpreting the *CP* related to the derivative of the angle of the sensor attached to it. Table 4.6 shows its output *CP* y_{BM} and the variables related to it.

Sentence	Back waist movement	Associated variables
$a_{1_{BM}}$	*Not moving*	$a_{2_{d\theta_3}}$
$a_{2_{BM}}$	*Moving backwards*	$a_{2_{d\theta_3}}$ OR $a_{3_{d\theta_3}}$
$a_{3_{BM}}$	*Moving forwards*	$a_{1_{d\theta_3}}$

Table 4.6: Back waist movement for the output *CP* y_{BM} and related variables.

This results in the following template:

$a_{[1:3]_{FM}} \rightarrow$ *"The back waist is {not moving | moving backwards | moving forwards}."*

Calves movement ***(PM_{CM})*** The last PM in this level provides information of the calves movement, as shown in Table 4.7.

Sentence	Calves movement	Associated variables
$a_{1_{CM}}$	*Not moving*	$a_{2_{d\theta_4}}$ AND $a_{2_{d\theta_5}}$
$a_{2_{CM}}$	*Moving to "bending backward pose"*	$(a_{1_{d\theta_4}}$ OR $a_{2_{d\theta_4}})$ AND $(a_{1_{d\theta_5}}$ OR $a_{2_{d\theta_5}})$

Table 4.7: Calves movement for the output CP y_{CM} and related variables.

The template below describes its set of NL sentences:

$a_{[1:2]_{CM}} \rightarrow$ *"The calves are {not moving | moving to "bending backward pose"}."*

Time instant level – Pose recognition level

This level allows to recognize the pose at each time instant by using a *special PM*, based on a FFSM, described below.

Pose ***(PM_{pose})*** This 2-PM, whose inputs are the outputs of the PMs of the level below it (PM_F, PM_B, PM_C, PM_{FM}, PM_{BM} and PM_{CM}), defines the elements of a pose. The output CP y_{pose} includes the following set of NL sentences:

$a_{0_{pose}} \rightarrow$ *"The current pose is 0: standing with arms falling in relaxed position."*
$a_{1_{pose}} \rightarrow$ *"The current pose is 1: standing with hands in mountain pose."*
$a_{2_{pose}} \rightarrow$ *"The current pose is 2: standing raising hands overhead."*
$a_{3_{pose}} \rightarrow$ *"The current pose is 3: standing forward fold, hands next to feet."*
$a_{4_{pose}} \rightarrow$ *"The current pose is 4: standing raising hands overhead."*
$a_{5_{pose}} \rightarrow$ *"The current pose is 5: standing with hands in mountain pose."*

The aggregation function (g_{pose}) calculates, at each time instant, the next value of the validity degrees for each sentence based on the previous validity degrees and current input CPs, the intermediate fuzzy variables described above. The aggregation function is, therefore, an expert knowledge-based FFSM.

The two main techniques used for human activity or behaviour recognition are template matching approaches [294] and state-space models [295]. The main advantage of using the template matching technique is its low computational cost. However, it is sensitive to noise and the time interval of the movements. On the other hand, state-space approaches overcome these drawbacks by defining each static posture as a state, although involving iterative computation, to predict, estimate and detect time series over a long period of time [1]. Following this technique, the application of FFSMs to model a series of poses corresponding to the Sun Salutation exercise is explored.

The concept of the traditional Finite State Machines (FSMs) can be extended using fuzzy logic [296], therefore, the FFSMs instead of processing crisp symbols, use fuzzy values both in the input and the output. This technique was first used for the analysis of quasi-periodic signals in [297] and, afterwards, applied to human body posture recognition [33] and human gait modelling [36]. Here, the complexity is increased by fusing information from various sensors to model an exercise which involves the movement of several body parts. A more detailed description of this paradigm and its applications can be found in [298, 299]. In general, a FFSM is described as a tuple $\{Q, S, U, Y, f, g\}$ where:

- $Q = \{q_0, q_1, q_2, \ldots, q_n\}$ is the set of n fuzzy states of the system.
- $S = \{s_0, s_1, s_2, \ldots, s_n\}$, with $s_i \in [0, 1]$, is the state activation vector which represents the state of the FFSM. It stores, in each of its components, the activation degree of the different states, considering that the system is always in a known state (see Equation 4.1).

$$\sum_{i=0}^{n} s_i = 1 \tag{4.1}$$

- $U = \{u_0, u_1, u_2, \ldots, u_n\}$ is the input vector of the system, *i.e.*, the set of fuzzy input variables.
- $Y = \{y_0, y_1, y_2, \ldots, y_n\}$ is the output vector. It is a summary of the relevant characteristics of the system while it remains in each state.

- f is the state transition function that calculates, at each instant of time, the next value of the state activation vector: $S[t+1] = f(U[t], S[t])$.
- g is the output function that calculates the set of output vectors of the system: $Y[t] = g(U[t], S[t])$.

Both the state transition function and the output function can be represented using fuzzy rules.

Figure 4.17 represents the state diagram of the FFSM designed for the reduced cycle of the Sun Salutation (an initial version of this FFSM has been published in [300]). This state diagram allows one to recognize the different poses depending on the PMs aggregated on PM_{pose}.

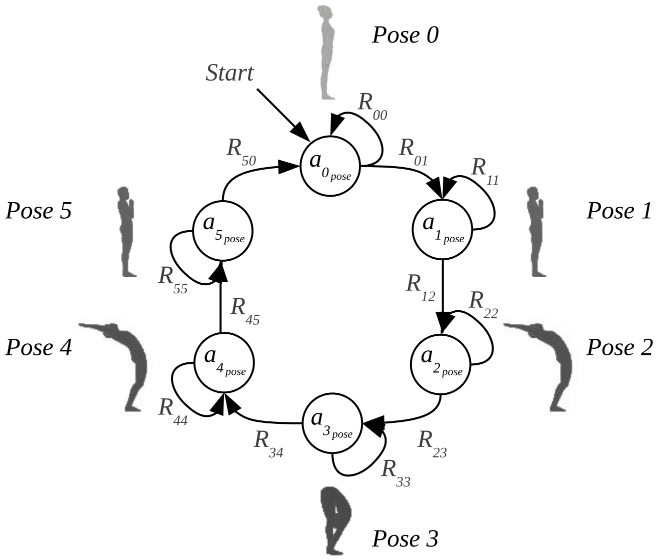

Figure 4.17: State diagram of the FFSM for the reduced cycle of the Sun Salutation.

The state transition function of the FFSM is implemented by using a set of zero-order Takagi-Sugeno-Kang (TSK) inference rules [301], distinguishing between rules to remain in each pose i ($R_{i \to i}$) and rules to change from one pose i to another pose j ($R_{i \to j}$). Due to the characteristics of the reduced Sun Salutation exercise and according to the state diagram previously shown in Figure 4.17, there are 12 fuzzy rules in total in the system, 6 rules to remain in each pose and other 6 to change between poses. The pose 0 was chosen as the initial one, *i.e.*, $w_{0_{pose}}$ has initially a value equal to 1. In this way, the FFSM will synchronize with the Sun Salutation exercise when the requirements for being in that pose are fulfilled, without the need of doing any previous segmentation of the signal. In this work, the set of fuzzy rules of the FFSM has been set up experimentally using the available expert knowledge about the Sun Salutation sequence. However, it is interesting to mention that in [33, 36] an automatic method for learning the model parameters is described, based on the hybridization of Fuzzy Finite State Machines and Genetic Algorithms leading to Genetic Fuzzy Finite State Machines. The rule base of g_{pose} is as follows:

$R_{0\to0}$: IF $a_{0_{pose}}$ AND a_{1_F} AND a_{1_B} AND a_{1_C} AND $a_{1_{FM}}$ AND $a_{1_{BM}}$ AND $a_{1_{CM}}$ THEN $a_{0_{pose}}$
$R_{1\to1}$: IF $a_{1_{pose}}$ AND a_{2_F} AND a_{1_B} AND a_{1_C} AND $a_{1_{FM}}$ AND $a_{1_{BM}}$ AND $a_{1_{CM}}$ THEN $a_{1_{pose}}$
$R_{2\to2}$: IF $a_{2_{pose}}$ AND a_{3_F} AND a_{2_B} AND a_{2_C} AND $a_{1_{FM}}$ AND $a_{1_{BM}}$ AND $a_{1_{CM}}$ THEN $a_{2_{pose}}$
$R_{3\to3}$: IF $a_{3_{pose}}$ AND a_{1_F} AND a_{3_B} AND a_{1_C} AND $a_{1_{FM}}$ AND $a_{1_{BM}}$ AND $a_{1_{CM}}$ THEN $a_{3_{pose}}$
$R_{4\to4}$: IF $a_{4_{pose}}$ AND a_{3_F} AND a_{2_B} AND a_{2_C} AND $a_{1_{FM}}$ AND $a_{1_{BM}}$ AND $a_{1_{Cm}}$ THEN $a_{4_{pose}}$
$R_{5\to5}$: IF $a_{5_{pose}}$ AND a_{2_F} AND a_{1_B} AND a_{1_C} AND $a_{1_{FM}}$ AND $a_{1_{BM}}$ AND $a_{1_{CM}}$ THEN $a_{5_{pose}}$
$R_{0\to1}$: IF $a_{0_{pose}}$ AND a_{2_F} AND a_{1_B} AND a_{1_C} AND $a_{2_{FM}}$ AND $a_{1_{BM}}$ AND $a_{1_{CM}}$ AND $T_{move_0}(d_0)$ THEN $a_{1_{pose}}$
$R_{1\to2}$: IF $a_{1_{pose}}$ AND a_{3_F} AND a_{2_B} AND a_{2_C} AND $a_{2_{FM}}$ AND $a_{2_{BM}}$ AND $a_{2_{CM}}$ AND $T_{move_1}(d_1)$ THEN $a_{2_{pose}}$
$R_{2\to3}$: IF $a_{2_{pose}}$ AND a_{1_F} AND a_{3_B} AND a_{1_C} AND $a_{3_{FM}}$ AND $a_{3_{BM}}$ AND $a_{1_{CM}}$ AND $T_{move_2}(d_2)$ THEN $a_{3_{pose}}$
$R_{3\to4}$: IF $a_{3_{pose}}$ AND a_{3_F} AND a_{2_B} AND a_{2_C} AND $a_{2_{FM}}$ AND $a_{2_{BM}}$ AND $a_{2_{CM}}$ AND $T_{move_3}(d_3)$ THEN $a_{4_{pose}}$
$R_{4\to5}$: IF $a_{4_{pose}}$ AND a_{2_F} AND a_{1_B} AND a_{1_C} AND $a_{3_{FM}}$ AND $a_{1_{BM}}$ AND $a_{1_{CM}}$ AND $T_{move_4}(d_4)$ THEN $a_{5_{pose}}$
$R_{5\to0}$: IF $a_{5_{pose}}$ AND a_{1_F} AND a_{1_B} AND a_{1_C} AND $a_{3_{FM}}$ AND $a_{1_{BM}}$ AND $a_{2_{CM}}$ AND $T_{move_5}(d_5)$ THEN $a_{0_{pose}}$

where:

- The first term in the antecedent computes the previous validity degree of the sentence $a_{i_{pose}}$, *i.e.*, $w_{i_{pose}}$. With this mechanism, the FFSM is only allowed to move from the pose i to the pose j (or to remain in pose i, when $i = j$). For example, $R_{0\to 0}$ computes the validity degree of the sentence *"The current pose is 0: standing with arms falling in relaxed position"* ($w_{0_{pose}}$).

- The second, third and fourth terms in the antecedents describe the constraints imposed on the positions of the forearms, the back and the calves, respectively. For example, in the case of the second antecedent, related with the position of the forearms, it computes the validity degree of one or various of the three possible sentences that this *CP* (u_F) has, *e.g.*, *"The forearms are in mountain pose"* (w_{2_F}).
- The fifth, sixth and seventh terms in the antecedents describe the constraints imposed on the movement of the forearms, the back and the calves, respectively. For example, in the case of the fifth antecedent, related with the movement of the forearms, it computes the validity degree of one or various of the three possible sentences that this *CP* (u_{FM}) has, *e.g.*, *"The forearms are moving down"* ($w_{2_{FM}}$).
- The eighth term in the antecedent, if present, describes the conditions that constrain the poses duration. To control the duration d_i of each pose a linguistic label is defined for each pose i: T_{move_i} (which is the minimum time that the pose i is expected to lasts before changing to pose j). For example, in $R_{1\to 2}$, the membership degree of d_1 to the linguistic label T_{move} is calculated. To calculate the duration of each pose d_i, Equation 4.2, which weights the duration of each pose with its validity degree $w_{i_{pose}}$, is used:

$$d_i[t] = \begin{cases} 0 & \text{if } w_{i_{pose}}[t] = 0 \\ d_i[t-1] + w_{i_{pose}}[t] \cdot T_s & \text{otherwise} \end{cases} \tag{4.2}$$

being $T_s = {}^1/_{f_s}$ the inverse of the sampling frequency (160Hz), which corresponds to the sampling period, 6.25ms.

Figure 4.18 shows an example of the linguistic label T_{move} used to define the temporal constraints for moving from one state to another. In agreement with the knowledge about the Sun Salutation, each pose is assigned a duration between 3 s and 15 s.

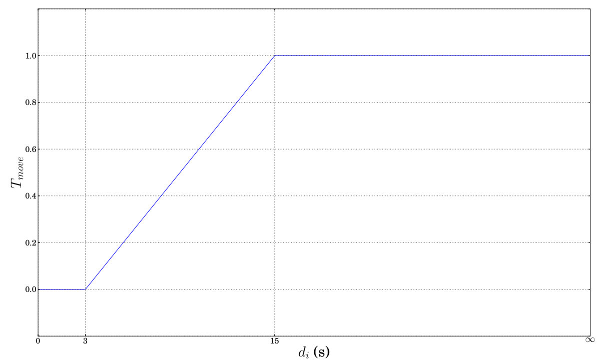

Figure 4.18: Temporal condition for T_{move}.

- Finally, the consequent of the rule defines the next pose. To calculate the validity degrees of the sentences associated with each pose j ($w_{j_{pose}}$), a weighted average using the firing degree of each rule R_{ij} (ϕ_{ij}) is computed as defined in Equation 4.3:

$$w_{j_{pose}} = \frac{\sum\limits_{i=0}^{5} \phi_{ij}}{\sum\limits_{i=0}^{5} \sum\limits_{j=0}^{5} \phi_{ij}} \tag{4.3}$$

  where (ϕ_{ij}) is calculated using the minimum for the AND operator and the bounded sum of Łukasiewicz [302] for the OR operator.

Note that each rule of this set is a complete linguistic expression as can be seen in the following expanded expression of the rule R_{44} to remain in pose 4: *"If the previous pose is 4, standing raising hands overhead, and the forearms are in overhead pose, and the back and the calves are bending backward, and none of them are moving, then the current pose is 4, standing raising hands overhead"*.

The output of the FFSM contains the activation degree of every state at each instant in time, which means providing information related to pose recognition. As an example of the performance of the proposal for the reduced Sun Salutation sequence, Figure 4.19 represents the validity degrees of the sentences associated to each pose together with the angles and their derivatives of each sensor (θ_i and ${}^{d\theta_i}/_{dt}$, respectively). It shows how this set of fuzzy rules is able to model and recognize the six poses of the selected sequence of positions.

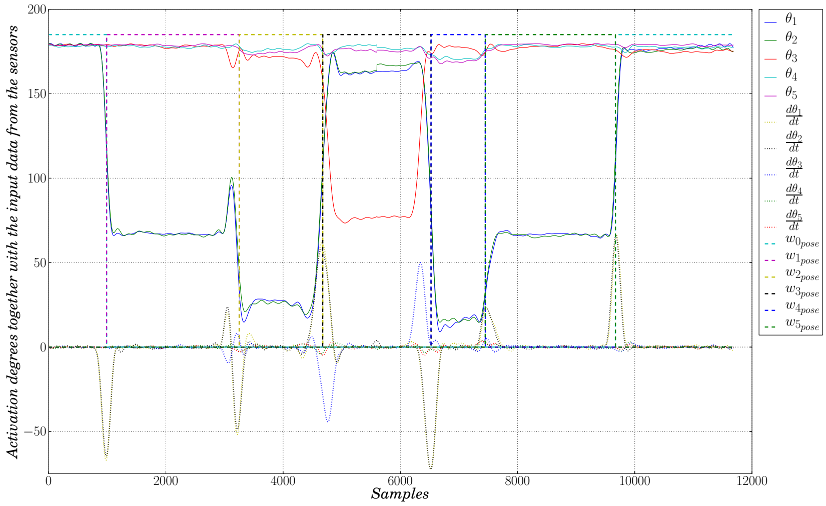

Figure 4.19: Graphical representation of the validity degrees of each sentence together with the evolution of angles and their derivatives for each one of the sensors (θ_i and ${}^{\mathrm{d}\theta_i}/_{\mathrm{d}t}$, respectively).

From this analysis, a preliminary feedback can be given to the user, with information about the duration of the poses and the whole exercise [81]. The duration refers to the amount of time during which each pose is recognized by the FFSM as the active pose. Table 4.8 shows the results obtained for each subject, reporting the average values and the corresponding standard deviation computed over the four datasets, for each of the sun salutation poses (state q_0 is not included as it is related to the calibration pose). The last two columns summarize the average and standard deviation for the duration of all the poses and of the whole exercise. As can be seen, in general, the duration of state q_4 is significantly shorter than that of the other states. This pose is considered the *most complex* of the sequence and, therefore, it is more difficult to maintain for a long period of time. The average duration of the poses and its standard deviation measure how uniformly the subject is performing the exercise, while the values referred to the whole exercise measure the homogeneity among different exercises performed by the same user. For example, Subject 2 performs the exercise at a smooth pace, but there are significant differences between the executions and even among the poses. Instead, Subject 6 performs the Sun Salutation with a more uniform duration of the poses and the various sequences present small differences in duration. The statistics show that the external feedback, given to all of the subjects except the two first ones, improves exercise performance because of the unfamiliarity of the subjects with developing a pacing strategy, as suggested in [55].

Pose level

The *PM*s here belong to an upper level of granularity (pose level). Their output *CP*s are calculated for each pose instead of being calculated at each time instant.

Forearms symmetry during the current pose (PM_{FS}) As can be seen in Figure 4.13, PM_{FS} has three *CP*s as inputs: the angle of the sensors on the forearms, 1 and 2, and the current pose, *i.e.*, $U = (u_{\theta_1}, u_{\theta_2}, u_{pose})$. The output *CP* y_{FS} includes the following set of NL sentences:

$a_{[1:3]_{FS}} \rightarrow$ *"The forearms symmetry in pose {i} is {low | medium | high}."*

The validity degrees ($w_{1_{FS}}$, $w_{2_{FS}}$, $w_{3_{FS}}$) are obtained by means of the aggregation function g_{FS}. This function makes use of the Jaccard index [303] as similarity function, which is defined using Equation 4.4, in order to compare the angles of both forearms during the pose. This is done for each instant of time and then averaged over its duration.

$$J(x,y) = \begin{cases} 1 & \text{if x = 0 and y = 0} \\ \frac{\min(x,y)}{\max(x,y)} & \text{otherwise} \end{cases} \tag{4.4}$$

Subject	**Duration of each state**					**Total summary**	
	q_1	q_2	q_3	q_4	q_5	**Pose**	**Exercise**
1	13.32 (0.82)	8.57 (0.40)	11.91 (2.78)	6.93 (1.24)	13.07 (1.08)	**10.75 (2.94)**	**53.80 (3.17)**
2	11.25 (1.38)	8.94 (1.62)	11.38 (1.18)	7.81 (0.82)	14.68 (3.95)	**10.81 (3.06)**	**54.04 (6.98)**
3	7.86 (0.69)	7.85 (0.69)	10.03 (1.91)	0.84 (0.09)	12.83 (4.05)	**7.88 (4.46)**	**39.41 (3.55)**
4	7.71 (0.76)	11.16 (8.64)	6.06 (3.51)	2.88 (2.39)	7.11 (4.94)	**6.98 (5.11)**	**34.92 (3.31)**
5	9.43 (5.03)	7.06 (0.28)	8.69 (1.49)	1.92 (1.47)	8.75 (2.54)	**7.17 (3.69)**	**35.84 (1.25)**
6	6.41 (0.61)	6.32 (0.63)	6.68 (0.46)	5.01 (0.47)	5.52 (0.66)	**5.99 (0.82)**	**29.95 (0.83)**
7	6.84 (1.13)	6.94 (1.02)	7.19 (0.51)	2.43 (1.72)	8.33 (3.09)	**6.35 (2.59)**	**31.73 (3.44)**
8	6.61 (0.21)	6.26 (0.76)	8.16 (0.12)	1.93 (1.78)	9.72 (2.32)	**6.53 (2.94)**	**32.67 (1.56)**
9	6.52 (0.74)	5.91 (0.27)	7.89 (0.69)	6.71 (0.63)	6.43 (0.71)	**6.69 (0.88)**	**33.46 (2.77)**
10	12.80 (0.38)	0.29 (0.10)	7.42 (0.67)	6.25 (0.34)	5.47 (0.51)	**6.44 (4.13)**	**32.22 (1.08)**

Table 4.8: Analysis of poses and exercise duration (mean and, in parenthesis, standard deviation, in seconds).

***Calves symmetry during the current pose** (PM_{CS})* This PM is equivalent to the previous one, but it takes into consideration the angle of the sensors in the calves, sensors 4 and 5, to calculate their symmetry for each pose. Therefore, its three CPs inputs are: the angles of the sensors 4 and 5, and the current pose, *i.e.*, $U = (u_{\theta_4}, u_{\theta_5}, u_{pose})$. The output CP y_{CS} includes the following set of NL sentences:

$a_{[1:3]_{CS}} \rightarrow$ *"The calves symmetry in pose {i} is {low | medium | high}."*

Following the same criteria as in the previous PM, the aggregation function g_{CS} makes use of the Jaccard index for comparing the angles of both calves during each pose.

***Stability during the current pose** (PM_{PST})* In order to give information about the stability, this PM considers the fluctuation of the validity degree of each sentence related to the pose. It is calculated as the average value of the validity degree for the current pose i along its duration (T_i) as shown in Equation 4.5.

$$w_{i_{PST}} = \frac{\sum_{t=0}^{T_i} w_{i_{pose}}[t]}{T_i} \tag{4.5}$$

The output CP y_{PST} includes the following set of NL sentences:

$a_{[1:3]_{PST}} \rightarrow$ *"The stability in pose {i} is {low | medium | high}."*

Sun Salutation sequence level

In Figure 4.13, these CPs are calculated for a complete sequence of the Sun Salutation instead of being calculated for each pose.

***Forearms symmetry during the Sun Salutation sequence** (PM_{AFS})* This perception mapping is in charge of analyzing the forearms symmetry during the Sun Salutation sequence. It has just one input CP, which corresponds to the lower level forearms symmetry for each pose, so the set is $U = (u_{FS})$. This PM includes a set of three NL sentences in its output *CP* (y_{AFS}) following the template below:

$a_{[1:3]_{AFS}} \rightarrow$ *"The forearms symmetry during the Sun Salutation is {low | medium | high}."*

The aggregation function (g_{AFS}) calculates the validity degree ($w_{i_{AFS}}$) of each sentence as shown in Equation 4.6:

$$w_{i_{AFS}} = \frac{\sum_{k=1}^{P} w_{i_{FS}}[k]}{P} \tag{4.6}$$

where *P* is the total number of poses, six in the case of the reduced version of the Sun Salutation sequence.

Calves symmetry during the Sun Salutation sequence (PM_{ACS}) This *PM* is equivalent to the previous one, but it analyses the calves symmetry during the Sun Salutation sequence, instead of the forearms symmetry. The input *CP* included in its set, $U = (u_{ACS})$, corresponds to the calves symmetry for each pose. Its set of three NL sentences in its output *CP* (y_{ACS}) is described by the following template:

$a_{[1:3]_{ACS}} \rightarrow$ *"The calves symmetry during the Sun Salutation is {low | medium | high}."*

Similarly to the previous *PM*, the equivalent aggregation function g_{ACS} calculates the validity degree of each sentence.

Duration of the Sun Salutation sequence (PM_D) This *PM* makes use of the duration of each pose (d_i) calculated using Equation 4.2 to estimate the total duration of the exercise, its output *CP* (y_D) being a set of three NL sentences defined by the template below:

$a_{[1:3]_D} \rightarrow$ *"The Sun Salutation has a {low | medium | high} duration."*

Variability of the duration of the Sun Salutation sequence (PM_{σ_D}) On the other hand, this *PM* provides information of the variability of the duration of the Sun Salutation sequence by considering the standard deviation of the duration of the individual poses. Its output is defined as follows:

$a_{[1:3]_{\sigma_D}} \rightarrow$ *"The variability of the duration of the Sun Salutation is {low | medium | high}."*

Symmetry during the Sun Salutation sequence (PM_S) This *PM* has two *CP*s as inputs: the symmetry of the forearms and the symmetry of the calves. Therefore, the set of input *CP*s is $U = (u_{AFS}, u_{ACS})$. This *PM* includes a set of three NL sentences in its output *CP* (y_S) following the template below:

$a_{[1:3]_S} \rightarrow$ *"The symmetry of the Sun Salutation is {low | medium | high}."*

The aggregation function (g_S) calculates the validity degrees (w_{i_S}) for each sentence. This function is defined by Equation 4.7, which calculates the average value of each pair of validity degrees of the input *CP*s associated with a low, medium, and high symmetry:

$$w_{i_S} = \frac{w_{i_{AFS}} + w_{i_{ACS}}}{2} \tag{4.7}$$

Stability during the Sun Salutation sequence (PM_{ST}) This *PM* has one *CP* as input: the stability of the poses along the Sun Salutation sequence. Therefore, the set of input *CP*s is $U = (u_{PST})$. This *PM* has a set of three NL sentences as output *CP* (y_{ST}) which are defined by the template below:

$a_{[1:3]_{ST}} \rightarrow$ *"The stability during the Sun Salutation is {low | medium | high}."*

The aggregation function (g_{ST}) calculates the validity degrees ($w_{i_{ST}}$) for each sentence. This function is defined by Equation 4.8, which calculates the average value of the three validity degrees of the input *CP*s associated with a low, medium, and high stability considering the values obtained previously for each of the poses:

$$w_{i_{ST}} = \frac{\sum_{k=1}^{P} w_{i_{PST}}[k]}{P} \tag{4.8}$$

being P the total number of poses of the reduced version of the Sun Salutation sequence.

Rhythm during the Sun Salutation sequence ***(PM_R)*** This *PM* makes use of the *CP*s corresponding to the duration of the Sun Salutation exercise and its variability between the poses. The output *CP* (y_R) of this *PM* includes a set of three NL sentences defined by the template below:

$a_{[1:3]_R} \rightarrow$ *"The rhythm of the Sun Salutation is {variable | adequate | optimal}."*

The aggregation function (g_R) is an expert knowledge based Fuzzy Rule-Based System (FRBS). Considering the three different sentences for each of the inputs, there are 9 different rules obtained when combining them:

R_1: IF a_{1_D} AND $a_{1_{\sigma_D}}$ THEN a_{2_R}
R_2: IF a_{2_D} AND $a_{1_{\sigma_D}}$ THEN a_{3_R}
R_3: IF a_{3_D} AND $a_{1_{\sigma_D}}$ THEN a_{2_R}
R_4: IF a_{1_D} AND $a_{2_{\sigma_D}}$ THEN a_{1_R}
R_5: IF a_{2_D} AND $a_{2_{\sigma_D}}$ THEN a_{2_R}
R_6: IF a_{3_D} AND $a_{2_{\sigma_D}}$ THEN a_{1_R}
R_7: IF a_{1_D} AND $a_{3_{\sigma_D}}$ THEN a_{1_R}
R_8: IF a_{2_D} AND $a_{3_{\sigma_D}}$ THEN a_{1_R}
R_9: IF a_{3_D} AND $a_{3_{\sigma_D}}$ THEN a_{1_R}

Quality of the Sun Salutation sequence ***(PM_Q)*** The top *PM*, PM_Q, has three *CP*s as inputs: the symmetry, the stability and the rhythm obtained from the Sun Salutation performance. Therefore, the set of input *CP*s is $U = (u_S, u_{ST}, u_R)$. Five different levels of quality are defined: very low, low, medium, high, and very high. Therefore, the output *CP* y_Q is a set of five possible sentences defined by the following template:

$a_{[1:5]_Q} \rightarrow$ *"The quality of the Sun Salutation execution is {very low | low | medium | high | very high}."*

The aggregation function (g_Q) in this case is also an expert knowledge FRBS. The combination of all possible values for each input would give a total of $3^3 = 27$ rules. After a rule simplification process according to [304, 305], the following 19 ones were obtained:

R_1: IF a_{1_S} AND $a_{1_{ST}}$ AND NOT a_{3_R} THEN a_{1_Q}
R_2: IF a_{1_S} AND $a_{2_{ST}}$ AND a_{1_R} THEN a_{1_Q}
R_3: IF a_{2_S} AND $a_{1_{ST}}$ AND a_{1_R} THEN a_{1_Q}
R_4: IF a_{1_S} AND $a_{1_{ST}}$ AND a_{3_R} THEN a_{2_Q}
R_5: IF a_{1_S} AND $a_{3_{ST}}$ AND a_{1_R} THEN a_{2_Q}
R_6: IF a_{3_S} AND $a_{1_{ST}}$ AND a_{1_R} THEN a_{2_Q}
R_7: IF NOT a_{3_S} AND $a_{2_{ST}}$ AND NOT a_{1_R} THEN a_{3_Q}
R_8: IF NOT a_{3_S} AND $a_{3_{ST}}$ AND a_{2_R} THEN a_{3_Q}
R_9: IF a_{2_S} AND $a_{1_{ST}}$ AND NOT a_{1_R} THEN a_{3_Q}
R_{10}: IF a_{2_S} AND NOT $a_{1_{ST}}$ AND a_{1_R} THEN a_{3_Q}
R_{11}: IF a_{3_S} AND $a_{1_{ST}}$ AND a_{2_R} THEN a_{3_Q}
R_{12}: IF a_{3_S} AND $a_{2_{ST}}$ AND a_{1_R} THEN a_{3_Q}
R_{13}: IF a_{1_S} AND $a_{3_{ST}}$ AND a_{3_R} THEN a_{4_Q}
R_{14}: IF a_{3_S} AND $a_{1_{ST}}$ AND a_{3_R} THEN a_{4_Q}
R_{15}: IF a_{3_S} AND $a_{2_{ST}}$ AND a_{2_R} THEN a_{4_Q}
R_{16}: IF a_{3_S} AND $a_{3_{ST}}$ AND a_{1_R} THEN a_{4_Q}
R_{17}: IF NOT a_{1_S} AND $a_{3_{ST}}$ AND a_{3_R} THEN a_{5_Q}
R_{18}: IF a_{3_S} AND $a_{2_{ST}}$ AND a_{3_R} THEN a_{5_Q}
R_{19}: IF a_{3_S} AND $a_{3_{ST}}$ AND a_{2_R} THEN a_{5_Q}

The consequents of the rules define the Sun Salutation quality. To calculate the validity degrees of the sentences associated to the different levels of the Sun Salutation quality (w_{i_Q}), a weighted average using the firing degree of each rule R_i (ϕ_i) is computed as defined in Equation 4.9:

$$w_{i_Q} = \frac{\phi_i}{\sum_{i=1}^{5} \phi_i} \tag{4.9}$$

Each rule of this set is a complete linguistic expression as can be seen in the following expanded expression of the rule R_{19} that predicts a very high value of the Sun Salutation quality: *"If the symmetry is high, the stability is high and the rhythm is optimal, then the Sun Salutation quality is very high"*.

4.3.3 Experimentation

This section presents the experimental results obtained with this approach. Table 4.9 shows the validity degrees of the sentences associated to the quality of one exercise randomly chosen from each person's among the four test samples. It also shows the validity degrees associated to the symmetry, stability and rhythm. The report provided by the proposed system is generated by using the sentences corresponding to the maximum validity degrees, which are boldfaced. As an example, three different sentences that have been generated are as follows:

- *"The quality of the Sun Salutation execution of subject 5 is medium because the symmetry is high, the stability is high and the rhythm is variable."*
- *"The quality of the Sun Salutation execution of subject 7 is high because the symmetry is high, the stability is high and the rhythm is variable."*
- *"The quality of the Sun Salutation execution of subject 10 is very high because the symmetry is high, the stability is high and the rhythm is adequate."*

It can be seen from the results that the quality of the Sun Salutation execution is always medium or greater, being high for three subjects and very high for six subjects. Their performance is mainly influenced by the rhythm that they maintain during the exercise. Thanks to the hierarchical structure of the GLMP, reports can be provided with a higher level of detail. As an example, in Table 4.10 the validity

Sentence	**Subject** 1	2	3	4	5	6	7	8	9	10
$w1_Q$	0.10	0.00	0.00	0.00	0.07	0.00	0.00	0.00	0.00	0.00
$w2_Q$	0.10	0.00	0.00	0.14	0.07	0.06	0.09	0.00	0.00	0.00
$w3_Q$	0.30	0.15	0.34	0.31	**0.47**	0.08	0.28	0.09	0.09	0.22
$w4_Q$	**0.50**	0.25	0.30	0.23	0.31	**0.86**	**0.59**	0.45	0.00	0.17
$w5_Q$	0.00	**0.60**	**0.36**	**0.32**	0.08	0.00	0.04	**0.46**	**0.91**	**0.61**
$w1_S$	0.00	0.00	0.00	0.26	0.01	0.06	0.10	0.00	0.00	0.00
$w2_S$	0.28	0.09	0.26	0.15	0.21	0.08	0.23	0.05	0.11	0.14
$w3_S$	**0.72**	**0.91**	**0.74**	**0.58**	**0.78**	**0.86**	**0.67**	**0.95**	**0.89**	**0.86**
$w1_{ST}$	0.14	0.00	0.00	0.00	0.17	0.00	0.00	0.00	0.00	0.00
$w2_{ST}$	0.08	0.29	0.00	0.00	0.17	0.00	0.00	0.00	0.00	0.00
$w3_{ST}$	**0.78**	**0.71**	**1.00**	**1.00**	**0.66**	**1.00**	**1.00**	**1.00**	**1.00**	**1.00**
$w1_R$	**1.00**	0.00	0.45	0.42	**0.77**	**1.00**	**0.96**	0.49	0.00	0.22
$w2_R$	0.00	**1.00**	**0.55**	**0.58**	0.23	0.00	0.04	**0.51**	**0.87**	**0.78**
$w3_R$	0.00	0.00	0.00	0.00	0.00	0.00	0.00	0.00	0.13	0.00

Table 4.9: Validity degrees of the sentences associated to the quality of one Sun Salutation sequence performed by the healthy participants.

Subject 5 Sun Salutation sequence lower level			
Sentence	1	2	3
w_{AFS}	0.03	0.41	**0.56**
w_{ACS}	0.00	0.00	**1.00**
w_D	**1.00**	0.00	0.00
w_{σ_D}	0.23	**0.77**	0.00

Table 4.10: Validity degrees of the sentences associated to the Sun Salutation sequence partial level for the exercise performed by Subject 5.

degrees associated to the Sun Salutation sequence partial level performed by Subject 5 are shown. The sentences that explain the symmetry and the rhythm of Subject 5 are as follows:

- *"The symmetry is high because the forearms symmetry is high and the calves symmetry is high."*
- *"The rhythm is variable because the duration of the Sun Salutation is low and the variability of the duration is medium."*

To check why the symmetry of the forearms does not have a very high value for the validity degree, one can descend to the pose level, whose validity degrees are shown in Table 4.11: *"The forearms symmetry is high because the symmetry of poses 0, 1, 2 and 3 is high and the symmetry of poses 4 and 5 is medium"*. At this level, the information of the stability of each pose could also be checked: *"The stability is high because the stability of poses 0, 1, 2 and 3 is high, the stability of pose 4 is medium and the stability of pose 5 is low."*.

Subject 5 Pose level									
Pose	w_{FS}			w_{CS}			w_{PST}		
	1	2	3	1	2	3	1	2	3
0	0.00	0.00	**1.00**	0.00	0.00	**1.00**	0.00	0.00	**1.00**
1	0.00	0.34	**0.66**	0.00	0.00	**1.00**	0.00	0.00	**1.00**
2	0.00	0.31	**0.69**	0.00	0.00	**1.00**	0.00	0.00	**1.00**
3	0.00	0.00	**1.00**	0.00	0.00	**1.00**	0.00	0.00	**1.00**
4	0.15	**0.85**	0.00	0.00	0.00	**1.00**	0.00	**1.00**	0.00
5	0.00	**0.97**	0.03	0.00	0.00	**1.00**	**1.00**	0.00	0.00

Table 4.11: Validity degrees of the sentences associated to the pose level for the exercise performed by Subject 5.

As can be seen, the tool developed provides a useful linguistic assessment of the selected exercise thanks to the interpretability of the computational model created to evaluate its quality, based on its symmetry, stability and rhythm, at different levels of granularity.

4.4 Hybrid neuro-fuzzy system

The artificial intelligence techniques based on fuzzy logic and artificial neural networks may be applied together in order to come out of the difficulties and inherent limitations of each of them [306]. While the fuzzy systems are able to represent inherent uncertainties of the human knowledge with linguistic variables and provide an easy interpretation of the results, they first depend on an expert to determine the inference logical rules, then they are not capable of generalizing. On the other hand, the main advantages of neural networks are their learning and generalization capacity, while causing a more difficult interpretation of the results. When used together in a combined way, they are called neuro-fuzzy systems.

Neuro-fuzzy systems have already been used in the medical field: for the characterization of movements [307], for designing a decision-support system for prognosis in stroke rehabilitative therapy [308], for extraction of angular information to predict ankle trajectories [309] and to “discover” relationships between fluctuation, treatment and disease severity in Parkinson [310], among other applications.

The approach to data analysis presented in this section is based on a neuro-fuzzy system for providing a linguistic description of the postural balance. Balance is defined as the ability of the body to statically and dynamically stabilize against resisting intrinsic and extrinsic forces. This system is focused on postural balance assessment due to its importance in physical therapies. For instance, in [79], balance retraining is included in conventional physical therapy following acute stroke. Deficits in balance and postural control are highly correlated with falls risk in elderly adults, since stroke patients are prone to particularly high risk of falling, too. This is the reason why several studies are focused on balance training and postural response assessment [311, 312, 313]. In [314], the results showed that balance training was beneficial for patients after hemiplegic stroke. In addition, it was found that the dynamic balance function showed significant improvements in patients with visual feedback training when compared with those receiving conventional therapy only. Similarly, the study done in [315] suggests that subjects receiving visual feedback within the rehabilitation program showed after 2 weeks better postural control than those receiving standard physiotherapy rehabilitation, while in [316] it is also concluded that visual feedback can enhance patients' balance performance.

The architecture of the proposed neuro-fuzzy system for assessing postural balance during the performance of the Sun Salutation exercise is shown in Figure 4.20.

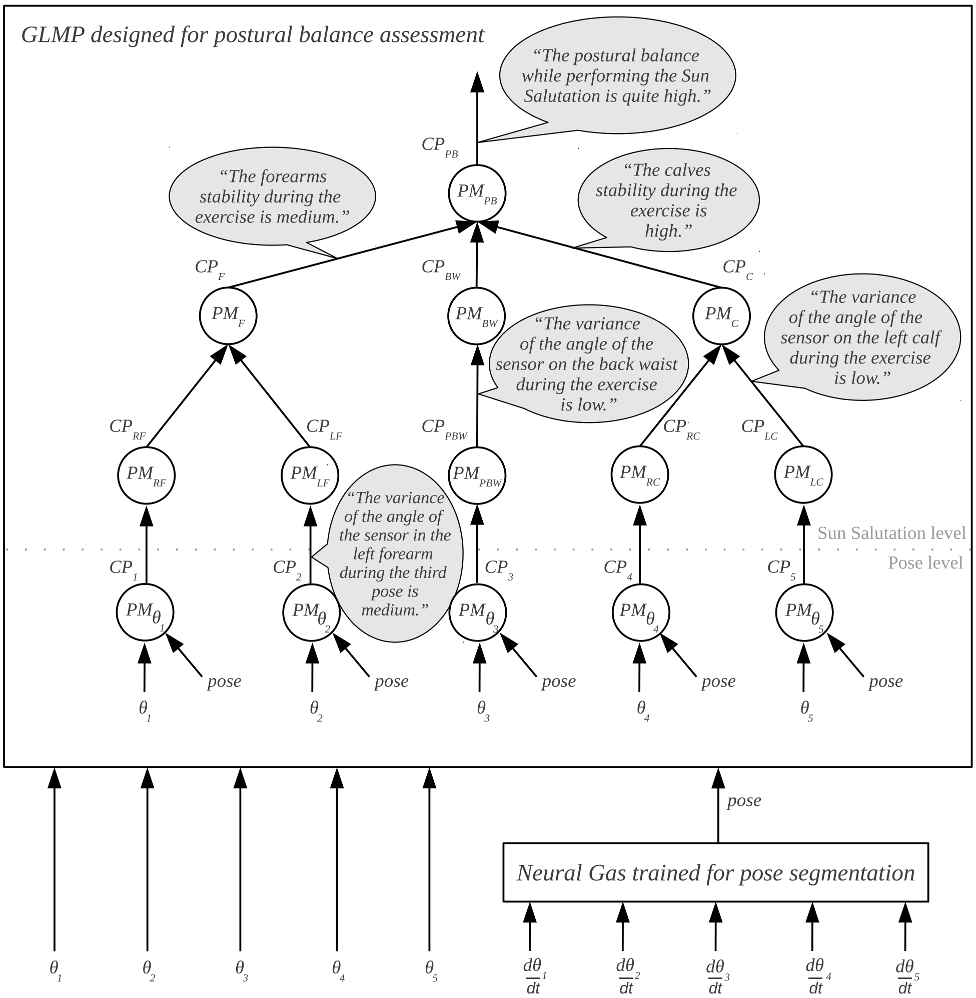

Figure 4.20: Proposed hybrid neuro-fuzzy system for postural balance assessment.

The artificial neural network has been implemented by using a neural gas for low-level perception and signal integration, exploiting its ability to recognize patterns, while the higher levels of the proposed network are based on the Granular Linguistic Model of a Phenomenon (GLMP), already introduced before, used for the reasoning aspects, since it is good at dealing with imprecision and at explaining the phenomena.

Combining both techniques in an intelligent hybrid system allows one to overcome their individual limitations while merging their advantages. In the proposed scheme both systems work independently, *i.e.*, the interaction between them occurs through data transfer. It is not a cooperative model, as in the case of cooperative neuro-fuzzy system where the artificial neural networks are used during a pre-processing phase to determine membership functions or fuzzy rules of the fuzzy inference system [317], but it could rather be considered a concurrent neuro-fuzzy system where both parts work continuously together with the neural network pre-processing the inputs of the fuzzy system.

The data input to the system include both the angle of the sensors with respect to the Z axis $(\theta_1, \theta_2, \theta_3, \theta_4, \theta_5)$, and the corresponding derivatives $\left({}^{d\theta_1}/_{dt}, {}^{d\theta_2}/_{dt}, {}^{d\theta_3}/_{dt}, {}^{d\theta_4}/_{dt}, {}^{d\theta_5}/_{dt}\right)$. During the initial phase of a rehabilitation therapy, it is not expected that the subject performs perfectly a specific posture, but, in the case of analysing her/his postural balance it is sufficient to see if she/he is capable of maintaining a pose for a few seconds. This is the reason why the neural gas network is trained here just with the derivatives, to recognize and differentiate between the poses and the transitions, without identifying each specific pose, which can be however correlated with the information provided by the video captured with Kinect. This network feeds the higher level with the information about the poses, their location in the sequence of data. The upper level, based on the GLMP, has been designed to take into consideration these data, plus the angles, fusing and interpreting them in order to provide a linguistic description of the postural balance while the person is performing the exercise.

4.4.1 Neural gas network for pose segmentation

The Self-Growing and Self-Organized Neural Gas (SGONG) has been chosen as neural gas algorithm to be part of the network due to its capacity to automatically adapt the number of output neurons to represent the input data. The architecture chosen for this reduced hMPF scheme is the one shown previously in Figure 4.6(a). But, in this case, it has been trained with data from the derivatives of the angles of the sensors acquired while the person was performing the Sun Salutation. The neural gas was intensively trained by using 8 different datasets. At the end of the training process, the network had 15 neurons aimed at describing the input data. Figure 4.21 shows, on the bottom left side, the input data provided during the test process, and, on the top right side, the output provided by the neural gas. The numbers, corresponding to the winner neuron ID, allows one to classify if the sample data corresponds to a transition or a pose (ID = 10). The right part of the figure shows the spatial topology of the network, where the colours of the neurons are associated to their corresponding activation degrees for the current data sample.

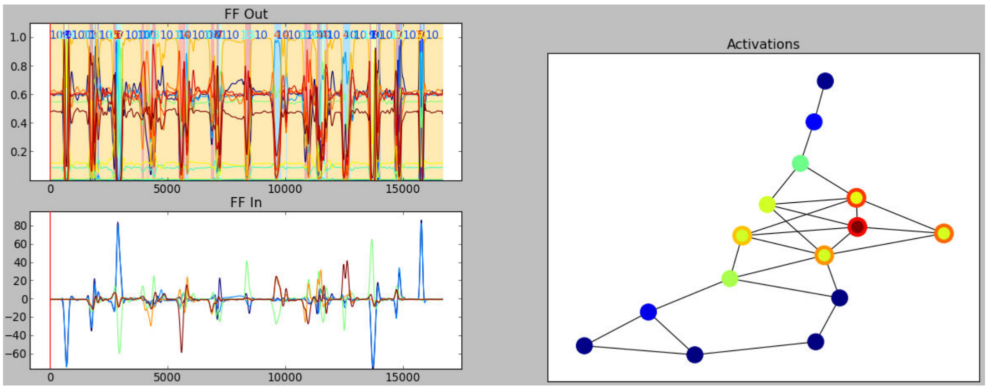

Figure 4.21: Input and output data with the network topology.

Figure 4.22 shows the input data together with the segmentation provided by the neural gas algorithm for one of the Sun Salutation sequences performed by Subject 8. This segmentation of the signals allows to indicate to the GLMP where to find the poses within the data in order to analyse them without taking into consideration the transitions, as this study is based on the capacity of the subject to stabilize a position for a few seconds.

In order to evaluate if the poses had been correctly segmented by using this

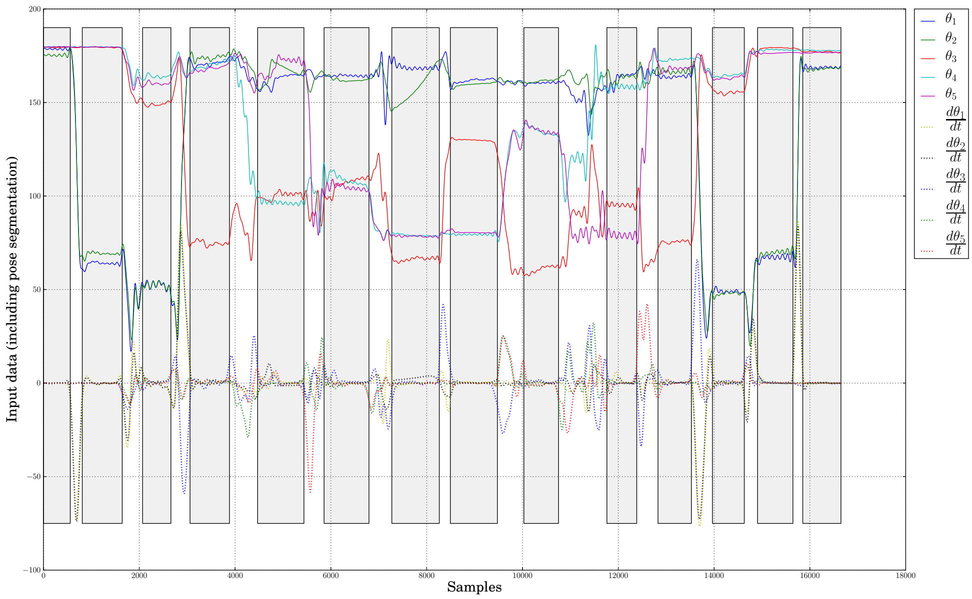

Figure 4.22: Input data with the segmentation given by the neural gas for Subject 8.

approach, the results were compared to three manually segmented sequences of data. Table 4.12 shows the comparison for each of the three datasets with respect both to the poses and the transitions.

Expert segmentation	**Neural gas segmentation (%)**					
	Dataset 1		Dataset 2		Dataset 3	
	Pose	*Trans.*	*Pose*	*Trans.*	*Pose*	*Trans.*
Pose	100.00	0.00	100.00	0.00	100.00	0.00
Transition	24.66	75.34	22.15	77.85	37.05	62.95

Table 4.12: Segmentation comparison among the results of the neural gas and the expert manual segmentation.

As can be seen, the poses were correctly identified in the 100% of the instances. The transitions, however, had a recognition rate among 62.95% and 75.34%. This means that this model is more restrictive than the expert classification, *i.e.*, it considers that the transitions are shorter by taking into account the derivatives information with a lower "virtual" threshold. However, this approach is still valid for being used in the current proposal. Once the poses are segmented, with the aim to analyse just that part of the signal in order to assess at the highest level the postural balance of the subject, the data taken into consideration will correspond to the central 80% of the poses segmented, giving the subject the required time to stabilize the acquired posture.

4.4.2 GLMP designed for postural balance assessment

In this section, each of the *PM*s which conform the GLMP designed for postural balance assessment is explained. In this approach, the analysis of the postural balance is based on the stability of the forearms, the back waist and the calves. While in the previous approach the stability during a pose considered the fluctuation of the validity degree of each sentence related to the pose by calculating its average value along the duration, here it is analysed at the lowest level on the variance of the signals corresponding to the angle of each of the sensors during the poses while performing the Sun Salutation. The variance provides a measure of how much a set of values is spread, which means that, if it is low, the signal is quite stable, while, if it is high, then the signal fluctuates significantly, meaning that the subject is not maintaining the pose appropriately.

Variance of the angle of the sensor (PM_{θ_i})

It is a 1-*PM* whose inputs are the corresponding pose and the numerical values of the angle formed by the vector given by the sensor *i* and the Z axis ($\theta_i \in [0^o, 180^o]$, $i \in [1,5]$). The output *CP* y_{θ_i}, gives a fuzzy description related to the variance of the angle during the pose. It includes the following set of NL sentences:

$a_{1_{\theta_i}} \rightarrow$ *"The variance of the angle of sensor 'i' in pose {j} is low."*
$a_{2_{\theta_i}} \rightarrow$ *"The variance of the angle of sensor 'i' in pose {j} is medium."*
$a_{3_{\theta_i}} \rightarrow$ *"The variance of the angle of sensor 'i' in pose {j} is high."*

which can be described by the following template:

$a_{[1:3]_{\theta_i}} \rightarrow$ *"The variance of the angle of sensor 'i' in pose {j} is {low | medium | high}."*

The validity degrees are obtained from the trapezoidal membership functions shown in Figure 4.23, which were designed empirically.

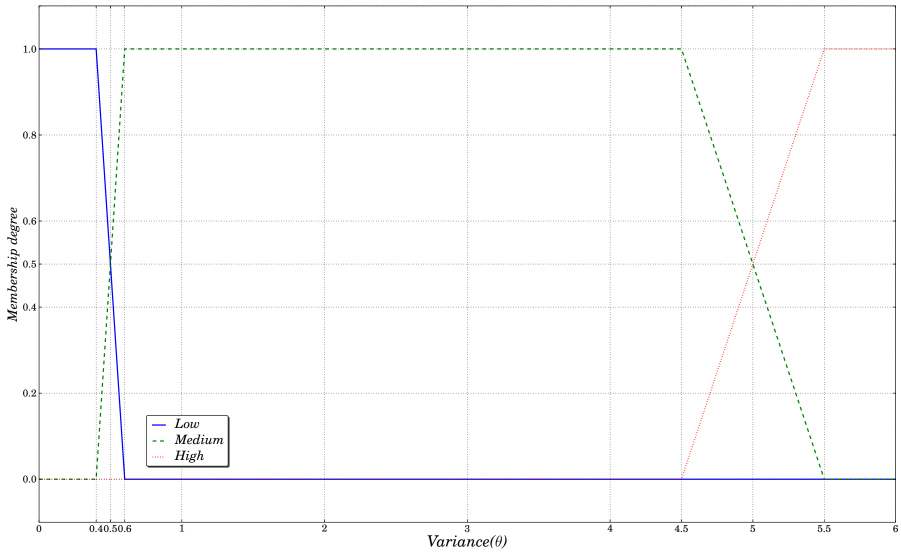

Figure 4.23: Trapezoidal membership functions for the variance of the angle.

Variance of the angle of the sensor during the exercise (PM_{RF}, PM_{LF}, PM_{PBW}, PM_{RC}, PM_{LC})

PM_{RF}, PM_{LF}, PM_{PBW}, PM_{RC} and PM_{LC} (where RF, LF, PBW, RC and LC stand for Right Forearm, Left Forearm, Partial Back Waist, Right Calf and Left Calf) are 2-*PM*s which describe the variance of the angle of the sensors while performing all the poses. The aggregation functions calculate the corresponding validity degrees as shown in Eq. 4.10:

$$w_{i_{RF}} = \frac{\sum_{t=0}^{T_i} w_{i_{\theta_1}}[t]}{T_i} \quad , \quad w_{i_{LF}} = \frac{\sum_{t=0}^{T_i} w_{i_{\theta_2}}[t]}{T_i} \quad , \quad w_{i_{PBW}} = \frac{\sum_{t=0}^{T_i} w_{i_{\theta_3}}[t]}{T_i}$$

$$w_{i_{RC}} = \frac{\sum_{t=0}^{T_i} w_{i_{\theta_4}}[t]}{T_i} \quad , \quad w_{i_{LC}} = \frac{\sum_{t=0}^{T_i} w_{i_{\theta_5}}[t]}{T_i} \tag{4.10}$$

The output *CP*s are described by the following templates:

$a_{[1:3]_{RF}} \rightarrow$ *"The variance of the angle of the sensor on the right forearm during the exercise is {low | medium | high}."*

$a_{[1:3]_{LF}} \rightarrow$ *"The variance of the angle of the sensor on the left forearm during the exercise is {low | medium | high}."*

$a_{[1:3]_{PBW}} \rightarrow$ *"The variance of the angle of the sensor on the back waist during the exercise is {low | medium | high}."*

$a_{[1:3]_{RC}} \rightarrow$ *"The variance of the angle of the sensor on the right calf during the exercise is {low | medium | high}."*

$a_{[1:3]_{LC}} \rightarrow$ *"The variance of the angle of the sensor on the left calf during the exercise is {low | medium | high}."*

Stability of the forearms and the calves during the exercise (PM_F, PM_C)

These *PM*s merge the data corresponding to the variance of the forearms and the calves in order to provide information about the stability of the limbs. The aggregation functions calculate their validity degrees as shown in Eq. 4.11:

$$w_{i_F} = \frac{w_{(3-i+1)_{RF}} + w_{(3-i+1)_{LF}}}{2} \quad , \quad w_{i_C} = \frac{w_{(3-i+1)_{RC}} + w_{(3-i+1)_{LC}}}{2} \tag{4.11}$$

The output CP of PM_F, for example, would include the following set of NL sentences:

a_{1_F} → *"The stability of the forearms during the exercise is low."*

a_{2_F} → *"The stability of the forearms during the exercise is medium."*

a_{3_F} → *"The stability of the forearms during the exercise is high."*

While dealing with the pure linguistic system described in the previous section, it was noticed that, depending on the values obtained for the validity degrees, the NL sentences provided by the output CPs would be more or less meaningful. For example, considering two different sets of validity degrees for the current PM: $w_{1_F} = 0.94$, $w_{2_F} = 0.06$, $w_{3_F} = 0.00$ and $w_{1_F} = 0.52$, $w_{2_F} = 0.48$, $w_{3_F} = 0.00$, and taking the sentence corresponding to the maximum validity degree, the output would correspond in both cases to a_{1_F}: *"The stability of the forearms during the exercise is low."*. However, it is obvious that the "relevance" or "importance" of this sentence, or how it could be perceived by a clinician or a patient, is not the same for the two sets. In the first one, w_{1_F} is clearly the maximum validity degree with a significant difference from the others (0.94 with respect to 0.06), while in the second set, this difference is much smaller (0.52 with respect to 0.48). With the aim to provide a more meaningful description of the phenomenon and to improve the usability of texts, it is proposed to include a modifier of intensity, as commonly done in human discourse [318]. The quantifier chosen to be considered when the maximum validity degree corresponds to the first or the third sentence (therefore to modify the adjectives "low" or "high", while it would not have much sense in natural language applying it to the adjective "medium") is *quite*.

In this context, the standard deviation among the weights provided by the PM is taken into consideration. If the standard deviation calculated is below a determined threshold, fixed experimentally at 0.2, which means that there is not a large difference among the weights, this quantifier is included in the text. Considering this, the output CP of PM_F includes the following set of NL sentences:

a_{1_F} → *"The stability of the forearms during the exercise is (quite) low."*

$a_{2_F} \rightarrow$ *"The stability of the forearms during the exercise is medium."*
$a_{3_F} \rightarrow$ *"The stability of the forearms during the exercise is (quite) high."*

Equivalently, the output *CP* of PM_C is expressed by the following sentences:

$a_{1_C} \rightarrow$ *"The stability of the calves during the exercise is (quite) low."*
$a_{2_C} \rightarrow$ *"The stability of the calves during the exercise is medium."*
$a_{3_C} \rightarrow$ *"The stability of the calves during the exercise is (quite) high."*

Stability of the back waist during the exercise (PM_{BW})

The other *PM* in this level transforms the variance of the angle of the sensor in the back waist in order to obtain its stability by calculating the corresponding validity degrees as described in Equation 4.12.

$$w_{i_{BW}} = w_{(3-i+1)_{PBW}} \tag{4.12}$$

The template of the output *CP* is:

$a_{[1:3]_{BW}} \rightarrow$ *"The stability of the back waist during the exercise is {low | medium | high}."*

Postural balance during the exercise (PM_{PB})

The *PM* at the highest level provides the output *CP* y_{PB} with a description of the postural balance based on the stability of each part of the body. The aggregation function (g_{PB}) calculates the validity degree ($w_{i_{PB}}$) of each sentence as shown in Eq. 4.13:

$$w_{i_{PB}} = \frac{w_{i_F} + w_{i_{BW}} + w_{i_C}}{\sum_{j=1}^{3} w_{j_F} + w_{j_{BW}} + w_{j_C}} \tag{4.13}$$

Considering the use of the quantifier *quite* as before, the output $CP\ y_{PB}$ includes the following set of NL sentences:

$a_{1_{PB}} \rightarrow$ *"The postural balance while performing the Sun Salutation is (quite) low."*

$a_{2_{PB}} \rightarrow$ *"The postural balance while performing the Sun Salutation is medium."*

$a_{3_{PB}} \rightarrow$ *"The postural balance while performing the Sun Salutation is (quite) high."*

4.4.3 Experimentation

Table 4.13 shows the validity degrees of the sentences associated to the postural balance of one exercise randomly chosen from each subject's among the test samples. It also shows the validity degrees associated to the stability of the forearms, the back waist and the calves. The report provided by the proposed system is generated by using the sentences corresponding to the maximum validity degrees, which are boldfaced, taking into account the consideration introduced previously about the standard deviation of the weights, also shown in the table. As an example, four different generated sentences are as follows:

- *"The postural balance of subject 1 while performing the Sun Salutation is quite high because during the exercise the stability of the forearms is quite high, the stability of the back waist is quite high and the stability of the calves is high."*
- *"The postural balance of subject 5 while performing the Sun Salutation is medium because during the exercise the stability of the forearms is medium, the stability of the back waist is medium and the stability of the calves is medium."*
- *"The postural balance of subject 8 while performing the Sun Salutation is quite high because during the exercise the stability of the forearms is medium, the stability of the back waist is quite high and the stability of the calves is high."*
- *"The postural balance of subject 9 while performing the Sun Salutation is high because during the exercise the stability of the forearms is high, the stability of the back waist is high and the stability of the calves is high."*

Sentence	Subject									
	1	2	3	4	5	6	7	8	9	10
$w1_B$	0.13	0.09	0.01	0.01	0.18	0.08	0.05	0.09	0.00	0.02
$w2_B$	0.34	**0.53**	0.35	**0.57**	**0.49**	0.31	**0.52**	0.43	0.35	**0.53**
$w3_B$	**0.53**	0.38	**0.64**	0.42	0.33	**0.61**	0.43	**0.48**	**0.65**	0.45
σ_B	**0.16**	0.18	0.25	0.24	0.12	0.22	0.21	**0.17**	0.27	0.23
$w1_F$	0.18	0.09	0.02	0.02	0.23	0.07	0.00	0.14	0.00	0.00
$w2_F$	0.36	**0.63**	0.41	**0.84**	**0.39**	**0.54**	**0.67**	**0.44**	0.35	**0.53**
$w3_F$	**0.46**	0.28	**0.57**	0.14	0.38	0.39	0.33	0.42	**0.65**	0.47
σ_F	**0.12**	0.22	0.23	0.36	0.08	0.20	0.27	0.13	0.26	0.23
$w1_{BW}$	0.14	0.12	0.00	0.00	0.22	0.14	0.07	0.07	0.00	0.01
$w2_{BW}$	0.35	**0.45**	0.40	0.42	**0.64**	0.10	**0.62**	0.46	0.43	**0.54**
$w3_{BW}$	**0.51**	0.43	**0.60**	**0.58**	0.14	**0.76**	0.31	**0.47**	**0.57**	0.45
σ_{BW}	**0.15**	0.15	0.25	0.25	0.22	0.30	0.22	**0.19**	0.24	0.23
$w1_C$	0.07	0.06	0.03	0.00	0.11	0.04	0.07	0.07	0.00	0.03
$w2_C$	0.29	**0.51**	0.23	0.46	**0.43**	0.27	0.29	0.38	0.27	**0.52**
$w3_C$	**0.64**	0.43	**0.74**	**0.54**	0.46	**0.69**	**0.64**	**0.55**	**0.73**	0.45
σ_C	0.23	0.19	0.30	0.24	0.16	0.27	0.24	0.20	0.30	0.21

Table 4.13: Validity degrees of the sentences associated to the postural balance during the Sun Salutation sequence performed by the healthy participants.

Taking for instance Subject 8 and going into a lower level, in Table 4.14 the validity degrees of the sentences associated to the variance of the angle of the sensors during the whole exercise are shown. From them, the following sentences are extracted for the report:

- *"The forearms stability is medium because the variance of the angle of the sensor on the right forearm during the exercise is low and the variance of the angle of the sensor on left forearm during the exercise is medium."*
- *"The back waist stability is quite high because the variance of the angle of the sensor on the back waist during the exercise is low."*
- *"The calves stability is high because the variance of the angle of the sensor*

on the right calf during the exercise is low and the variance of the angle of the sensor on the left calf during the exercise is low."

Sentence	**Perception Mapping**				
	RF	LF	PBW	RC	LC
w_1	**0.43**	0.41	**0.47**	**0.57**	**0.53**
w_2	0.43	**0.45**	0.46	0.36	0.40
w_3	0.14	0.14	0.07	0.07	0.07

Table 4.14: Validity degrees of the sentences associated to the variance of the angle of the sensors during the whole exercise for Subject 8.

Table 4.15 shows the validity degrees associated to the variance of the angle of the sensors on the forearms, θ_1 and θ_2, for the the analysis done at the pose level. The following sentences explain the variance of these angles for the whole exercise depending on the variance for each pose:

- *"The variance of the angle of the sensor on the right forearm for the whole exercise is low because it is low for poses 0, 1, 5, 8, 10 and 13, it is medium for poses 2, 4, 6, 7, 11 and 12 and it is high for poses 4 and 9."*
- *"The variance of the angle of the sensor on the left forearm for the whole exercise is medium because it is low for poses 0, 1, 7, 8 and 13, it is medium for poses 2, 3, 5, 9, 10, 11 and 12 and it is high for poses 4 and 6."*

The proposed approach allows to provide a feedback on the postural balance through the use of the Granular Linguistic Model of a Phenomenon theory, while simplifying the lower level perception considering the use of a neural gas within the hMPF architecture.

Pose	Perception Mapping					
	θ_1			θ_2		
	$w1_{\theta_1}$	$w2_{\theta_1}$	$w3_{\theta_1}$	$w1_{\theta_2}$	$w2_{\theta_2}$	$w3_{\theta_2}$
0	**1**	0	0	**1**	0	0
1	**1**	0	0	**1**	0	0
2	0	**1**	0	0	**1**	0
3	0	**1**	0	0	**1**	0
4	0	0	**1**	0	0	**1**
5	**1**	0	0	0	**1**	0
6	0	**1**	0	0	0	**1**
7	0	**1**	0	**1**	0	0
8	**1**	0	0	**1**	0	0
9	0	0	**1**	0	**1**	0
10	**1**	0	0	0	**1**	0
11	0	**1**	0	0	**0.75**	0.25
12	0	**1**	0	0	**1**	0
13	**1**	0	0	**1**	0	0

Table 4.15: Validity degrees of the sentences associated to the variance of the angle of the sensors on the forearms for each pose for Subject 8.

4.5 Summary

Three different methods have been presented for the analysis of motion data, each of which has its advantages and its inconveniences, which could be summed up as follows.

In Section 4.2 the Memory Prediction Framework has been introduced and neural gas algorithms have been investigated within its implementation by Henesis. Having the advantage of an unsupervised learning and the capacity of generalization, the preliminary results encourage to continue the research on this direction, *e.g.*, including feedback connections within the architecture for providing information to the lower levels about the current interpretations of the higher levels, as the actual brain does. Some of the inconveniences related to this approach are, on the one hand, the large amount of data needed during the training phase (becoming both a time consuming and computationally expensive process, even more when the network has several levels or layers) and the complexity of finding the right parameters for the correct performance of the chosen algorithms and, on the other hand, the difficulty of interpreting the results and providing an adequate feedback to the subject.

Section 4.3 introduced the Granular Linguistic Model of a Phenomenon, based on which and in combination with a Fuzzy Finite State Machine, an application which generates linguistic descriptions for assessing the subject's performance, considering symmetry, stability and rhythm, has been developed. While this approach solves the problem of interpreting the results easily and providing a useful feedback to the patient, the definition of the whole system, *i.e.*, which levels of the signals should be considered during the fuzzification process or how the information is analysed in each node, are defined manually by the designer.

Finally, Section 4.4 proposed a hybrid neuro-fuzzy system for postural balance assessment, combining the technologies used in the previous approaches, in order to merge their advantages and trying to reduce their drawbacks. Thus, the neural part of the system learns how to differentiate the poses from the transitions without supervision, while the fuzzy sector provides a linguistic description of the exercise based on the stability of the subject during the duration of the poses. Additionally, in this approach, the inclusion of a modifier of intensity in the sentences for improving the usability of texts when providing a feedback is proposed.

Chapter 5

Conclusions and Future Work

A story has no beginning or end: arbitrarily one chooses that moment of experience from which to look back or from which to look ahead.

Graham Greene

5.1 Conclusions

The work done in this thesis contributes to the field of assessment of rehabilitation exercises by proposing a hardware and software suite, both for human motion acquisition and tracking and data analysis.

Firstly, to capture human motion, a prototypical wearable sensing system, based on a robust communication scheme and a data alignment algorithm, has been developed. The integration of five small wireless modules, worn by the subject, which can acquire accelerometer data at high frequency, synchronized by an external master device, makes the system ideal for patient monitoring since it is easily wearable and does not interfere with the movements. Moreover, it provides significant flexibility, allowing to monitor different parts of the body with the same modules just by changing the placement of the elastic bands. While some exercises might require the use of the five slave modules for the correct monitoring of both the inferior and superior limbs, having a reference point next to the centre of mass of the body, other exercises, such as monitoring a single arm during a rehabilitation therapy, could require fewer modules. Thanks to the versatility of the system, it could be used in this case in a simpler configuration without affecting its capabilities.

The successful working of the system has been demonstrated during the experiments carried out to assess the communication performance, which has been focused on data synchronization, data loss, jitter measurements and battery life. Furthermore, the system functionality has been tested analysing the data acquired with it in the task of activity classification using standard classifiers.

The resulting system operates in real time and in a wireless network, guaranteeing data correctness while being portable and easy to manipulate, which are crucial factors for the target application. The system also includes Kinect for video acquisition during the training sessions in order to provide additional visual feedback to the patient, which is considered to have a great impact in the therapy. A software with a GUI for easy management of the sessions is included in the suite.

Human motion analysis is then performed by modelling a physical complex exercise. The case study chosen is the Sun Salutation sequence, which is an interesting example of a phenomenon evolving in time, a yoga exercise which involves the movement of different parts of the body. Three different methods have been considered for analysing the temporal series of measures that contains a numerical description of this exercise.

The first method is based on the Memory Prediction Framework, and neural gas algorithms have been investigated to be included in its implementation. The results obtained show that this type of algorithms can effectively be used for analysing motion data, for classification doing pose recognition and for adding prediction capabilities by taking into consideration the temporal context. The second approach is based on the Computational Theory of Perceptions. The Granular Linguistic Model of a Phenomenon in combination with a Fuzzy Finite State Machine have been used to develop a tool able to analyse the exercise and provide a linguistic assessment of it. A computational model which evaluates the quality of the exercise based on its symmetry, stability and rhythm during the movements at different levels of granularity, being highly interpretable, has been created. The last method proposes a hybrid neuro-fuzzy system for postural balance assessment which merges the technologies used in the previous approaches in order to exploit the learning and generalization capacity of neural networks and the easiness of the interpretation of the results of the fuzzy system. Additionally, in order to improve the usability of the texts used when providing a feedback to the patient, the use of a modifier of intensity, a quantifier, is suggested.

From the experimental results obtained, it can be concluded that, both from a practical and a theoretical point of view, the proposed suite can introduce improvements in the current state of the art in the field of human motion monitoring for rehabilitation.

5.2 Future work

Due to the multidisciplinary character of this thesis, a wide range of future steps and research lines has been opened.

First, in order to complete the field validation of the system, the assessment of the clinicians is needed. Thus, the next steps should involve testing the suite in a rehabilitation centre with a patient wearing the sensors while doing the exercises. This would allow to interact directly with the people involved in the rehabilitation environment, the subject and the doctors, by providing them with the results obtained with the different methods proposed and the visual feedback. Clinicians could then evaluate the patient's performance both subjectively and making use of the objective results given by the system for assessing her/his achievement during the physical therapy.

On the other hand, the prototype of the wearable system can be further developed and improved working on its miniaturization, by re-engineering the base module used in the architecture. This would allow to reduce the size and weight of the sensors. While the actual characteristics and configuration of the system allow a maximum of five slave modules because just one communication channel is being used, creating a multi-channel system would consent to introduce more sensors and, therefore, to have more motion data available.

With respect to the data analysis, future work could be focused on the automatic configuration of neural gas algorithms, *e.g.*, using the iterated racing procedure to find the most appropriate settings for optimizing the parametrization. Deepening on the use of the temporal context and the addition of feedback connections between different levels of the Memory Prediction Framework implementation is recommended. In order to make data more accessible to people, within the Granular Linguistic Model of a Phenomenon the concept of relevancy of a Computational Perception could be explored for providing descriptions highlighting the relevant and hiding the irrelevant data according to the subject's specific goals. Further study on hybrid neuro-fuzzy systems would allow to boost the potentiality demonstrated in this field as they join the advantages of two different methods while compensating their drawbacks.

In addition, considering that the proposed system also includes video acquisition, this type of data could be considered for future analysis through computer vision techniques, which would allow to complement the analysis done on the accelerometer data.

Finally, it should be pointed out that even if this thesis has been focused on the development of a suite for application in rehabilitation, virtual training and gaming could be other potential fields of interest.

Bibliography

[1] J. K. Aggarwal and Q. Cai, "Human motion analysis: A review," in *Proceedings of the IEEE Nonrigid and Articulated Motion Workshop*, pp. 90–102, June 1997.

[2] H. Zhou, T. Stone, H. Hu, and N. Harris, "Use of multiple wearable inertial sensors in upper limb motion tracking," *Medical Engineering & Physics*, vol. 30, no. 1, pp. 123–133, 2008.

[3] R. P. Van Peppen, G. Kwakkel, S. Wood-Dauphinee, H. J. Hendriks, P. J. Van der Wees, and J. Dekker, "The impact of physical therapy on functional outcomes after stroke: what's the evidence?," *Clinical Rehabilitation*, vol. 18, no. 8, pp. 833–862, 2004.

[4] A. Cutti, A. Giovanardi, L. Rocchi, and A. Davalli, "A simple test to assess the static and dynamic accuracy of an inertial sensors system for human movement analysis," in *28th Annual International Conference of the IEEE Engineering in Medicine and Biology Society (EMBS)*, pp. 5912–5915, 2006.

[5] H. Zhou and H. Hu, "Human Motion Tracking for Rehabilitation – A Survey," *Biomedical Signal Processing and Control*, vol. 3, no. 1, pp. 1–18, 2008.

[6] T. Hester, R. Hughes, D. Sherrill, B. Knorr, M. Akay, J. Stein, and P. Bonato, "Using wearable sensors to measure motor abilities following stroke," in *International Workshop on Wearable and Implantable Body Sensor Networks*, pp. 4–8, 2006.

[7] S. Patel, D. Sherrill, R. Hughes, T. Hester, N. Huggins, T. Lie-Nemeth, D. Standaert, and P. Bonato, "Analysis of the severity of dyskinesia in patients with Parkinson's disease via wearable sensors," in *International Workshop on Wearable and Implantable Body Sensor Networks*, pp. 123–126, 2006.

[8] F. Naghdy, "Fuzzy clustering of human motor motion," *Applied Soft Computing*, vol. 11, no. 1, pp. 927–935, 2011.

[9] XSens, "Xbus Kit: Measurement of human motion." [Online]. Available: `www.xsens.com/en/general/xbus-kit`, 2013. Last visit: [8 May 2013].

[10] T. Martin, E. Jovanov, and D. Raskovic, "Issues in wearable computing for medical monitoring applications: A case study of a wearable ecg monitoring device," in *Proceedings of the 4th IEEE International Symposium on Wearable Computers*, pp. 43–48, IEEE Computer Society, 2000. ISWC '00, Washington, DC, USA.

[11] C. Otto, A. Milenković, C. Sanders, and E. Jovanov, "System architecture of a wireless body area sensor network for ubiquitous health monitoring," *Journal of Mobile Multimedia*, vol. 1, pp. 307–326, January 2005.

[12] "Henesis S.r.l.." [Online]. Available: `www.henesis.eu`. Last visit: [14 Aug 2013].

[13] A. Sant'Anna, *A Symbolic Approach to Human Motion Analysis Using Inertial Sensors : Framework and Gait Analysis Study*. PhD thesis, Halmstad University, Sweden, 2012.

[14] World Health Organization, "Stroke, cerebrovascular accident." [Online]. Available: `www.who.int/topics/cerebrovascular_accident`, 2013. Last visit: [28 Mar 2013].

[15] J. Díaz-Guzmán, J. Egido-Herrero, R. Gabriel-Sánchez, G. Barberà, B. Fuentes, C. Fernández-Pérez, and S. Abilleira, "Incidencia de ictus en España. Bases metodológicas del estudio Iberictus.," *Revista de Neurología*, vol. 47, no. 12, pp. 617–623, 2008.

[16] E. Martínez-Vila, P. Irimia, E. Urrestarazu, and J. Gállego, "The cost of the stroke," *ANALES Sis San Navarra*, vol. 23, no. 3, pp. 33–38, 2000.

[17] M. J. Medrano Albero, R. Boix Martínez, E. Cerrato Crespán, and M. Ramírez Santa-Pau, "Incidence and prevalence of ischaemic heart disease and cerebrovascular disease in Spain: a systematic review of the literature," *Revista Española de Salud Pública*, vol. 80, pp. 5–15, January 2006.

[18] S. Molinelli, "Lo stroke – epidemiologia, patofisiologia, classificazione." Fisiobrain, February 2007.

[19] P. Langhorne, F. Coupar, and A. Pollock, "Motor recovery after stroke: a systematic review," *Lancet Neurology*, vol. 8, pp. 741–754, August 2009.

[20] R. van Peppen, *Towards evidence-based physiotherapy for patients with stroke*. PhD thesis, Utrecht University, 2008.

[21] T. Beth, I. Boesnach, M. Haimerl, J. Moldenhauer, K. Bös, and V. Wank, "Characteristics in Human Motion – From Acquisition to Analysis," in *IEEE International Conference on Humanoid Robots*, 2003.

[22] Vicon, "Motion Capture Systems." [Online]. Available: `www.vicon.com`. Last visit: [28 Mar 2013].

[23] NDI, "Optotrack, Optical Tracker System." [Online]. Available: `www.ndigital.com/industrial/products-opticaltracker.php` . Last visit: [28 Mar 2013].

[24] S. Patel, H. Park, P. Bonato, L. Chan, and M. Rodgers, "A review of wearable sensors and systems with application in rehabilitation," *Journal of NeuroEngineering and Rehabilitation*, vol. 9, no. 21, pp. 1–17, 2012.

[25] P. Bonato, "Advances in wearable technology and applications in physical medicine and rehabilitation," *Journal of NeuroEngineering and Rehabilitation*, vol. 2, no. 2, pp. 1–4, 2005.

[26] L. Moreno-Hagelsieb, X. Tang, O. Bulteel, N. V. Overstraeten-Schlögel, N. André, , P. Dupuis, J.-P. Raskin, L. Francis, D. Flandre, P. Fonteyne, J.-L. Gala, and Y. Nizet, "Miniaturized and low cost innovative detection systems for medical and environmental applications," in *2nd Workshop on Circuits and*

Systems for Medical and Environmental Applications (CASME), (Merida, Yucatan, Mexico), pp. 1–4, December 2010.

[27] B. Latré, B. Braem, I. Moerman, C. Blondia, and P. Demeester, “A survey on wireless body area networks,” *Wireless Networks*, vol. 17, pp. 1–18, January 2011.

[28] E. Jovanov, A. Milenkovic, C. Otto, P. De Groen, B. Johnson, S. Warren, and G. Taibi, “A WBAN system for ambulatory monitoring of physical activity and health status: Applications and challenges,” in *27th Annual International Conference of the Engineering in Medicine and Biology Society (EMBS)*, pp. 3810–3813, 2005.

[29] J. Yang, S. Wang, N. Chen, X. Chen, and P. Shi, “Wearable accelerometer based extendable activity recognition system,” in *IEEE International Conference on Robotics and Automation (ICRA)*, pp. 3641–3647, May 2010.

[30] M. J. Mathie, A. C. Coster, N. H. Lovell, and B. G. Celler, “Accelerometry: providing an integrated, practical method for long-term, ambulatory monitoring of human movement,” *Physiological Measurement*, vol. 25, pp. 1–20, April 2004.

[31] C.-C. Yang and Y.-L. Hsu, “A review of accelerometry-based wearable motion detectors for physical activity monitoring,” *Sensors*, vol. 10, pp. 7772–7788, August 2010.

[32] N. Ravi, D. Nikhil, P. Mysore, and M. L. Littman, “Activity recognition from accelerometer data,” in *17th Conference on Innovative Applications of Artificial Intelligence (IAAI)*, vol. 3, pp. 1541–1546, AAAI Press, 2005.

[33] A. Alvarez-Alvarez, G. Trivino, and O. Cordón, “Body posture recognition by means of a genetic fuzzy finite state machine,” in *IEEE 5th International Workshop on Genetic and Evolutionary Fuzzy Systems (GEFS)*, pp. 60–65, April 2011.

[34] M. Guler and S. Ertugrul, "Measuring and transmitting vital body signs using MEMS sensors," in *1st Annual RFID Eurasia*, pp. 1–4, September 2007.

[35] K. M. Culhane, M. O'Connor, D. Lyons, and G. M. Lyons, "Accelerometers in rehabilitation medicine for older adults," *Age and Ageing*, vol. 34, pp. 556–560, November 2005.

[36] A. Alvarez-Alvarez, G. Trivino, and O. Cordón, "Human Gait Modeling Using a Genetic Fuzzy Finite State Machine," *IEEE Transactions on Fuzzy Systems*, vol. 20, no. 2, pp. 205–223, 2012.

[37] A. Alvarez-Alvarez and G. Trivino, "Linguistic description of the human gait quality," *Engineering Applications of Artificial Intelligence*, vol. 26, pp. 13–23, January 2013.

[38] M. Sung, C. Marci, and A. Pentland, "Wearable feedback systems for rehabilitation," *Journal of NeuroEngineering and Rehabilitation*, vol. 2, no. 1, p. 17, 2005.

[39] S. Cagnoni, G. Matrella, M. Mordonini, F. Sassi, and L. Ascari, "Sensor fusion-oriented fall detection for assistive technologies applications," in *Proceedings of the 9th International Conference on Intelligent Systems Design and Applications (ISDA)*, (Washington, DC, USA), pp. 673–678, IEEE Computer Society, 2009.

[40] F. Sassi, L. Ascari, and S. Cagnoni, "Classifying human body acceleration patterns using a hierarchical temporal memory," in *11th International Conference on Emergent Perspectives in Artificial Intelligence*, AI*IA, pp. 496–505, 2009.

[41] K. Altun, B. Barshan, and O. Tunçel, "Comparative study on classifying human activities with miniature inertial and magnetic sensors," *Pattern Recognition*, vol. 43, pp. 3605–3620, October 2010.

[42] M. Milenkovic, E. Jovanov, J. Chapman, D. Raskovic, and J. Price, "An accelerometer-based physical rehabilitation system," in *Proceedings of the 34th Southeastern Symposium on System Theory*, pp. 57–60, 2002.

[43] E. Jovanov, A. Milenkovic, C. Otto, and P. de Groen, "A wireless body area network of intelligent motion sensors for computer assisted physical rehabilitation," *Journal of NeuroEngineering and Rehabilitation*, vol. 2, pp. 1–10, March 2005.

[44] H. Zhou, H. Hu, and Y. Tao, "Inertial measurements of upper limb motion," *Medical and Biological Engineering and Computing*, vol. 44, pp. 479–487, 2006.

[45] "Xsens." [Online]. Available: `www.xsens.com`. Last visit: [20 Aug 2013].

[46] "Inertia Technology." [Online]. Available: `inertia-technology.com`. Last visit: [20 Aug 2013].

[47] XSens, "MTw Development Kit." [Online]. Available: `www.xsens.com/en/mtw`. Last visit: [20 Aug 2013].

[48] XSens, "MVN BIOMECH." [Online]. Available: `www.xsens.com/en/mvn-biomech`. Last visit: [20 Aug 2013].

[49] XSens, "MVN BIOMECH Awinda." [Online]. Available: `www.xsens.com/en/mvn-biomech-awinda`, 2013. Last visit: [20 Aug 2013].

[50] Inertia Technology, "ProMove-3D." [Online]. Available: `inertia-technology.com/promove-3d`. Last visit: [20 Aug 2013].

[51] RM Ingénierie, "BioVal." [Online]. Available: `www.rmingenierie.net/analysis-rehabilitation/bioval`. Last visit: [20 Aug 2013].

[52] Movea, "SmartMotion Development Kit." [Online]. Available: `www.movea.com/products/development-tools/smdk`. Last visit: [20 Aug 2013].

[53] CoRehab, "Riablo." [Online]. Available: `www.corehab.com/riablo`, 2013. Last visit: [20 Aug 2013].

[54] A. Rizzo and G. J. Kim, "A SWOT analysis of the field of virtual reality rehabilitation and therapy," *Presence: Teleoperators and Virtual Environments*, vol. 14, pp. 119–146, April 2005.

[55] C. M. Carroll and C. B. Dixon, "The effect of feedback on exercise performance in recreationally-active young adults," *Keystone Journal of Undergraduate Research*, vol. 1, no. 1, pp. 37–40, 2011.

[56] J. Doyle, D. Kelly, M. Patterson, and B. Caulfield, "The effects of visual feedback in therapeutic exergaming on motor task accuracy," in *International Conference on Virtual Rehabilitation*, June 2011.

[57] V. S. Ramachandran and E. L. Altschuler, "The use of visual feedback, in particular mirror visual feedback, in restoring brain function," *Brain*, vol. 132, pp. 1693–1710, 2009.

[58] A. Sanecki, "Development of a multidimensional balance exercise program with the use of visual feedback in patients with stroke: A case report," in *Physical Therapy Case Study Collection*, Carroll University Library, May 2011.

[59] B. R. Brewer, *Visual Feedback Manipulation for Hand Rehabilitation in a Robotic Environment*. Doctor of Philosophy in Robotics, Carnegie Mellon University, May 2006.

[60] G. Mousa, A. Hassan, and M. El-Bahrawy, "The impact of visual feedback training on postural control in chronic mechanical low back pain patients.," *Bull. Fac. Ph. Th. Cairo Univer.*, vol. 13, pp. 169–181, January 2008.

[61] D. Sayenko, M. Alekhina, K. Masani, A. Vette, H. Obata, M. Popovic, and K. Nakazawa, "Positive effect of balance training with visual feedback on standing balance abilities in people with incomplete spinal cord injury," *Spinal Cord*, vol. 48, pp. 886–893, December 2010.

[62] A. Ledebt, J. Becher, J. Kapper, R. Rozendaalr, B. R., L. I.C., and S. G.J., "Balance training with visual feedback in children with hemiplegic cerebral palsy: effect on stance and gait," *Motor Control*, vol. 9, pp. 459–468, October 2005.

[63] "Isokinetic." [Online]. Available: www.isokinetic.com. Last visit: [14 Aug 2013].

[64] "Henesis WiModule." [Online]. Available: www.henesis.eu/prod-wimodule-eng.htm. Last visit: [14 Aug 2013].

[65] S. Microelectronics, "LIS3LV02DQ MEMS Inertial Sensor." [Online]. Available: www.st.com/internet/com/TECHNICAL_RESOURCES/TECHNICAL_LITERATURE/DATASHEET/CD00047926.pdf. Last visit: [5 Sep 2012].

[66] Microchip, "MRF24J40 RF Transceiver." [Online]. Available: ww1.microchip.com/downloads/en/DeviceDoc/ 39776C.pdf. Last visit: [5 Sep 2012].

[67] Microchip, "PIC18F87J11 Microcontroller." [Online]. Available: ww1.microchip.com/downloads/en/DeviceDoc/ 39778e.pdf. Last visit: [5 Sep 2012].

[68] LAN/MAN Standards Committee – IEEE Computer Society, "IEEE standard for local and metropolitan area networks – part 15.4: Low-rate wireless personal area networks (LR-WPANs)," 2011.

[69] W. Tao, T. Liu, R. Zheng, and H. Feng, "Gait analysis using wearable sensors," *Sensors*, vol. 12, pp. 2255–2283, 2012.

[70] C. Bouten, K. Koekkoek, M. Verduin, R. Kodde, and J. Janssen, "A triaxial accelerometer and portable data processing unit for the assessment of daily physical activity," *IEEE Transactions on Biomedical Engineering*, vol. 44, pp. 136–147, March 1997.

[71] A. Milenković, C. Otto, and E. Jovanov, "Wireless sensor networks for personal health monitoring: Issues and an implementation," *Computer Communications*, vol. 29, no. 13–14, pp. 2521–2533, 2006. Wireless Sensor Networks and Wired/Wireless Internet Communications.

[72] S. Ahmed and T. Chen, “Minimizing the effect of sampling jitters in wireless sensor networks,” *IEEE Signal Processing Letters*, vol. 18, pp. 219–222, April 2011.

[73] F. Sivrikaya and B. Yener, “Time synchronization in sensor networks: A survey,” *IEEE Network*, vol. 18, no. 4, pp. 45–50, 2004.

[74] J. Elson, L. Girod, and D. Estrin, “Fine-grained network time synchronization using reference broadcasts,” in *Proceedings of the 5th Symposium on Operating Systems Design and Implementation*, vol. 36, (New York, NY, USA), ACM, 9–11 December 2002.

[75] M. Paavola and J. Kemppainen, “Wireless monitoring of a steam boiler - performance measurements in industrial environment,” in *IEEE International Symposium on Industrial Electronics (ISIE)*, pp. 1166–1171, July 2008.

[76] J. S. Lee, “Performance evaluation of IEEE 802.15.4 for low-rate wireless personal area networks,” *IEEE Trans. on Consumer Electronics*, vol. 52, no. 3, pp. 742–749, 2006.

[77] L. Mo, S. Liu, R. Gao, D. John, J. Staudenmayer, and P. Freedson, “Wireless design of a multi-sensor system for physical activity monitoring,” *IEEE Transactions on Biomedical Engineering*, vol. 59, no. 59, pp. 3230–3237, 2012.

[78] K. Kunze and P. Lukowicz, “Using acceleration signatures from everyday activities for on-body device location,” in *11th IEEE International Symposium on Wearable Computers*, pp. 115–116, October 2007.

[79] C. Walker, B. J. Brouwer, and E. G. Culham, “Use of visual feedback in retraining balance following acute stroke,” *Physical Therapy*, vol. 80, pp. 886–895, 2000.

[80] L. González-Villanueva, L. Chiesi, and L. Mussi, “Wireless Human Motion Acquisition System for Rehabilitation Assessment,” in *Proceedings of the 25th IEEE International Symposium on Computer-Based Medical Systems*, June 2012.

[81] L. González-Villanueva, S. Cagnoni, and L. Ascari, "Design of a wearable sensing system for human motion monitoring in physical rehabilitation," *Sensors*, vol. 13, pp. 7735–7755, June 2013.

[82] Microchip, "ZENA Network Analyzer." [Online]. Available: `www.microchip.com/stellent/idcplg?IdcService=SS_GET_PAGE&nodeId=1406&dDocName=en520682`. Last visit: [24 Feb 2012].

[83] F. Wilcoxon, "Individual comparisons by ranking methods," *Biometrics Bulletin*, vol. 1, pp. 80–83, December 1945.

[84] M. Hall, E. Frank, G. Holmes, B. Pfahringer, P. Reutemann, and I. H. Witten, "The WEKA data mining software: an update," *SIGKDD Explorations Newsletter*, vol. 11, no. 1, pp. 10–18, 2009.

[85] J. R. Quinlan, *C4.5: programs for machine learning*. San Francisco, CA, USA: Morgan Kaufmann Publishers Inc., 1993.

[86] J. Platt, *Fast Training of Support Vector Machines using Sequential Minimal Optimization*, vol. Advances in Kernel Methods – Support Vector Learning. MIT Press, 1998.

[87] T. Mitchell, *Machine Learning*. McGraw-Hill, 1997.

[88] P. Ahmadian, S. Sanei, L. Ascari, L. González-Villanueva, and M. A. Umiltà, "Constrained blind source extraction of readiness potentials from EEG," *IEEE Transactions on Neural Systems and Rehabilitation Engineering*, vol. 21, pp. 567–575, July 2013.

[89] P. Ahmadian, S. Sanei, L. González-Villanueva, M. A. Umiltà, and L. Ascari, "A framework for detection of readiness potentials in single trials of EEG," in *Proceedings of the International Conference on Medical Imaging Using Bio-Inspired and Soft Computing (MIBISOC2013)*, pp. 261–266, May 2013.

[90] J. A. Raub, “Psychophysiologic effects of hatha yoga on musculoskeletal and cardiopulmonary function: a literature review,” *The Journal of Alternative and Complementary Medicine*, vol. 8, no. 6, pp. 767–812, 2002.

[91] T. Field, “Yoga clinical research review,” *Complementary Therapies in Clinical Practice*, vol. 17, pp. 1–8, 2011.

[92] S. Telles, “Yoga for rehabilitation: An overview,” in *Science of Holistic Living and Its Global Application*, (Bangalore), pp. 67–71, 2006.

[93] N. N. Nayak and K. Shankar, “Yoga: a therapeutic approach,” *Physical Medicine and Rehabilitation Clinics of North America*, vol. 15, no. 4, pp. 783–98, 2004.

[94] S. Telles and K. V. Naveen, “Yoga for rehabilitation: An overview,” *Indian Journal of Medical Sciences*, vol. 51, no. 4, pp. 123–127, 1997.

[95] C. E. F. Hart and B. L. Tracy, “Yoga as steadiness training: Effects on motor variability in young adults,” *Journal of Strength & Conditioning Research*, vol. 22, pp. 1659–1669, September 2008.

[96] K. A. Williams, J. Petronis, D. Smith, D. Goodrich, J. Wu, N. Ravi, E. J. D. Jr, R. G. Juckett, M. M. Kolar, R. Gross, and L. Steinberg, “Effect of iyengar yoga therapy for chronic low back pain,” *Pain*, vol. 115, no. 1–2, pp. 107–117, 2005.

[97] S. N. Omkar, M. Mour, and D. Das, “Motion analysis of sun salutation using magnetometer and accelerometer,” *International Journal of Yoga*, vol. 2, pp. 62–68, July-December 2009.

[98] S. N. Omkar, B. Badri Narayanan, R. Ashwini, B. Rohit, and K. Sachin, “A comparative study on performance analysis of sun-salutation using fast fourier transform, wavelet transform and hilbert-huang transform,” *International Journal of Sports Science and Engineering*, vol. 6, pp. 54–64, March 2012.

[99] S. Omkar, M. Mour, and D. Das, "A mathematical model of effects on specific joints during practice of the sun salutation – a sequence of yoga postures," *Journal of bodywork and movement therapies*, vol. 15, pp. 201–208, April 2011.

[100] D. Kelly, D. Fitzgerald, J. Foody, D. Kumar, T. Ward, B. Caulfield, and C. Markham, "The e-motion system: Motion capture and movement-based biofeedback game," in *Proceedings of the 9th International Conference on Computer Games Artificial Intelligence and Mobile Systems (CGAMES)*, pp. 19–23, 2006.

[101] D. Fitzgerald, D. Kelly, T. Ward, C. Markham, and B. Caulfield, "Usability evaluation of e-motion: A virtual rehabilitation system designed to demonstrate, instruct and monitor a therapeutic exercise programme," in *Virtual Rehabilitation*, pp. 144–149, August 2008.

[102] I. Arel, D. Rose, and T. Karnowski, "Deep machine learning - a new frontier in artificial intelligence research," *IEEE Computational Intelligence Magazine*, vol. 5, no. 4, pp. 13–18, 2010.

[103] J. Hawkins and S. Blakeslee, *On intelligence*. Times Books, 2004.

[104] D. George, *How the Brain Might Work: A Hierarchical and Temporal Model for Learning and Recognition*. PhD thesis, Stanford University, June 2008.

[105] F. Sassi, *Studio e sviluppo di un sistema neurocomputazionale per l'analisi e la predizione di sequenze temporali multidimensionali*. PhD thesis, University of Parma, 2012.

[106] D. Kit, B. Sullivan, and D. Ballard, "Novelty detection using Growing Neural Gas for visuo-spatial memory," in *IEEE International Conference on Intelligent Robots and Systems*, pp. 1194–1200, 2011.

[107] T. Kohonen, "Self-organized formation of topologically correct feature maps," *Biological Cybernetics*, vol. 43, no. 1, pp. 59–69, 1982.

[108] T. Martinetz and K. Schulten, "A "neural-gas" network learns topologies," *Artificial Neural Networks*, vol. I, pp. 397–402, 1991.

[109] F. Questier, Q. Guo, B. Walczak, D. L. Massart, C. Boucon, and S. De Jong, "The neural-gas network for classifying analytical data," *Chemometrics and Intelligent Laboratory Systems*, vol. 61, no. 1–2, pp. 105–121, 2002.

[110] L.-n. Jin and S. Ouyang, "Algorithm for data visualization by hybridizing neural gas network and Sammon's mapping," *Journal of Electronics and Information Technology*, vol. 30, no. 5, pp. 1118–1121, 2008.

[111] F. Camastra and A. Vinciarelli, "Combining neural gas and learning vector quantization for cursive character recognition," *Neurocomputing*, vol. 51, pp. 147–159, 2003.

[112] K. Kishida, H. Miyajima, and M. Maeda, "Destructive fuzzy modeling using neural gas network," *IEICE Transactions on Fundamentals of Electronics, Communications and Computer Sciences*, vol. E80-A, no. 9, pp. 1578–1584, 1997.

[113] A.-M. Cretu, J. Lang, and E. Petriu, "A composite neural gas-Elman network that captures real-world elastic behavior of 3D objects," in *Proceedings of the IEEE Instrumentation and Measurement Technology Conference*, IMTC, pp. 1063–1068, 2006.

[114] A.-M. Cretu, P. Payeur, and E. Petriu, "Selective vision sensing with neural gas networks," in *IEEE Conference on Instrumentation and Measurement Technology Conference*, pp. 478–483, 2008.

[115] A.-M. Cretu, P. Payeur, and E. Petriu, "Selective range data acquisition driven by neural-gas networks," *IEEE Transactions on Instrumentation and Measurement*, vol. 58, no. 8, pp. 2634–2642, 2009.

[116] F.-M. Schleif, T. Villmann, and B. Hammer, "Supervised neural gas for classification of functional data and its application to the analysis of clinical pro-

teom spectra," in *Computational and Ambient Intelligence*, vol. 4507 of *Lecture Notes in Computer Science*, pp. 1036–1044, Springer Berlin Heidelberg, 2007.

[117] A. Date and K. Kurata, "Separation of position and direction information of robots by a product model of self-organizing map and neural gas," *Systems and Computers in Japan*, vol. 36, no. 11, pp. 1–11, 2005.

[118] A. Meyer-Baese, "Medical image compression by "neural-gas" network and principal component analysis," in *Proceedings of the International Joint Conference on Neural Networks*, vol. 5, pp. 489–493, 2000.

[119] O. Lange, A. Meyer-Baese, and A. Wismueller, "Small mammographic lesions evaluation based on neural gas network," in *Proceedings of the International Society for Optical Engineering*, vol. 6560 of *SPIE*, pp. 65600V–65600V–9, 2007.

[120] L. E. Peterson, S. Ather, V. Divakaran, A. Deswal, B. Bozkurt, and D. L. Mann, "Improved Propensity Matching for Heart Failure using Neural Gas and Self-Organizing Maps," in *Proceedings of the International Joint Conference on Neural Networks*, pp. 2517–2524, 2009.

[121] S. I. Dimitriadis, N. A. Laskaris, V. Tsirka, S. Erimaki, M. Vourkas, S. Micheloyannis, and S. Fotopoulos, "A novel symbolization scheme for multichannel recordings with emphasis on phase information and its application to differentiate eeg activity from different mental tasks," *Cognitive Neurodynamics*, vol. 6, pp. 107–113, February 2012.

[122] A.-M. Cretu, J. Lang, and E. Petriu, "Adaptive acquisition of virtualized deformable objects with a neural gas network," in *IEEE International Workshop on Haptic Audio Visual Environments and their Applications*, HAVE, pp. 165–170, October 2005.

[123] T. Koga, K. Horio, and T. Yamakawa, "Learning of SOR network employing soft-max adaptation rule of neural gas network," *International Congress Series*, vol. 1291, pp. 165–168, 2006.

[124] P. A. Estévez, C. J. Figueroa, and K. Saito, "Cross-entropy embedding of high-dimensional data using the neural gas model," *Neural Networks*, vol. 18, no. 5–6, pp. 727–737, 2005.

[125] P. A. Estévez, C. J. Figueroa, and K. Saito, "Cross-entropy approach to data visualization based on the neural gas network," in *Proceedings of the International Joint Conference on Neural Networks*, vol. 5, pp. 2724–2729, 2005.

[126] P. A. Estévez, A. M. Chong, C. M. Held, and C. A. Pérez, "Nonlinear projection using geodesic distances and the neural gas network," in *Proceedings of the 16th international conference on Artificial Neural Networks - Volume Part I* (Springer-Verlag, ed.), ICANN, pp. 464–473, 2006.

[127] P. A. Estévez and C. J. Figueroa, "Online data visualization using the neural gas network," *Neural Networks*, vol. 19, no. 6–7, pp. 923–934, 2006.

[128] P. A. Estévez and A. M. Chong, "Geodesic nonlinear mapping using the neural gas network," in *Proceedings of the IEEE International Conference on Neural Networks*, pp. 3287–3294, 2006.

[129] S. Ridella, S. Rovetta, and R. Zunino, "Generalization-based approach to plastic vector quantization," in *World Congress on Neural Networks*, vol. 1, pp. 505–508, July 1995.

[130] Y. Xiao, C.-Z. Han, Q.-H. Zheng, and X. Zan, "Analyzing intrusion alerts based on kernel neural-gas clustering," *Systems Engineering and Electronics*, vol. 28, no. 9, pp. 1442–1446, 2006.

[131] D. J. Lutz, "Using neural gas for a better machine identity description," in *Proceedings of the 11th IASTED International Conference on Artificial Intelligence and Soft Computing*, pp. 7–12, 2007.

[132] O. Kurasova and A. Molyte, “Quality of quantization and visualization of vectors obtained by neural gas and self-organizing map,” *Informatica*, vol. 22, no. 1, pp. 115–134, 2011.

[133] F. Ancona, S. Ridella, S. Rovetta, and R. Zunino, “On the importance of sorting in “neural gas” training of vector quantizers,” in *Proceedings of the IEEE International Conference on Neural Networks*, vol. 3, pp. 1804–1808, 1997.

[134] A. Witoelar, M. Biehl, A. Ghosh, and B. Hammer, “Learning dynamics and robustness of vector quantization and neural gas,” *Neurocomputing*, vol. 71, no. 7–9, pp. 1210–1219, 2008.

[135] A. Witoelar and M. Biehl, “Phase transitions in vector quantization and neural gas,” *Neurocomputing*, vol. 72, no. 7–9, pp. 1390–1397, 2009.

[136] F. Ancona, S. Rovetta, and R. Zunino, “Implementing neural gas networks on distributed architectures,” in *Proceedings of the World Congress on Neural Networks*, WCNN, September 1996.

[137] F. Ancona, S. Rovetta, and R. Zunino, “Hardware implementation of the neural gas,” in *Proceedings of the IEEE International Conference on Neural Networks*, vol. 2, pp. 991–994, 1997.

[138] F. Ancona, S. Rovetta, and R. Zunino, “Parallel approach to plastic neural gas,” in *Proceedings of the IEEE International Conference on Neural Networks*, vol. 1, pp. 126–130, 1996.

[139] S. Rovetta and R. Zunino, “Efficient training of neural gas vector quantizers with analog circuit implementation,” *IEEE Transactions on Circuits and Systems II: Analog and Digital Signal Processing*, vol. 46, no. 6, pp. 688–698, 1999.

[140] M. Winter, G. Metta, and G. Sandini, “Adding reinforcement learning features to the neural-gas method,” in *Proceedings of the International Joint Conference on Neural Networks*, vol. 4, pp. 539–542, 2000.

[141] M. Winter, G. Metta, and G. Sandini, "Neural-gas for function approximation: A heuristic for minimizing the local estimation error," in *Proceedings of the International Joint Conference on Neural Networks*, vol. 4, pp. 535–538, 2000.

[142] P. N. Suganthan, "Attributed relational graph matching by neural-gas networks," *Proceedings of the IEEE Workshop on Neural Networks for Signal Processing*, vol. 1, pp. 366–375, 2000.

[143] G. Vachkov, "Growing model algorithm for process identification based on neural-gas learning and local linear mapping," in *Proceedings of the 4th International Conference on Hybrid Intelligent Systems*, HIS, pp. 222–227, 2005.

[144] J. C. Claussen and T. Villmann, "Magnification control in winner relaxing neural gas," *Neurocomputing*, vol. 63, no. SPEC. ISS., pp. 125–137, 2005.

[145] C. Saavedra, S. Moreno, R. Salas, and H. Allende, "Robustness analysis of the neural gas learning algorithm," in *Proceedings of the 11th Iberoamerican conference on Progress in Pattern Recognition, Image Analysis and Applications*, CIARP, pp. 559–568, 2006.

[146] T. Villmann, B. Hammer, and M. Biehl, "Some theoretical aspects of the neural gas vector quantizer," in *Similarity-Based Clustering*, vol. 5400 of *Lecture Notes in Computer Science*, pp. 23–34, Springer Berlin Heidelberg, 2009.

[147] C. S.-T. Choy and W.-C. Siu, "Fast sequential implementation of "neural-gas" network for vector quantization," *IEEE Transactions on Communications*, vol. 46, no. 3, pp. 301–304, 1998.

[148] F.-M. Schleif, A. Gisbrecht, and B. Hammer, "Accelerating kernel neural gas," in *Proceedings of the 21th international conference on Artificial neural networks - Volume Part I*, ICANN, pp. 150–158, 2011.

[149] B. Hammer, M. Strickert, and T. Villmann, "Supervised neural gas with general similarity measure," *Neural Processing Letters*, vol. 21, no. 1, pp. 21–44, 2005.

[150] B. Fritzke, "Growing cell structures - a self-organizing network for unsupervised and supervised learning," *Neural Networks*, vol. 7, pp. 1441–1460, 1993.

[151] B. Fritzke, "A growing neural gas network learns topologies," in *Advances in Neural Information Processing Systems 7*, pp. 625–632, MIT Press, 1995.

[152] B. Fritzke, "A self-organizing network that can follow non-stationary distributions," in *Proceedings of International Conference on Artificial Neural Networks*, ICANN, pp. 613–618, 1997.

[153] M. Teixeira, G. Zaverucha, V. da Silva, and G. Ribeiro, "Recurrent neural gas in electric load forecasting," in *Proceedings of the International Joint Conference on Neural Networks*, vol. 5, pp. 3468–3473, 1999.

[154] A. S. Atukorale and P. N. Suganthan, "Hierarchical overlapped neural gas network with application to pattern classification," *Neurocomputing*, vol. 35, pp. 165–176, 2000.

[155] M. Aupetit, P. Couturier, and P. Massotte, "A "recruiting neural-gas" for function approximation," in *Proceedings of the International Joint Conference on Neural Networks*, vol. 3, pp. 91–96, 2000.

[156] T. Villmann and B. Hammer, "Supervised neural gas for learning vector quantization," in *Proceedings of the 5th German Workshop on Artificial Life*, GWAL, pp. 9–16, 2002.

[157] J. Huhse, T. V., P. Merz, and A. Zell, "Evolution strategy with neighborhood attraction using a neural gas approach," in *Proceedings of the 7th International Conference on Parallel Problem Solving Nature*, pp. 391–400, 2002.

[158] H. Allende, S. Moreno, C. Rogel, and R. Salas, "Robust neural gas for the analysis of data with outliers," in *Proceedings of the International Conference of the Chilean Computer Science Society*, SCCC, pp. 149–155, 2004.

[159] A. K. Qin and P. N. Suganthan, "A robust neural gas algorithm for clustering analysis," in *Proceedings of International Conference on Intelligent Sensing and Information Processing*, ICISIP, pp. 342–347, 2004.

[160] F.-M. Schleif, U. Clauss, T. Villmann, and B. Hammer, "Supervised relevance neural gas and unified maximum separability analysis for classification of mass spectrometric data," in *Proceedings of the International Conference on Machine Learning and Applications*, ICMLA, pp. 374–379, 2004.

[161] R. Andonie and A. Caţaron, "Feature ranking using supervised neural gas and informational energy," in *Proceedings of the International Joint Conference on Neural Networks* [176], pp. 1269–1273.

[162] A. K. Qin and P. N. Suganthan, "Kernel neural gas algorithms with application to cluster analysis," in *Proceedings of the International Conference on Pattern Recognition*, vol. 4, pp. 617–620, 2004.

[163] A. K. Qin and P. N. Suganthan, "Enhanced neural gas network for prototype-based clustering," *Pattern Recognition*, vol. 38, no. 8, pp. 1275–1288, 2005.

[164] M. Cottrell, B. Hammer, A. Hasenfuß, and T. Villmann, "Batch neural gas," in *Proceedings of the 5th Workshop on Self-Organizing Maps*, WSOM, pp. 275–282, 2005.

[165] M. Cottrell, B. Hammer, A. Hasenfuß, and T. Villmann, "Batch and median neural gas," *Neural Networks*, vol. 19, no. 6–7, pp. 762–771, 2006.

[166] B. Hammer, A. Hasenfuss, F.-M. Schleif, and T. Villmann, "Supervised batch neural gas," in *Proceedings of the Second international conference on Artificial Neural Networks in Pattern Recognition*, ANNPR, pp. 33–45, 2006.

[167] M. Pena and C. Fyfe, "The topographic neural gas," in *Proceedings of the 7th international conference on Intelligent Data Engineering and Automated Learning*, IDEAL, pp. 241–248, 2006.

[168] I. Licata and L. Lella, "Evolutionary neural gas (ENG) : A model of self organizing network from input categorization," *Electronic Journal of Theoretical Physics*, vol. 4, no. 14, pp. 31–50, 2007.

[169] S. Moreno, H. Allende, R. Salas, and C. Saavedra, "Fusion of neural gas," in *Proceedings of the 2nd international work-conference on The Interplay Between Natural and Artificial Computation, Part I: Bio-inspired Modeling of Cognitive Tasks*, IWINAC, pp. 558–567, 2007.

[170] X. Fang, G. Liu, and T.-Z. Huang, "Boosting the hierarchical hyperellipsoidal neural gas networks," in *Proceedings of the 4th International Conference on Natural Computation*, vol. 3 of *ICNC*, pp. 126–130, 2008.

[171] K. Labusch, E. Barth, and T. Martinetz, "Learning data representations with sparse coding neural gas," in *Proceedings of the 16th European Symposium on Artificial Neural Networks,* (M. Verleysen, ed.), pp. 233–238, D-Side Publishers, 2008.

[172] K. Labusch, E. Barth, and T. Martinetz, "Sparse coding neural gas for the separation of noisy overcomplete sources," in *Proceedings of the 18th international conference on Artificial Neural Networks, Part I*, ICANN, pp. 788–797, 2008.

[173] K. Labusch, E. Barth, and T. Martinetz, "Approaching the time dependent cocktail party problem with online sparse coding neural gas," in *Proceedings of the 7th International Workshop on Advances in Self-Organizing Maps*, WSOM, pp. 145–153, 2009.

[174] K. Labusch, E. Barth, and T. Martinetz, "Demixing jazz-music: Sparse coding neural gas for the separation of noisy overcomplete sources," *Neural Network World*, vol. 19, no. 5, pp. 581–596, 2009.

[175] K. Labusch, E. Barth, and T. Martinetz, "Sparse coding neural gas: Learning of overcomplete data representations," *Neurocomputing*, vol. 72, no. 7–9, pp. 1547–1555, 2009.

[176] A. Caţaron and R. Andonie, "Energy supervised relevance neural gas for feature ranking," *Neural Processing Letters*, vol. 32, no. 1, pp. 59–73, 2010.

[177] B. Arnonkijpanich and B. Hammer, "Global coordination based on matrix neural gas for dynamic texture synthesis," in *Proceedings of the 4th Conference on Artificial Neural Networks in Pattern Recognition*, ANNPR, pp. 84–95, 2010.

[178] Z. Yu, J. You, and G. Wen, "Neural gas based cluster ensemble algorithm and its application to cancer data," in *Proceedings of the International Conference on Machine Learning and Cybernetics*, vol. 1, pp. 15–20, 2011.

[179] J. Hagenauer and M. Helbich, "Contextual neural gas for spatial clustering and analysis," *International Journal of Geographical Information Science*, vol. 1, no. 1, pp. 1–16, 2012.

[180] R. Moller and H. Hoffmann, "An extension of neural gas to local PCA," *Neurocomputing*, vol. 62, no. 1–4, pp. 305–326, 2004.

[181] I. Machón-González, H. López-García, and J. L. Calvo-Rolle, "The complexity of the batch neural gas extended to local PCA," in *Proceedings of the 10th International Work-Conference on Artificial Neural Networks: Part I: Bio-Inspired Systems: Computational and Ambient Intelligence*, IWANN, pp. 212–219, 2009.

[182] I. Aleo, P. Arena, and L. Patané, "Incremental learning for visual classification using neural gas," in *Proceedings of the International Joint Conference on Neural Networks*, 2010.

[183] X. Fang, G. Liu, and T.-Z. Huang, "A principal components analysis neural gas algorithm for anomalies clustering," *WSEAS Transactions on Systems*, vol. 9, no. 1, pp. 42–51, 2010.

[184] B. Hammer and A. Hasenfuss, "Relational neural gas," in *Proceedings of the 30th Annual German conference on Advances in Artificial Intelligence*, KI, pp. 190–204, 2007.

[185] A. Hasenfuss, B. Hammer, and F. Rossi, "Patch relational neural gas - clustering of huge dissimilarity datasets," in *Proceedings of the 3rd IAPR workshop on Artificial Neural Networks in Pattern Recognition*, ANNPR, pp. 1–12, 2008.

[186] S. M. Zaki and H. Yin, "A semi-supervised learning algorithm for growing neural gas in face recognition," *Journal of Mathematical Modelling and Algorithms*, vol. 7, no. 4, pp. 425–435, 2008.

[187] M. P. Shiralkar and R. J. Schalkoff, "Multiple-class spatiotemporal flow estimation using a modified neural gas algorithm," *Optical Engineering*, vol. 48, no. 1, pp. 017003–017003–11, 2009.

[188] B. Hammer, A. Hasenfuss, and T. Villmann, "Magnification control for batch neural gas," *Neurocomputing*, vol. 70, no. 7–9, pp. 1225–1234, 2007.

[189] C. Mirabello, R. Rizzo, A. Urso, and S. Gaglio, "Clustering bacteria species using neural gas: Preliminary study," in *Computational Intelligence Methods for Bioinformatics and Biostatistics*, pp. 167–176, Springer-Verlag, 2009.

[190] A. Hasenfuss, B. Hammer, F. . Schleif, and T. Villmann, "Neural gas clustering for dissimilarity data with continuous prototypes," in *Proceedings of the 9th International Work Conference on Artificial neural networks*, IWANN, pp. 539–546, 2007.

[191] A. I. González, A. D'Anjou, M. T. García-Sebastian, and M. Graña, "SOM and neural gas as graduated nonconvexity algorithms," in *Proceedings of the International Conference on Computational Science and Its Applications - Volume Part III*, ICCSA, pp. 1143–1152, 2006.

[192] O. Kurasova and A. Molyte, "Integration of the self-organizing map and neural gas with multidimensional scaling," *Information Technology and Control*, vol. 40, no. 1, pp. 12–20, 2011.

[193] M. Daszykowski, B. Walczak, and D. L. Massart, "On the optimal partitioning of data with K-means, growing K-means, neural gas, and growing neural

gas," *Journal of Chemical Information and Computer Sciences*, vol. 42, no. 6, pp. 1378–1389, 2002.

[194] T. Martinetz and K. Schulten, "Topology representing networks," *Neural Networks*, vol. 7, pp. 507–522, March 1994.

[195] M. A. Montes De Oca, L. Garrido, and J. L. Aguirre, "An hybridization of an ant-based clustering algorithm with growing neural gas networks for classification task," in *Proceedings of the ACM Symposium on Applied Computing*, vol. 1, pp. 9–13, 2005.

[196] K. Lalonde, "Investigations into the analysis of remote sensing images with a growing neural gas pattern recognition algorithm," in *Proceedings of the International Joint Conference on Neural Networks*, vol. 3, pp. 1698–1703, 2005.

[197] S. Chelloug, S. Meshoul, and M. Batouche, "Clustering microarray data within amorphous computing paradigm and Growing Neural Gas algorithm," in *Proceedings of the 19th international conference on Advances in Applied Artificial Intelligence: industrial, Engineering and Other Applications of Applied Intelligent Systems*, IEA/AIE, pp. 809–818, 2006.

[198] J. A. F. Costa and R. S. Oliveira, "Cluster analysis using Growing Neural Gas and graph partitioning," in *Proceedings of the IEEE International Conference on Neural Networks*, pp. 3051–3056, 2007.

[199] R. M. Rodríguez-Pena, B. Pérez-Sánchez, and O. Fontenla-Romero, "A novel local classification method using Growing Neural Gas and proximal support vector machines," in *Proceedings of the IEEE International Conference on Neural Networks*, pp. 1607–1612, 2007.

[200] I. T. Podolak and K. Bartocha, "A hierarchical classifier with growing neural gas clustering," in *Proceedings of the 9th International Conference on Adaptive and Natural Computing Algorithms*, ICANNGA, pp. 283–292, 2009.

[201] R. Rizzo and A. Urso, "Identifying clusters using Growing Neural Gas: First results," in *Proceedings of the 19th International Conference on Artificial Neural Networks: Part I*, ICANN, pp. 536–545, 2009.

[202] A. Adam, S. Leuoth, S. Dienelt, and W. Benn, "Performance gain for clustering with Growing Neural Gas using parallelization methods," in *Proceedings of the 12th International Conference on Enterprise Information Systems*, ICEIS, pp. 264–269, 2010.

[203] J. Acevedo-Rodríguez, S. Maldonado-Bascón, R. López-Sastre, P. Gil-Jiménez, and A. Fernández-Caballero, "Clustering of trajectories in video surveillance using Growing Neural Gas," in *Proceedings of the 4th international conference on Interplay between natural and artificial computation - Volume Part I*, IWINAC, pp. 461–470, 2011.

[204] S. V. Mitsyn and G. A. Ososkov, "The Growing Neural Gas and clustering of large amounts of data," *Optical Memory and Neural Networks*, vol. 20, no. 4, pp. 260–270, 2011.

[205] S. Mohd Zaki and H. Yin, "Semi-supervised growing neural gas for face recognition," in *Proceedings of the 9th International Conference on Intelligent Data Engineering and Automated Learning*, IDEAL, pp. 525–532, 2008.

[206] O. Linda and M. Manic, "GNG-SVM framework - classifying large datasets with Support Vector Machines using Growing Neural Gas," in *Proceedings of the International Joint Conference on Neural Networks*, pp. 1820–1826, 2009.

[207] O. Beyer and P. Cimiano, "Online labelling strategies for growing neural gas," in *Proceedings of the 12th international conference on Intelligent Data Engineering and Automated Learning*, IDEAL, (Berlin, Heidelberg), pp. 76–83, 2011.

[208] J. García, F. Flórez, J. M. García, and A. Hernández, "Characterization and synthesis of objects using Growing Neural Gas," in *Proceedings of the 8th*

international conference on Artificial Neural Networks: Computational Intelligence and Bioinspired Systems, IWANN, pp. 630–636, 2005.

[209] J. García, F. Flórez-Revuelta, and J. M. García, "Growing Neural Gas for vision tasks with time restrictions," in *Proceedings of the 16th international conference on Artificial Neural Networks - Volume Part II*, ICANN, pp. 578–586, 2006.

[210] J. García-Rodríguez, F. Flórez-Revuelta, and J. M. García-Chamizo, "Adaptive representation of objects topology deformations with Growing Neural Gas," in *Proceedings of the 9th international work conference on Artificial Neural Networks*, IWANN, pp. 244–251, 2007.

[211] J. García-Rodríguez, F. Flórez-Revuelta, and J. M. García-Chamizo, "Image compression using Growing Neural Gas," in *Proceedings of the IEEE International Conference on Neural Networks*, pp. 366–370, 2007.

[212] J. García-Rodríguez, F. Flórez-Revuelta, and J. M. García-Chamizo, "Learning topologic maps with Growing Neural Gas," in *Knowledge-Based Intelligent Information and Engineering Systems*, Lecture Notes in Computer Science, pp. 469–476, Springer Berlin Heidelberg, 2007.

[213] N. Kubota and M. Satomi, "Growing neural gas with triangulation for reconstructing a 3D surface model," in *World Automation Congress*, WAC, 2008.

[214] N. Kubota, T. Narita, and B. H. Lee, "3D topological reconstruction based on Hough transform and growing neural gas for informationally structured space," in *Proceedings of the IEEE/RSJ International Conference on Intelligent Robots and Systems*, IROS, pp. 3459–3464, 2010.

[215] J. García-Rodríguez, A. Angelopoulou, and A. Psarrou, "Growing Neural Gas (GNG): A soft competitive learning method for 2D hand modelling," *IEICE Transactions on Information and Systems*, vol. E89-D, no. 7, pp. 2124–2131, 2006.

[216] A. Angelopoulou, A. Psarrou, and J. García Rodríguez, "A Growing Neural Gas algorithm with applications in hand modelling and tracking," in *Proceedings of the 11th international conference on Artificial neural networks conference on Advances in computational intelligence - Volume Part II*, IWANN, pp. 236–243, 2011.

[217] J. Rivera-Rovelo, S. Herold-García, and E. Bayro-Corrochano, "Object segmentation using Growing Neural Gas and generalized gradient vector flow in the geometric algebra framework," in *Progress in Pattern Recognition, Image Analysis and Applications*, no. 4225 in Lecture Notes in Computer Science Volume , 2006, pp 306-315, pp. 306–315, 2006.

[218] A.-M. Cretu, E. Petriu, and P. Payeur, "Evaluation of Growing Neural Gas networks for selective 3D scanning," in *IEEE International Workshop on Robotic and Sensors Environments Proceedings*, ROSE, pp. 108–113, 2008.

[219] L. De Oliveira Martins, A. C. Silva, A. C. De Paiva, and M. Gattass, "Detection of breast masses in mammogram images using Growing Neural Gas algorithm and Ripley's K function," *Journal of Signal Processing Systems*, vol. 55, no. 1–3, pp. 77–90, 2009.

[220] E. Fatemizadeh, C. Lucas, and H. Soltanian-Zadeh, "Automatic landmark extraction from image data using modified Growing Neural Gas network," *IEEE Transactions on Information Technology in Biomedicine*, vol. 7, no. 2, pp. 77–85, 2003.

[221] A. Angelopoulou, A. Psarrou, J. G. Rodríguez, and K. Revett, "Automatic landmarking of 2d medical shapes using the growing neural gas network," in *Proceedings of the First international conference on Computer Vision for Biomedical Image Applications*, CVBIA, pp. 210–219, 2005.

[222] G. S. Donatti and R. P. Würtz, "Using Growing Neural Gas networks to represent visual object knowledge," in *Proceedings of the 21st IEEE International Conference on Tools with Artificial Intelligence*, ICTAI, pp. 54–58, 2009.

[223] G. Donatti, O. Lomp, and R. W´uandrtz, "Evolutionary optimization of Growing Neural Gas parameters for object categorization and recognition," in *Proceedings of the International Joint Conference on Neural Networks*, pp. 1–8, 2010.

[224] H. Sasaki, N. Kubota, K. Sekiyama, and T. Fukuda, "Multiple object detection for intelligent robot vision by using Growing Neural Gas," in *International Symposium on Micro-NanoMechatronics and Human Science*, pp. 80–85, 2009.

[225] H. Sasaki, T. Fukuda, M. Satomi, and N. Kubota, "Growing Neural Gas for intelligent robot vision with range imaging camera," in *IEEE International Conference on Mechatronics and Automation*, ICMA, pp. 3269–3274, 2009.

[226] M. Satomi, H. Masuta, and N. Kubota, "Hierarchical Growing Neural Gas for information structured space," in *Proceedings of the IEEE Workshop on Robotic Intelligence in Informationally Structured Space*, RiiSS, pp. 54–59, 2009.

[227] C. Zhong, S. Liu, and X. Qiu, "Autonomous cognitive of the environment map based on Growing Neural Gas in unknown environment," in *Proceedings of the 29th Chinese Control Conference*, CCC, pp. 3768–3772, 2010.

[228] M. Cirrincione, M. Pucci, and G. Vitale, "Growing Neural Gas (gng) based maximum power point tracking for high performance voc-foc based wind generator system with an induction machineas," in *IEEE Energy Conversion Congress and Exposition*, ECCE, pp. 1603–1610, 2009.

[229] M. Cirrincione, M. Pucci, and G. Vitale, "Growing Neural Gas based mppt of variable pitch wind generators with induction machines," in *IEEE Energy Conversion Congress and Exposition*, ECCE, pp. 3762–3771, September 2010.

[230] M. Pucci, "Sensors-less neural maximum power point tracking control of induction machines wind generators by Growing Neural Gas and minor compo-

nent analysis exin + reduced order observer," *IET Control Theory and Applications*, vol. 4, no. 9, pp. 1627–1638, 2010.

[231] M. Cirrincione, M. Pucci, and G. Vitale, "Growing Neural Gas (gng)-based maximum power point tracking for high-performance wind generator with an induction machine," *IEEE Transactions on Industry Applications*, vol. 47, no. 2, pp. 861–872, 2011.

[232] M. Cirrincione, M. Pucci, and G. Vitale, "Growing Neural Gas-based mppt of variable pitch wind generators with induction machines," *IEEE Transactions on Industry Applications*, vol. 48, pp. 1006–1016, May–June 2012.

[233] F. J. Mora-Gimeno, F. Maciá-Pérez, I. Lorenzo-Fonseca, J. A. Gil-Martínez-Abarca, D. Marcos-Jorquera, and V. Gilart-Iglesias, "Security alert correlation using Growing Neural Gas," in *Proceedings of the 4th international conference on Computational intelligence in security for information systems*, CISIS, pp. 76–83, 2011.

[234] T. Chen, A. Bansal, S. Zhong, and X. Chen, "Protecting data privacy in Growing Neural Gas," *Neural Computing and Applications*, vol. 21, pp. 1255–1262, September 2012.

[235] H. Shen, D.-W. Hu, and X.-S. Wen, "Identification of chaotic systems using a new growing neural-gas network," *Acta Automatica Sinica*, vol. 27, no. 3, pp. 401–405, 2001.

[236] P. Baldassarri, P. Puliti, A. Montesanto, and G. Tascini, "Self-organizing maps versus Growing Neural Gas in a robotic application," in *Proceedings of the 7th International Work-Conference on Artificial and Natural Neural Networks: Part II: Artificial Neural Nets Problem Solving Methods*, IWANN, pp. 201–208, 2003.

[237] M. Y. Kim, H. Cho, and J.-h. Kim, "Obstacle modeling for environment recognition of mobile robots using Growing Neural Gas network," *International Journal of Control, Automation and Systems*, vol. 1, no. 1, pp. 134–141, 2003.

[238] T. Hermann and H. Ritter, "Neural gas sonification - growing adaptive interfaces for interacting with data," in *Proceedings of the International Conference on Information Visualization*, vol. 8, pp. 871–878, 2004.

[239] M. Cirrincione, M. C. Di Piazza, M. Pucci, and G. Vitale, "Real-time simulation of photovoltaic arrays by Growing Neural Gas controlled dc-dc converter," in *Proceedings of the IEEE Annual Power Electronics Specialists Conference*, pp. 2004–2010, June 2008.

[240] H. F. Satizábal, A. Pérez-Uribe, and M. Tomassini, "Prototype proliferation in the Growing Neural Gas algorithm," in *Proceedings of the 18th International Conference on Artificial Neural Networks, Part II*, (Berlin, Heidelberg), pp. 793–802, Springer-Verlag, 2008.

[241] M. C. Di Piazza, M. Pucci, A. Ragusa, and G. Vitale, "A Growing Neural Gas network based mppt technique for multi-string pv plants," in *IEEE International Symposium on Industrial Electronics*, pp. 544–549, July 2010.

[242] F. Flentge, "Locally weighted interpolating growing neural gas," *IEEE Transactions on Neural Networks*, vol. 17, no. 6, pp. 1382–1393, 2006.

[243] D. Chavez, G. Laures, K. Loayza, and R. Patino, "A stopping criteria for the growing neural gas based on a validity separation index for clusters," in *Proceedings of the 11th International Conference on Hybrid Intelligent Systems*, HIS, pp. 578–583, 2011.

[244] J. Graham and J. A. Starzyk, "A hybrid self-organizing neural gas based network," in *Proceedings of the International Joint Conference on Neural Networks*, pp. 3806–3813, 2008.

[245] M. Kortkamp and S. Wachsmuth, "Continuous visual codebooks with a limited branching tree growing neural gas," in *Proceedings of the 20th international conference on Artificial neural networks: Part III*, ICANN, pp. 188–197, 2010.

[246] X. Cao and P. N. Suganthan, "Hierarchical overlapped growing neural gas networks with applications to video shot detection and motion characterization,"

in *Proceedings of the International Joint Conference on Neural Networks*, vol. 2, pp. 1069–1074, 2002.

[247] X. Cao and P. N. Suganthan, "Video shot motion characterization based on hierarchical overlapped growing neural gas networks," *Multimedia Systems*, vol. 9, no. 4, pp. 378–385, 2003.

[248] G. Cheng and A. Zell, "Double growing neural gas for disease diagnosis," in *Proceedings of Artificial Neural Networks in Medicine and Biology Conference*, ANNIMAB, pp. 309–314, 2000.

[249] D. Hu and H. Shen, "A new algorithm for chaotic system identification based on self-organizing neural gas," in *Proceedings of the World Congress on Intelligent Control and Automation*, vol. 3 of *WCICA*, pp. 2211–2214, 2000.

[250] S. Marsland, J. Shapiro, and U. Nehmzow, "A self-organising network that grows when required," *Neural Networks*, vol. 15, pp. 1041–1058, October 2002.

[251] A. K. Qin and P. N. Suganthan, "Robust growing neural gas algorithm with application in cluster analysis," *Neural Networks*, vol. 17, no. 8–9, pp. 1135–1148, 2004.

[252] Y. Prudent and A. Ennaji, "An incremental growing neural gas learns topologies," in *Proceedings of the International Joint Conference on Neural Networks*, vol. 2, pp. 1211–1216, 2005.

[253] H. Hamza, Y. Belaïd, A. Belaïd, and B. B. Chaudhuri, "Incremental classification of invoice documents," in *19th International Conference on Pattern Recognition*, ICPR, pp. 1–4, 2008.

[254] J.-C. Lamirel, Z. Boulila, M. Ghribi, and P. Cuxac, "A new incremental growing neural gas algorithm based on clusters labeling maximization: Application to clustering of heterogeneous textual data," in *Proceedings of the 23rd international conference on Industrial engineering and other applications of applied intelligent systems - Volume Part III*, IEA/AIE, pp. 139–148, 2010.

[255] J.-C. Lamirel, R. Mall, P. Cuxac, and G. Safi, "Variations to incremental growing neural gas algorithm based on label maximization," in *Proceedings of the International Joint Conference on Neural Networks*, pp. 956–965, 2011.

[256] K. A. J. Doherty, R. G. Adams, and N. Davey, "Hierarchical growing neural gas," in *Proceedings of the International Conference on Adaptive and Natural Computing Algorithms*, pp. 140–143, 2005.

[257] Z. Cselényi, "Mapping the dimensionality, density and topology of data: The growing adaptive neural gas," *Computer methods and programs in biomedicine*, vol. 78, no. 2, pp. 141–156, 2005.

[258] R. Mayrhofer and H. Radi, "Extending the growing neural gas classifier for context recognition," in *Proceedings of the 11th international conference on Computer aided systems theory*, EUROCAST, pp. 920–927, 2007.

[259] F. Canales and M. Chacón, "Modification of the growing neural gas algorithm for cluster analysis," in *Proceedings of the 12th Iberoamerican Conference on Progress in Pattern Recognition, Image Analysis and Applications*, CIARP, pp. 684–693, 2007.

[260] A. Jirayusakul and S. Auwatanamongkol, "A supervised growing neural gas algorithm for cluster analysis," *International Journal of Hybrid Intelligent Systems*, vol. 4, pp. 129–141, April 2007.

[261] S. Gancev and D. Davcev, "Monitoring wireless sensor network system based on classification of adopted supervised growing neural gas algorithm," in *ICT Innovations*, vol. 83 of *Communications in Computer and Information Science*, pp. 316–324, Springer Berlin Heidelberg, 2011.

[262] I. J. Sledge and J. M. Keller, "Growing neural gas for temporal clustering," in *Proceedings of the International Conference on Pattern Recognition*, 2008.

[263] Y. Holdstein and A. Fischer, "Three-dimensional surface reconstruction using meshing growing neural gas (MGNG)," *Visual Computer*, vol. 24, no. 4, pp. 295–302, 2008.

[264] H. Frezza-Buet, "Following non-stationary distributions by controlling the vector quantization accuracy of a growing neural gas network," *Neurocomputing*, vol. 71, no. 7–9, pp. 1191–1202, 2008.

[265] S. Gancev and A. Kulakov, "Modified growing neural gas algorithm for faster convergence on signal distribution sudden change," in *XXII International Symposium on Information, Communication and Automation Technologies*, ICAT, pp. 1–5, October 2009.

[266] J. García-Rodríguez, A. Angelopoulou, J. M. García-Chamizo, A. Psarrou, S. Orts-Escolano, and V. Morell-Giménez, "Fast autonomous growing neural gas," in *Proceedings of the International Joint Conference on Neural Networks*, pp. 725–732, 2011.

[267] R. Berlich and M. Kunze, "A comparison between the performance of feed forward neural networks and the supervised growing neural gas algorithm," *Nuclear Instruments and Methods in Physics Research, Section A: Accelerators, Spectrometers, Detectors and Associated Equipment*, vol. 389, no. 1–2, pp. 274–277, 1997. Cited By (since 1996): 4.

[268] D. Heinke and F. H. Hamker, "Comparing neural networks: A benchmark on growing neural gas, growing cell structures, and fuzzy ARTMAP," *IEEE Transactions on Neural Networks*, vol. 9, no. 6, pp. 1279–1291, 1998.

[269] F. F. Revuelta, J. M. G. Chamizo, J. G. Rodríguez, and A. H. Sánchez, "Analysis of the topology preservation of accelerated growing neural gas in the representation of bidimensional objects," in *Current Topics in Artificial Intelligence*, vol. 3040 of *Lecture Notes in Computer Science*, pp. 167–176, 2004.

[270] J. Holmström, "Growing neural gas – experiments with GNG, GNG with Utility and Supervised GNG," Master's thesis, Uppsala University Department of Information Technology Computer Systems, 2002.

[271] J. García-Rodríguez, A. Angelopoulou, V. Morell, S. Orts, A. Psarrou, and J. M. García-Chamizo, "Fast image representation with GPU-based growing

neural gas," in *Proceedings of the 11th international conference on Artificial neural networks conference on Advances in computational intelligence - Volume Part II*, IWANN, pp. 58–65, 2011.

[272] A. Atsalakis, N. Papamarkos, and I. Andreadis, "Image dominant colors estimation and color reduction via a new self-growing and self-organized neural gas," in *Proceedings of the 10th Iberoamerican Congress Conference on Progress in Pattern Recognition, Image Analysis and Applications*, CIARP, pp. 977–988, Springer Verlag Berlin, 2005.

[273] A. Atsalakis and N. Papamarkos, "Color reduction by using a new self-growing and self-organized neural network," in *Second International Conference on Vision, Video and Graphics*, pp. 53–60, 2005.

[274] A. Atsalakis and N. Papamarkos, "Color reduction and estimation of the number of dominant colors by using a self-growing and self-organized neural gas," *Engineering Applications of Artificial Intelligence*, vol. 19, no. 7, pp. 769–786, 2006.

[275] E. Stergiopoulou and N. Papamarkos, "Hand gesture recognition using a neural network shape fitting technique," *Engineering Applications of Artificial Intelligence*, vol. 22, pp. 1141–1158, December 2009.

[276] D. P. Papadopoulos, S. A. Chatzichristofis, and N. Papamarkos, "Video summarization using a self-growing and self-organized neural gas network," in *Proceedings of the 5th international conference on Computer vision/computer graphics collaboration techniques*, MIRAGE, pp. 216–226, 2011.

[277] T. M. Martinetz, S. G. Berkovich, and K. J. Schulten, ""neural-gas" network for vector quantization and its application to time-series prediction," *IEEE Transactions on Neural Networks*, vol. 4, no. 4, pp. 558–569, 1993.

[278] M. Strickert and B. Hammer, "Merge {SOM} for temporal data," *Neurocomputing*, vol. 64, pp. 39–71, March 2005. Trends in Neurocomputing: 12th European Symposium on Artificial Neural Networks.

[279] A. Andreakis, N. V. Hoyningen-Huene, and M. Beetz, "Incremental unsupervised time series analysis using merge growing neural gas," in *Advances in Self-Organizing Maps*, vol. 5629 of *Lecture Notes in Computer Science*, pp. 10–18, Springer Berlin Heidelberg, 2009.

[280] A. Ultsch, "Clustering with SOM: U*C," in *Proceedings of the Workshop on Self-Organizing Maps*, pp. 75–82, 2008.

[281] L. González-Villanueva, A. Alvarez-Alvarez, L. Ascari, and G. Trivino, "A tool for linguistic assessment of rehabilitation exercises," *Applied Soft Computing*, vol. 14, Part A, pp. 120–131, January 2014. Special Issue on Hybrid Intelligent Methods for Health Technologies.

[282] M. G. Sánchez-Torrubia, C. Torres-Blanc, and G. Trivino, "An approach to automatic learning assessment based on the computational theory of perceptions," *Expert Systems with Applications*, vol. 39, no. 15, pp. 12177–12191, 2012.

[283] L. A. Zadeh, "From computing with numbers to computing with words – from manipulation of measurements to manipulation of perceptions," *IEEE Transactions on Circuits and Systems - I: Fundamental theory and applications*, vol. 45, no. 1, pp. 105–119, 1999.

[284] L. A. Zadeh, *Fuzzy Sets and information granularity*. Amsterdam, The Netherlands: North-Holland, 1979.

[285] L. A. Zadeh, "Towards a theory of fuzzy information granulation and its centrality in human reasoning and fuzzy logic," *Fuzzy Sets and Systems*, vol. 90, pp. 111–127, 1997.

[286] L. A. Zadeh, "Toward human level machine intelligence – is it achievable? the need for a paradigm shift," *IEEE Computational Intelligence Magazine*, vol. 3, pp. 11–22, August 2008.

[287] L. A. Zadeh, "The concept of a linguistic variable and its application to approximate reasoning - I," *Information Sciences*, vol. 8, no. 3, pp. 199–249, 1975.

[288] L. A. Zadeh, "The concept of a linguistic variable and its application to approximate reasoning - II," *Information Sciences*, vol. 8, no. 4, pp. 301–357, 1975.

[289] L. A. Zadeh, "The concept of a linguistic variable and its application to approximate reasoning - III," *Information Sciences*, vol. 9, no. 1, pp. 43–80, 1975.

[290] L. Eciolaza, M. Pereira-Fariña, and G. Trivino, "Automatic linguistic reporting in driving simulation environments," *Applied Soft Computing*, vol. 13, pp. 3956–3967, September 2013.

[291] A. Alvarez-Alvarez, D. Sanchez-Valdes, G. Trivino, A. Sánchez, and P. D. Suárez, "Automatic linguistic report of traffic evolution in roads," *Expert Systems with Applications*, vol. 39, pp. 11293–11302, September 2012.

[292] H. Chaudhry, T. Findley, K. S. Quigley, Z. Ji, M. Maney, T. Sims, B. Bukiet, and R. Foulds, "Postural stability index is a more valid measure of stability than equilibrium score," *The Journal of Rehabilitation Research and Development*, vol. 42, no. 4, pp. 547–556, 2005.

[293] T. Platz, R. G. Brown, and C. D. Marsden, "Training improves the speed of aimed movements in parkinson's disease," *Brain*, vol. 121, pp. 505–514, 1998.

[294] R. Polana and R. Nelson, "Low level recognition of human motion (or how to get your man without finding his body parts)," in *In Proc. of IEEE Comp. Soc. Workshop on Motion of Non-Rigid and Articulated Objects*, pp. 77–82, 1994.

[295] A. F. Bobick and A. D. Wilson, "A state-based technique for the summarization and recognition of gesture," in *Proc. of the 5th Int. Conf. on Computer Vision*, pp. 382–388, 1995.

[296] J. N. Mordeson and D. S. Malik, *Fuzzy Automata and Languages: Theory and Applications*. Chapman & Hall, 2002.

[297] A. Alvarez and G. Trivino, "Comprehensible model of a quasi-periodic signal," in *9th Int. Conf. on Intelligent Systems Design and Applications*, pp. 450–455, 2009.

[298] A. Alvarez-Alvarez, J. Alonso, and G. Trivino, "Human activity recognition in indoor environments by means of fusing information extracted from intensity of WiFi signal and accelerations," *Information Sciences (in press)*, 2013.

[299] G. Trivino, A. Alvarez-Alvarez, and G. Bailador, "Application of the computational theory of perceptions to human gait pattern recognition," *Pattern Recognition*, vol. 43, pp. 2572–2581, July 2010.

[300] L. González-Villanueva, A. Alvarez-Alvarez, L. Ascari, and G. Trivino, "Computational model of human body motion performing a complex exercise by means of a Fuzzy Finite State Machine," in *Proceedings of the International Conference on Medical Imaging Using Bio-Inspired and Soft Computing (MIBISOC2013)*, May 2013.

[301] M. Sugeno, *Industrial applications of fuzzy control*. Elsevier Science Pub. Co., 1985.

[302] C. Alsina, M. J. Frank, and B. Schweizer, *Associative Functions: Triangular Norms and Copulas*. Singapore: World Scientific Publishing Company, 2006.

[303] L. Hamers, Y. Hemeryck, G. Herweyers, M. Janssen, H. Keters, R. Rousseau, and A. Vanhoutte, "Similarity measures in scientometric research: The Jaccard index versus Salton's cosine formula," *Information Processing and Management*, vol. 25, no. 3, pp. 315–318, 1989.

[304] J. M. Alonso and L. Magdalena, "Generating understandable and accurate fuzzy rule-based systems in a java environment," in *Lecture Notes in Artificial Intelligence - 9th International Workshop on Fuzzy Logic and Applications*, pp. 212–219, 2011.

[305] J. M. Alonso and L. Magdalena, "HILK++: an interpretability-guided fuzzy modeling methodology for learning readable and comprehensible fuzzy rule-based classifiers," *Soft Computing*, vol. 15, pp. 1959–1980, October 2011.

[306] J. Vieira, F. Morgado Dias, and A. Mota, "Neuro-fuzzy systems: A survey," in *5th WSEAS International Conference on Neural Networks and Applications*, 2004.

[307] A. Balbinot and G. Favieiro, "A neuro-fuzzy system for characterization of arm movements," *Sensors*, vol. 13, no. 2, pp. 2613–2630, 2013.

[308] Y. Wang and J. Winters, "An event-driven dynamic recurrent neuro-fuzzy system for adaptive prognosis in rehabilitation," in *Proceedings of the 25th Annual International Conference of the IEEE Engineering in Medicine and Biology Society*, vol. 2, pp. 1256–1259, 2003.

[309] S. Micera, W. Jensen, F. Sepulveda, R. Riso, and T. Sinkjaer, "Neuro-fuzzy extraction of angular information from muscle afferents for ankle control during standing in paraplegic subjects: an animal model," *IEEE Transactions on Biomedical Engineering*, vol. 48, no. 7, pp. 787–794, 2001.

[310] S. Begum, J. Westin, P. Funk, and M. Dougherty, "Induction of an adaptive neuro-fuzzy inference system for investigating fluctuations in parkinson's disease," in *Proceedings of 23rd Annual Workshop of the Swedish Artificial Intelligence Society*, pp. 67–71, 2006.

[311] L. Walsh, B. Greene, D. McGrath, A. Burns, and B. Caulfield, "Development and validation of a clinic based balance assessment technology," in *Annual International Conference of the IEEE Engineering in Medicine and Biology Society (EMBC)*, pp. 1327–1330, 2011.

[312] M. Kennedy, J. Schmiedeler, C. Crowell, M. Villano, A. Striegel, and J. Kuitse, "Enhanced feedback in balance rehabilitation using the nintendo wii balance board," in *13th IEEE International Conference on e-Health Networking Applications and Services (Healthcom)*, pp. 162–168, 2011.

[313] I. Cikajlo and Z. Matjacic, "Directionally specific objective postural response assessment tool for treatment evaluation in stroke patients," *IEEE Transactions on Neural Systems and Rehabilitation Engineering*, vol. 17, no. 1, pp. 91–100, 2009.

[314] I.-C. Chen, P.-T. Cheng, C.-L. Chen, S.-C. Chen, C.-Y. Chung, and T.-H. Yeh, "Effects of balance training on hemiplegic stroke patients," *Chang Gung Medical Journal*, vol. 25, pp. 583–590, September 2002.

[315] O. Čakrt, M. Chovanec, T. Funda, P. Kalitová, J. Betka, E. Zvěřina, P. Kolář, and J. Jeřábek, "Exercise with visual feedback improves postural stability after vestibular schwannoma surgery," *European Archives of Oto-Rhino-Laryngology*, vol. 267, pp. 1355–1360, September 2010.

[316] P. V. Vliet and G. Wulf, "Extrinsic feedback for motor learning after stroke: What is the evidence?," *Disability and Rehabilitation*, vol. 28, no. 13–14, pp. 831–840, 2006.

[317] A. Abraham, "Neuro fuzzy systems: Sate-of-the-art modeling techniques," in *Proceedings of the 6th International Work-Conference on Artificial and Natural Neural Networks: Connectionist Models of Neurons, Learning Processes and Artificial Intelligence-Part I*, IWANN '01, (London, UK, UK), pp. 269–276, Springer-Verlag, 2001.

[318] L. A. Zadeh, "A computational approach to fuzzy quantifiers in natural languages," *Computers & Mathematics with applications*, vol. 9, no. 1, pp. 149–184, 1983.

Acknowledgements

First of all I would like to acknowledge the funding sources that made this happen: the EU project "Medical Imaging using Bio-Inspired and Soft Computing" (MIBISOC), a Marie Curie Initial Training Network funded by the European Commission's 7^{th} Framework Programme (FP7-PEOPLE-ITN-2008, GA n. 238819).

This dissertation has been possible thanks to the help of many people, to their suggestions and support. Starting from the very beginning, Félix and Gustavo (my professors, my mentors, my friends) encouraged me to start this adventure and *let me go*. They will always be an inspiration to me, both in the professional and the personal aspect.

I owe my gratitude to Henesis, and Luca Ascari in particular, for choosing me for being part of this experience, which has definitely and completely changed my life. I am sincerely thankful to Prof. Stefano Cagnoni for his endless availability and advice during the PhD.

Within MIBISOC I have found, not just incredibly well prepared people and colleagues, but also very good friends. The other 17 ESRs (Pablo, Pouya, Youssef, Michela, David, Maddalena, Jérémie, Luis, Andrea, Nicola, Benjamin, Esmeralda, Alessandro, Viktor, Torbjörn, Gabriele and Bartosz) have made me not feeling alone in the loneliness of a thesis, sharing both the good moments and the bad ones. I cannot forget the rest of the members of MIBISOC: the Coordinator, Óscar Cordón, his team (Carmen Peña, Óscar Ibáñez…) and the principal researchers, among others. There is no space to name and thank them all for their support.

During the PhD I did two research stays, at the University of Nottingham and the European Centre for Soft Computing, under the supervision of Prof. Bai Li and Dr.

Gracián Triviño, respectively. I am very grateful to both of them for sharing with me their knowledge. And especially to Gracián, for his kindness and for helping me to recover my self-confidence when I needed it more. I would also like to thank Alberto for his valuable contributions.

I acknowledge all of the subjects who participated in the experiments for their *patience and enthusiasm*. Several more people have been around and helped me along the way, regrettably it is impossible to mention them all by name here. I thank them for sharing with me their thoughts, their time, their friendship.

Inoltre ringrazio tutte le persone, amici e familiari, che in Italia, grazie ai bei momenti passati insieme, hanno contribuito e contribuiscono a rendere meno difficile la lontananza da casa.

Doy las gracias especialmente a mis padres y a mi hermana porque, junto con el resto de mi familia y amigos, han creído siempre en mí, han estado a mi lado en la distancia y han sabido darme ánimos cuando los he necesitado.

E, finalmente, ringrazio e dedico questa tesi a te, Matteo. Solo tu sai bene quanto è stato difficile arrivare fin qui e quanto sono stati importanti il tuo amore e sostegno. Grazie per darmi idee, consigli e inspirazione per il mio lavoro ma, sopratutto, grazie per condividere la tua vita con me.

Ahora empieza otra aventura.

Muchas gracias a todos.

Lara González Villlanueva

Parma, September 2013

Puedo escribir los versos más tristes esta noche.

Escribir, por ejemplo: "La noche está estrellada,
y tiritan, azules, los astros, a lo lejos."

El viento de la noche gira en el cielo y canta.

Puedo escribir los versos más tristes esta noche.
Yo la quise, y a veces ella también me quiso.

En las noches como ésta la tuve entre mis brazos.
La besé tantas veces bajo el cielo infinito.

Ella me quiso, a veces yo también la quería.
Cómo no haber amado sus grandes ojos fijos.

Puedo escribir los versos más tristes esta noche.
Pensar que no la tengo. Sentir que la he perdido.

Oír la noche inmensa, más inmensa sin ella.
Y el verso cae al alma como al pasto el rocío.

Qué importa que mi amor no pudiera guardarla.
La noche está estrellada y ella no está conmigo.

Eso es todo. A lo lejos alguien canta. A lo lejos.
Mi alma no se contenta con haberla perdido.

Como para acercarla mi mirada la busca.
Mi corazón la busca, y ella no está conmigo.

La misma noche que hace blanquear los mismos árboles.
Nosotros, los de entonces, ya no somos los mismos.

Ya no la quiero, es cierto, pero cuánto la quise.
Mi voz buscaba el viento para tocar su oído.

De otro. Será de otro. Como antes de mis besos.
Su voz, su cuerpo claro. Sus ojos infinitos.

Ya no la quiero, es cierto, pero tal vez la quiero.
Es tan corto el amor, y es tan largo el olvido.

Porque en noches como ésta la tuve entre mis brazos,
Mi alma no se contenta con haberla perdido.

Aunque éste sea el último dolor que ella me causa,
y éstos sean los últimos versos que yo le escribo.

Pablo Neruda
Veinte poemas de amor y una canción desesperada, Poema 20